UNIVERSITÀ
DEGLI STUDI
DI PADOVA

Head Office: Università degli Studi di Padova

Department of Biology

Ph.D. COURSE IN: BIOSCIENCES
CURRICULUM: CELL BIOLOGY AND PHYSIOLOGY
SERIES XXXI

Synergic interaction of chemotherapy and PDT by co-delivery of DTX and photosensitizers in nanoparticles

Coordinator: Prof. Ildikò Szabò
Supervisor: Prof. Elena Reddi
Co-Supervisor: Dr. Francesca Moret

Ph.D. student: Elisa Gaio

Contents

List and summary of papers……3

Abstract……...……...7

Abbreviations……...……..9

Introduction……...……..11

Aim of the thesis……...……...33

Papers

Paper I……...35

Paper II……..57

Paper III……83

Conclusions……...……109

References……...……...111

List and summary of papers

The thesis is based on the following papers, which are referred to by roman numerals in the text:

I. Elisa Gaio, Claudia Conte, Diletta Esposito, Giovanni Miotto, Fabiana Quaglia, Francesca Moret, Elena Reddi.

"Co-delivery of docetaxel and disulphonate tetraphenyl chlorin in one nanoparticle produces strong synergism between chemo- and photodynamic therapy in drug-sensitive and -resistant cancer cells."

II. Elisa Gaio, Claudia Conte, Fabiana Quaglia, Francesca Moret, Elena Reddi.

"Synergic effects of chemo- and photodynamic therapy in 3D tumor cell models treated with nanoparticles co-delivering docetaxel and disulphonate tetraphenyl chlorin"

III. Elisa Gaio[#], Andrea Guerrini[#], Marco Ballestri, Greta Varchi, Claudia Ferroni, Annalisa Aluigi, Francesca Moret, Elena Reddi.

"Keratin nanoparticles co-delivering Docetaxel and Chlorin e6 for synergic chemo- and photodynamic anticancer effect"

[#] *The authors contributed equally to the study*

The papers were written in co-authorship, reflecting the collaboration among authors.
Paper I is already published in Molecular Pharmaceutics and reports the results on the efficacy of the combination of chemotherapy using the chemotherapeutic docetaxel (DTX) and photodynamic therapy (PDT) with the photosensitizer (PS) disulphonate tetraphenyl chlorin (TPCS2a) loaded in layer-by-layer nanoparticles for treating chemo –sensitive and –resistant cancer cells grown in the 2D condition. Paper II, prepared for submission to Biomacromolecules, is the extension and continuation of the investigation published in Paper I, and reports data on the ability of layer-by-layer nanoparticles to induce synergistic killing effects in 3D tumor models as multicellular tumor spheroids and tumor spheres enriched in cancer stem cells. These two papers are the results of the collaboration of my research group at the Department of Biology in Padova and the research group of prof. Fabiana Quaglia at the Department of Pharmacy of University of Napoli Federico II. The latter research group takes care of the synthesis, drug loading and characterization of the nanonanoparticle, while all the *in vitro* cell experiments and the statistical analysis of the obtained data were carried out in the lab in Padova.
Paper III, prepared for submission to Material Science and Engineering: C, deals with the evaluation of the efficacy of the combination photo-chemotherapy performed co-loading the photosensitizer chlorin e6 (Ce6) and DTX in keratin nanoparticles. These nanoparticles were synthetized by the group of dr. Greta Varchi from the Italian National Research Council (CNR) of Bologna. The biological studies were performed by my research group in Padova.
In all the three papers my name appears as the first author since the large majority of the data were produced in my research group and during my PhD experience.

Summary of Paper I

The paper reports the design, synthesis and characterization and the evaluation of the efficacy of hyaluronic acid (HA) targeted polymeric layer-by-layer nanoparticles for performing combination therapy with the co-delivery of DTX and TPCS2a to cancer cells overexpressing CD44 HA receptor. Thus PLGA-PEI nanoparticles loaded with the two drugs at a fixed drug ratio, previously identified as optimal for obtaining synergic effects, were prepared and their ability in inducing synergism in DTX –sensitive and –resistant cancer cells was compared to

that observed with the combination of the two drugs loaded in separate vehicles and co-administered as free molecules in standard solvent. The Compusyn software was used to evaluate the type of interaction between chemotherapy and PDT and quantify their desired synergistic interaction. In addition, cell death mechanisms elicited by monotherapies and their combination and the drug intracellular uptake and localization were investigated. The study highlighted how the co-loading of DTX and TPCS2a in one nanoparticle gives the higher extent of synergism in all the three cell lines considered (HeLa, MDA-MB-231 and DTX –resistant HeLa cells). Importantly, the nanoparticles co-loaded with DTX and TPCS2a gave the highest synergism in drug-resistant cells indicating the possibility to overcome drug-resistant efflux pumps.

Summary of Paper II

The study reports the extension of the work presented in Paper I. Here DTX and TPCS2a were co-loaded in layer-by-layer nanoparticles at three different concentration ratios and were tested in two different types of 3D tumor models namely, multicellular spheroids and tumor spheres. Cell killing efficiency, nanoparticle penetration inside the 3D culture and ability in inducing synergism of nanoparticles loaded with the different drug ratios were compared in spheroids of cells sensitive (HeLa) as well as resistant to docetaxel (HeLa-R). Moreover, mammosphere cultures enriched with cancer stem cells (CSCs) were used to evaluate the capacity of our nanosystem to target and kill this cell subpopulation. The results confirmed the validity of the strategy based on the co-delivery of DTX and the photosensitizer TPCS2a for obtaining synergic effects between chemo- and photodynamic therapy. The results reported here have however highlighted that the drug concentration ratios giving synergism in these 3D models are much different from those found previously for 2D cultures and raise the question of the most suitable in vitro models for preclinical studies on combinatorial therapies. Nanoparticles co-loaded with the two drugs demonstrated also some extent of efficacy in decreasing the stemness or in reducing the capacity to form spheres in MCF-7 and MDA-MB-231 cell lines.

Summary of Paper III

The study highlighted potentialities and limitations of keratin nanoparticles as drug delivery vehicle for DTX and Ce6. In this work keratin NPs were synthetized using aggregation method in aqueous solution taking advantage of the aggregation ability of DTX. This aspect limits the possibility to modulate the drug concentration ratio between the two drugs. Notwithstanding the analysis of the efficacy of this nanoparticle against DTX -sensitive and -resistant HeLa cancer cells, cultured in 2D condition as well as in 3D arrangement, underlined again the occurrence of a synergistic interaction when the two therapeutic agents were co-loaded in the same nanocarrier. Synergism was found in spheroids of DTX -sensitive and -resistant HeLa cells and co-loading of DTX and Ce6 in the same nanoparticle showed higher efficacy in inducing cancer cell mortality compared to NPs loaded with single drugs. These results were reinforced by the significant reduction of tumor spheroid volume due to the release of the external layer of cells induced by the treatment with the co-loaded nanoparticle. The extent of damages observed correlated with the evaluation of cell penetration of keratin NPs that was limited to the more external layers of the tumor model.

Abstract

The combinations of two or more drugs/treatment modalities are increasingly considered very useful tools to increase efficacy and reduce side effects of anticancer therapies. To this aim, photodynamic therapy (PDT) is being widely investigated in combination with established therapeutic modalities including chemotherapy. In this connection, the progresses in the field of nanomedicine led to the production of nanocarriers offering opportunities to ameliorate the control of drug concentration ratios that is a prerequisite for obtaining synergic effects in combination therapy.

In this PhD thesis, PLGA-PEI hyaluronic acid (HA)-targeted nanoparticles (NPs) and keratin NPs were used for the co-delivery to cancer cells *in vitro* of the chemotherapeutic docetaxel (DTX) in combination with the PDT photosensitizers meso-tetraphenyl chlorin disulphonate (TPCS2a) or chlorin e6 (Ce6). To improve tumor selectivity, in the design of PLGA-PEI NPs, HA was selected for the active targeting of CD44 receptor overexpressed by cancer cells. PLGA-PEI NPs co-loaded with DTX and TPCS2a at fixed drug ratios were tested in DTX –sensitive (HeLa, MDA-MB-231 and MCF-7) and –resistant (HeLa-R) cells grown in 2D and 3D cultures. As 3D cultures, spheroids and mammospheres were used as avascular tumor models and cultures enriched of cancer stem cells (CSCs), respectively. In HeLa and MDA-MB-231 monolayers the highest synergism, evaluated by the Combination index (CI), between chemotherapy and PDT was found at DTX/TPCS2a ratio of 1:35 and co-loaded in the same NP (DTX/TPCS2a-NPs). Interestingly, strong synergism of chemotherapy and PDT was found also in the DTX -resistant cells where the dose of chemotherapeutic could be reduced by ~100 times with DTX/TPCS2a-NPs with respect to monotherapy. In spheroids, the DTX/TPCS2a-NPs at 1:35 ratio gave a strong antagonism (CI >1), while, in these 3D tumor cell models, DTX/TPCS2a ratios 1:3 and 1:5 gave synergism. In spheroids generated from DTX –resistant cells the 1:3 concentration ratio was significantly better in terms of synergism as shown by lower CI values. Combination treatments with DTX and TPCS2a co-loaded in the same NP suppressed also sphere formation, due to the presence of CSCs. Different results were obtained with mammospheres generated from MDA-MB-231 and MCF-7 breast cancer cells, very likely because of the different percentages of CSCs in the two culture models. Based on these results, we demonstrated the advantage of using HA-targeted layer-by-layer NPs as carriers of DTX

and TPCS2a to finely control the drug ratio inside the NPs and to precisely deliver the payloads in cancer cells.

Combination of chemotherapy and PDT was also performed co-encapsulating DTX and Ce6 in keratin-based NPs (DTX/Ce6-KNP) prepared by the aggregation method and with a ratio 1.8:1. The cytotoxic effects of combined chemotherapy and PDT, in comparison with monotherapies, and CI analysis were investigated in HeLa and HeLa-R cells in monolayers as well as 3D tumor spheroids. Combination therapy using DTX/Ce6-KNP caused only slight synergism in DTX – sensitive cell monolayers while clear synergism was found in drug resistant cells. Notably, the combination of free drugs caused antagonism. The efficacy of DTX/Ce6-KNP was also assessed in spheroids of DTX -sensitive and -resistant cells where strongest synergism and highest reduction of spheroid volume were observed. In conclusion, these results highlight that: i) the co-delivery of PSs for PDT and chemotherapeutics in NPs allows the control of drug concentration ratios for obtaining synergic interactions; ii) optimized drug ratios determined in 2D cell tumor models do not reproduce synergic interactions in the 3D models and poses the question of the most reliable *in vitro* models for screening combination therapy; iii) combination of chemotherapy and PDT appears particularly useful for treating drug-resistant tumors.

Abbreviations

5-ALA: 5-aminolevulinic acid

Alg: alginate

BCRP: breast cancer resistance protein

BCSCs: breast cancer stem cells

Ce6: chlorin e6

CI: combination index

CNTs: carbon nanotubes

CSCs: cancer stem cells

DOX: doxorubicine

DRI: dose reduction index

DSX: dextran sulfate

DTX: docetaxel

EPR: enhanced permeability and retention effect

Fa: fraction affected

FDA: Food and Drug Administration

HA: hyaluronic acid

HARE: hyaluronic acid receptor for endocytosis

HPD: hematoporphyrin derivative

ICG: indocyanine green

LUVs: large unilamellar vesicles

MB: methylene blue

MDR: multidrug resistance

MEP: median effect principle

MLVs: multilamellar vesicles

MPS: mononuclear phagocytic system

MRI: magnetic resonance imaging

MRP1: multidrug resistance-associated protein 1

MSN: mesoporus silica nanoparticles

MTSs: multicellular tumor spheroids

MWCNTs: multiwalled nanotubes

NPs: nanoparticles

PACA: poly-alkyl-cyanoacrylates

PAMAM: poly(amidoamine)

PCI: photochemical internalization

PCL: poly- ε-caprolactone

PDT: photodynamic therapy

PEG: poltethylene glycol

PEHAM: poly(etherhydroxylamine)

PEI: polyethylenimine

P-glyc: P-glycoprotein

PLA: polylactic acid

PLGA: poly(lactic-co-glycolic acid)

PPI: poly(propylene imine)

PS: photosensitizer

PTX: paclitaxel

RES reticulo-endothelial system

RHAMM: receptor for hyaluronan mediated motility

ROS: reactive oxygen species

SPIONs: superparamagnetic iron oxide nanoparticles

SUVs: small unilamellar vesicles

SWCNTs: single-walled nanotubes

TPCS2a: meso-tetraphenyl chlorin disulphonate

VP-16: etoposide

Introduction

Cancer is one of the most relevant diseases that affect modern society. It can result from different events such as spontaneous genetic mutations, exposure to environmental carcinogens and to a lesser extent has an inherited origin. With the term cancer are included a group of malignant diseases characterized by an abnormal cell growth that can result in tumor cell spread and metastasis[1]. As reported in 2014 by the World Health Organization, 8.2 million people died for cancer in 2012 and this number is destined to reach 22 million in 2035[2]. Conventional therapies include surgery, radiation therapy and chemotherapy. The first two therapeutic modalities are considered local treatments and are currently employed for non-metastatic cancer cure. The intravenous administration of toxic drugs, known as chemotherapy, is instead the choice for treatment of metastatic cancer in which tumor cells diffuse throughout the body far from the site of tumor origin. Unfortunately, these treatments show cytotoxicity and adverse effects that limit their use. Chemotherapy is characterized by an intrinsic drug toxicity of chemotherapeutic agents, the lack of selectivity due to the inability of these molecules to recognize tumor cells among the normal ones, and the development of multidrug resistance (MDR) that is one of the main reasons responsible of treatment failure[3]. To overcome these problems and to obtain an increase of the efficiency of delivery of the therapeutics and subsequent enhancement in tumor selectivity, cancer chemotherapy is realized through the employment of various types of nanostructures. The key role of the nanocarriers would be to improve the selective targeting of cancer cells reducing damages to healthy tissues, as well as to circumvent MDR pumps and to render cells sensitive to chemotherapeutics therefore increasing the therapeutic efficiency[4]. Moreover, recently, the use of nanomaterials is largely exploited for the concomitant delivery of two or more drugs for exploring the potential of treatments based on the combination of two or more chemotherapeutics or modalities of treating cancer. In the following paragraphs are discussed more in depth the concept of combination therapy with particular attention on the development of different nanovehicles able to host drugs with different characteristics in term of superficial charge and solubility. The investigations on these therapeutic modalities, usually performed in the most simple cell monolayer, gives only partial vision of their potential application *in vivo*. In this work, the need of more complex 3D tumor models, which more closely recapitulate the situation of a solid tumor, is highlighted.

Nanotechnology and drug delivery

The fabrication, characterization and use of materials with size between 1 and 100 nm is known as nanotechnology[5]. Nanotechnology applied to medicine is defined nanomedicine. The emerging science of nanotechnology manipulates matter at the nanoscale level, obtaining completely new properties of the materials, with several potential applications in several fields such as engineering, physics, biology and medicine[6]. Nano-sized materials, which have at least one dimension in the range 1-100 nm, are comparable in size with the biological molecules and being at least 100 times smaller than a cell are clearly particularly appealing for medicine applications. A hundred of materials have been investigated to synthetize nanoparticles ranging from biodegradable materials like polymers, proteins, lipids to non-biodegradable materials like gold, iron, silica or semiconductor materials obtaining nanoparticles with completely different characteristic and suitable for applications ranging from cosmetics, additive for industrial food, textile, computer components, regenerative medicine and drug delivery[7]. The use of nanoparticles offers unprecedented opportunity to ameliorate pharmaceutical delivery since the presence of a nanosystem can protect the drug by the recognition and the clearance by the immune system cells and the release can be fine tuned once in the target organs, sometimes bypassing drug resistance mechanisms[8]. A single nanoparticle can transport two or more drugs together with contrasting agents or fluorescent tracers allowing to the so called theragnostic, i.e. the simultaneous diagnosis and therapy using a single nanovehicle. Moreover, the development of multifunctional nanoparticles designed ad hoc based on the characteristics of one specific tumor open a window for a efficacious personalized medicine. The 1950s was revolutionary for drug delivery thanks to the introduction of Spansule®, a novel formulation capsule allowing the slow release of a drug for 12 h[9]. After this first example of controlled-release formulation, from the discovery of liposomes in 1960s, many nanosystems for drug delivery have been studied in the last 50 years and some of them have reached clinical application. Among liposomes the PEGylated Doxil® has been the first approved by the Food and Drug Administration (FDA) in 1995 for the treatment of Kaposi sarcoma[10], followed by the non-PEGylated liposomal doxorubicin Myocet® present in clinics from 2000. More recently, in 2013 the targeted ado-trastuzumab emtansine (DM1) also called Kadcyla® was recognized by FDA for the treatment of HER2-positive breast cancer[11]. Other examples of nanodrugs that entered the market are represented by the albumin-based nanoparticle

Abraxane® and the polymeric micelle Genexol®-PM both loaded with paclitaxel (PTX) and approved for the treatment of breast cancer in 2005 and 2007, respectively[12,13]. Despite several nanomaterials have found application in clinics, this field of research is still continuously expanding. According to Pubmed, 81.000 articles on nanodrug formulations have been published until the end of 2013 and the majority were published after 2010 demonstrating the exponential development of the nanomedical research[14]. Many of the works published in the last years report an improvement of the efficacy of cancer therapy using nanomedicine. A recent review has however underlined that less than 1% of the nanoparticles administered intravenously can reach the tumor site[15] and this demonstrates the need to find new approaches to improve the accumulation in the target tissue of drugs delivered in nanovehicles.

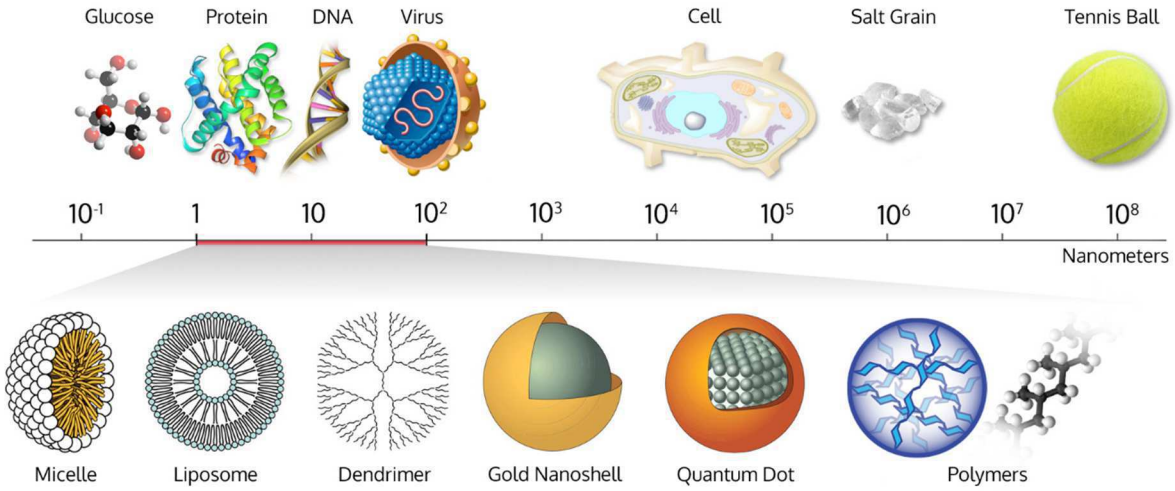

Figure 1: Relative size of nanoparticles (figure from McNeil, 2005[16]).

Passive and active targeting of drug delivery systems

After systemic administration, nanostructures must cross some physical barriers to reach the tumor tissue[17]. They must escape opsonization and recognition by the mononuclear phagocytic system (MPS) in order to circulate for long time and guarantee efficient accumulation in tumors. The superficial coverage with polyethylene glycol (PEG) is currently used to avoid the removal from circulation by phagocytes[18]. Then nanosystems must cross the vascular endothelium. In the normal physiological conditions of the healthy tissues, nanoformulations with size higher than 5-6 nm are unable to cross endothelial cells and reach the extracellular matrix. In the

pathological conditions, characterized instead by the presence of highly permeable and disorganized vasculature, also macromolecules of higher dimension can pass through the fenestrae of the endothelium and preferentially reach the tumor site. In any case, the tumor extracellular matrix represents an additional obstacle. Here the diffusion of therapeutic agents far from blood vessels can be limited because of the high pressure in the tumor interstitial fluid. The concomitant reduction of pH value and oxygen supply due to Warburg effect interfere with the internalization of several therapeutic agents and delivery systems into cancer cells. Nevertheless, there are evidences that nanocarriers can improve efficiency and selectivity of drug accumulation in tumors by exploiting passive and active mechanisms of targeting. Nanoparticles are so appealing for treating cancer mainly because conventional therapies such as surgery, radiation therapy and chemotherapy are only partially effective and chemotherapy in particular is highly cytotoxic due to drug accumulation also in healthy tissues and only at sub-optimal concentrations in tumors. The protection of drugs from recognition and degradation from the cells of the immune system together with the enhancement of specificity of targeting and the controlled release of the payload are some of the reasons that encourage the use of anticancer drug nanoformulations in clinics. It has been reported that the nanometric dimension of NPs allows their preferential accumulation in malignant lesions due to passive mechanism of targeting. In fact nanosystems take advantage of enhanced permeability and retention (EPR) effect, firstly described by Maeda and Matsumura in 1986, and resulting from the high permeability of tumor vasculature and lack of efficient lymphatic drainage[19]. This phenomenon allows the increase of drug accumulation in the tumor by 70-fold[20]. While the vascular system of healthy tissue is characterized by hierarchically organized structure, strong alteration of this organization and the formation of large fenestrations between adjacent endothelial cells are observed in pathological conditions. These gaps with a dimension between 10 and 1000 nm allow the extravasation of nanoparticles containing the drug that is less likely to occur in normal tissues[21]. Usually, after its administration, a therapeutic agent with low molecular weight enters arteries through which circulate in arterioles and then in capillaries. In this way it can be spread homogeneously in the normal tissue. Due to irregular and tortuous organization of blood vessels of the tumors, drugs are distributed heterogeneously. However, in the tumor, the lack of an efficient lymphatic drainage causes the prolonged entrapment of the nanosystems in this region. Taking advantage of these mechanisms, the passive accumulation of NPs in the tumor extracellular matrix can be realized allowing the enhancement of

therapeutic effect. The ability to overcome biological barriers and selectivity of targeting are also dependent on nanoparticle's properties such as size, shape and surface characteristics. Size is one of the most important parameters affecting the cellular uptake. It has been reported that diameter below 200 nm is required for an effective drug carrier[22]. Cabral *et al*. investigated on the uptake efficiency of platinum-loaded nanoparticles with different size (30, 50, 70 and 100 nm) in hyperpermeable and poorly permeable tumors in mice[23]. In the first case, the particle size did not affect distribution, while with low permeable vasculature only particles with a size < 70 nm showed an efficient accumulation in tumors. The shape is another parameter to consider in the design of a nanocarrier. Gold nanoparticles of four different shapes showed different cellular uptake with the higher accumulation of spherical shape and the lower with hollow particles[24]. Surface charge is particularly important to escape the opsonization by plasma components such as serum proteins leading to the recognition and removal of materials identified as foreign by the reticulo-endothelial system (RES). It is well established that the coverage of the delivery system with chemical entities that minimize opsonins association lead to the formation of long circulating nanocarriers. To this purpose, PEG is usually employed as hydrophilic polymer to decorate nanoparticles. Since 1990s the ability of PEGylation to increase circulation time of liposomes has been demonstrated[25]. Despite the modulation of these parameters can be used to exploit passive mechanisms of targeting, this mechanism suffers of some limitations based on the lack of selectivity. An additional strategy to reach target tissues is represented by the so called active targeting. In this case, the selective recognition between ligands associated to nanovehicles surface and a specific receptor over-expressed by cancer cells or endothelium of the tumor vasculature is involved. This strategy has the potential to increase the toxicity of anticancer agents reducing, at the same time, unwanted side effects on healthy tissue. Moreover, its ability to overcome multidrug resistance often developed by cancer cells has been reported[26]. To minimize drug accumulation in healthy tissues, the selection of targeting agents and ligands associated with nanoparticles (NPs) surface has a key role. Molecules used to decorate nanocarriers must be specific for receptors overexpressed by cancer cells but only minimally present in normal cells[27]. Peptides, vitamins, antibody, carbohydrates or other molecules can be used as ligands for receptors over-expressed by neoplastic cells. The use of folate[28], hyaluronic acid (HA)[29], transferrin[30], PSMA aptamer[31], anti-epidermal growth factor antibodies (Cetuximab and Herceptin®)[32] and RGD peptide[33] are reported as useful tools to realize targeted drug delivery. HA is an anionic polysaccharide made

of glucuronic acid and N-acetilglucosamine that represents a major component of the extracellular matrix. Among the many biomedical and pharmaceutical applications, its targeting potential has been extensively investigated due to the specific interaction with receptors over-expressed by cancer cells. In addition to its principal receptor CD44, hyaluronic acid represents a ligand also for RHAMM (receptor for hyaluronan-mediated motility), HARE (hyaluronic acid receptor for endocytosis) and Toll-like receptor-2 and -4[34]. The biocompatible, non-immunogenic and biodegradable nature of HA is an additional property that encourages its employment as targeting agent in drug delivery. The increase in cellular uptake via HA receptor mediated endocytosis has been demonstrated for different nanosystems such as mesoporus silica nanoparticles (MSN) and liposomes[35,36]. HA has been used to decorate the PLGA-PEI layer-by-layer NPs discussed in the papers I and II of this PhD thesis as vehicles to target CD44 over-expressing cancer cells. Despite the advantage of active targeting, only few nanoproducts derived by this technology has entered the clinical practice up to now. The density of the targeting ligand, its orientation and the different methodologies for conjugation of targeting agents are the major parameters that affect NPs blood circulation time and their ability to be specifically internalized by cancer cells[14]. The number of ligand molecules associated to NPs has to be finely tuned. In fact, it was demonstrated that this value has to reach a minimum to obtain a successful binding, but that over a certain ligand density on the NP surface, a reduction of binding affinity together with the occurrence of non-specific interactions with normal cells are observed. This leads to the clearance of the nanoparticles with a reduced treatment efficacy[37].

Drug delivery systems for cancer therapy

One aim when using nanostructures for drug delivery is the successful transport of drug to target tissues without its structural and functional modifications. Therefore, a number of nanostructures for the delivery of drugs able to preserve their pharmacological properties have been developed through the use of new nanomaterials. In this way drugs can reach the tumor site at therapeutic concentration avoiding at the same time their internalization in healthy tissues with the consequent side effects[38]. The properties and applications of the major inorganic and organic drug delivery systems are described in the following paragraphs. Particular attention will be focused on polymer-based nanoparticles because used as drug delivery systems in the

work reported in this PhD thesis (layer-by-layer NPs in paper I and II and keratin NPs in paper III).

Inorganic nanoparticles

Nanoparticles can also be made by different inorganic materials such as metal oxide, metal and silica. Among inorganic NPs, metal oxide, gold NPs and carbon nanotubes have been deeply investigated in recent years. Iron oxide formulations have been mainly used for the treatment of anemia associated with kidney diseases[39]. Others have been investigated as contrasting agents in magnetic resonance imaging (MRI). These are called superparamagnetic iron oxide nanoparticles (SPIONs)[40]. Feridex® and GastroMARK™, after their approval by FDA, have been withdrawn by the market. Feraheme® is still used for the treatment of patients affected by anemia. Due to their interaction with a magnetic field that leads to energy release, SPIONs are used also as agents for hyperthermia. Maier-Hauff *et al.* demonstrated the efficacy of hyperthermia using iron oxide NPs in combination with radiotherapy in the treatment of glioblastoma[41]. Gold NPs show unique optical and magnetic properties that encouraged their employment in many biotechnological applications including drug delivery, tumor imaging and photothermal and photodynamic therapy[42]. Moreover, gold NPs are considered highly biocompatible and with low toxicity. Cui *et al.* demonstrated the efficacy of PEGylated gold NPs for the delivery of DOX[43]. Moreover, with the conjugation of gold NPs via hydrazone bonds, DOX showed efficacy in the treatment of cancer stem cells (CSCs)[44]. Carbon nanotubes (CNTs) are cylindrical structure of carbon atoms with a diameter of 1-4 nm and a length between 1 and 100 μm. The walls of this structure are made of sheets of carbon atoms called graphene. Based on the number of these sheets CNTs can be classified in single-walled nanotubes (SWCNTs) and multiwalled nanotubes (MWCNTs)[4]. Thanks to their optical and mechanical properties these nanocarriers are useful tools for drug delivery, tumor imaging and tissue engineering. Wang *et al*. demonstrated the higher efficacy of SWCNTs conjugated with docetaxel (DTX) and NGR (Asn-Gly-Arg) peptide against PC3 cell line compared to the effect of free docetaxel[45]. Hyaluronan receptor overexpressed by A549 human lung cells has been exploited to target nanotubes conjugated with hyaluronic acid and loaded with doxorubicin (DOX). These strategies increase treatment efficacy compared to the use of free DOX[46]. Despite several types of carbon nanotubes have been investigated and led to promising pre-clinical

results, none has been approved for the treatment of human diseases up to now. The major drawback preventing their translation into clinics is the high cytotoxicity of these nanocarriers. However, the chemical modification of their structure can be used to minimize the toxic effects enhancing the biocompatibility.

Organic nanoparticles

Liposomes

Described for the first time in 1965, liposomes are spherical vesicles made by one or more phospholipidic bilayers surrounding an aqueous core. This peculiar structure allows liposomes to encapsulate both hydrophilic and hydrophobic molecules in the internal core and hydrophobic external membrane respectively[47]. Since the major components of these nanostructures are phospholipids and cholesterol, which are the major components of the cellular membranes, liposomes are highly biocompatible. Liposomes can be synthetized through different methods and based on the dimension and the number of bilayers can be classified in three groups: multilamellar vesicles (MLVs), large unilamellar vesicles (LUVs) and small unilamellar vesicles (SUVs)[48]. The first generation of liposomal formulations showed several drawbacks due to the inability in the retention of drugs and their rapid removal by reticulo-endothelial system. The administration of a pre-dosage of empty liposomes has been proposed to overcome this problem and prolong the circulation time of liposomes loaded with drug administered later[49]. The surface coating with hydrophilic polymers such as PEG characterizes the second generation of liposomes. This polymer shows some advantageous properties which include good solubility in aqueous medium, elevated flexibility of polymer chains and the low toxicity and immunogenicity, essential requirements to consider for materials used for the synthesis of a nanocarrier. PEG chains with a molecular weight lower than 20 KDa are eliminated through renal excretion, between 20 and 50 KDa are mainly eliminated via biliary excretion. Finally, if the size exceeds 50 KDa the removal of PEG occurs only through the biliary way. As reported in literature, PEG chains with a molecular weight between 3 and 5 KDa are the ideal to obtain nanoformulations with prolonged time of circulation in the blood stream[50]. The first liposomal formulation approved in 1995 by FDA was Doxil® for the delivery of doxorubicin. The protection of drugs from recognition and removal by RES leads to a longer half-life compared to free doxorubicin. Moreover, the size of

this nanoformulation allows its extravasation through the endothelial fenestration of tumor vasculature leading to a selective accumulation in tumor site that is not observed when the free drug is administered. This formulation is currently employed for the treatment of Kaposi sarcoma, ovarian and breast cancer[2]. After Doxil® only other four liposomal formulations have been approved for its use in clinics probably because despite several advantages of liposomes, they present also some limitations in particular due to the difficulty to control drug. Thus, recent investigations are directed to the development of carriers in which drug release can be triggered by different stimuli such as light[51], ultrasound[52], pH[53] and temperature[54].

Dendrimers

Dendrimers are branched macromolecules of 10-100 nm with a highly organized tridimensional architecture originating from a central core through a series of polymerization reaction. This synthesis method gives rise to a highly uniform structure in term of shape, molecular weight and polydispersity index. These properties allow them to cross the cancer cell membrane and to escape, at the same time, the removal from the circulation. Several therapeutic agents can be entrapped in the core or conjugated with one of the branches modified with different functional groups[55]. High drug loading ability together with biocompatibility and biodegradability make dendrimers a promising class of anticancer drug carriers. Poly(amidoamine) (PAMAM), poly(propylene imine) (PPI) and poly(etherhydroxylamine) (PEHAM) dendrimers have been used in association with different therapeutic agents in order to improve their delivery efficiency and reducing side effects[56]. As an example Malik *et al.* demonstrated the efficacy of a PEGylated PAMAM dendrimer associated with cisplatin in the treatment of B16F10 solid melanoma tumor[57].

Polymeric micelles

Polymeric micelles are made of self-assembled block copolymers with a hydrophobic core surrounded by the hydrophilic shell that has the function to impart stealth properties to NPs avoiding the interaction with serum proteins leading to the increased time of circulation. This particular structure allows the encapsulation of drugs with different characteristics in the different particle's compartments. This property together with the high stability and the dimension between 1 and 100 nm encouraged their use in clinics in particular as delivery vehicle for poorly water-soluble or hydrophobic drugs[55]. Poly(lactic-co-glycolic acid) NPs

loaded with DOX have been used by Liu *et al.* for the treatment of K562 leukemic cancer cells[58].

Polymeric nanoparticles

Very efficacious nanovectors for obtaining prolonged drug release are polymeric nanoparticles characterized by a colloidal spherical structure made of solid polymers with a size < 1 μm with a matrix in which is encapsulated the drug. They can be made of synthetic materials such as PEG or natural materials as dextran, albumin and collagen[59]. Polymeric NPs are usually classified in two categories: nanocapsules in which the liquid core accommodates the drug and nanospheres in which drug is absorbed on the matrix surface of the NPs[21]. Polylactic acid (PLA), poly-ε-caprolactone (PCL), poly-alkyl-cyanoacrylates (PACA), chitosan and poly(lactic-co-glycolic acid (PLGA) are the most used polymers in the synthesis of these nanocarriers[60]. Among these, PLGA is the most common. Its biodegradation occurs through hydrolysis that lead to the production of lactic acid and glycolic acid accompanied by a very low toxicity. Due to their high biocompatibility and flexibility in chemical modification that allows the functionalization with various types of molecules with different tasks, polymeric nanoformulations have been widely investigated for drug delivery applications. Recently, among polymeric nanoformulations, layer-by-layer nanoparticles have been developed by alternating the deposition of thin layers of cationic and anionic polymers on a solid substrate that forms the core of the nanostructure. The-layer-by layer method takes advantage of electrostatic interactions, hydrogen bonding or other types of interactions and it can be employed in many different applications such as drug and gene delivery and tissue engineering[61]. For cancer treatment, these novel drug delivery platforms are particularly interesting for the possibility to realize the simultaneous encapsulation of drugs with different features in different layers of the vehicle. Every charged layer surrounding the central core can accommodate molecules of different nature. Chemotherapeutic agents, photosensitizers (PS) or molecules affecting gene expression can be carried by these nanosystems. Furthermore, taking advantage of water-based synthesis, different therapeutic agents can be encapsulated without altering their biological and functional properties. Deng *et al.* used a layer-by-layer NP for the simultaneous delivery of doxorubicin and siRNA against triple-negative breast cancer cells[62]. The efficacy of multilayered NPs co-loaded with DTX and the PS TPCS2a for the treatment of DTX –sensitive and –resistant cells will be discussed in this work in paper I and II. Long

circulation time of this type of nanovehicle is ensured by the superficial coverage usually made of negatively charged materials including hyaluronic acid (HA), alginate (Alg) and dextran sulfate (DXS) that impart stealth properties to NPs. These negatively charged polymers are very efficient in imparting stealth properties to the particles enabling them to escape the capture by the phagocytic cells and have been proposed for replacement of the currently used PEG[63]. In conclusion, this method represents a clinically relevant promising approach for future therapeutic innovations. Natural biodegradable polymers like proteins have also been examined as suitable materials for the synthesis of NPs. Being non-toxic, abundant in nature, inexpensive, and biodegradable, they represent a promising tool for drug delivery. Albumin has been widely used. Protein-bound paclitaxel (Abraxane®) has been approved by FDA for the treatment of different malignancies. Moreover, it allows the improvement of drug solubility reducing its toxicity[64]. Other albumin-based nanoparticles are currently in clinical trial[2]. Few works reported instead the use of Keratin, the most abundant non-food protein, for the synthesis of nanoparticles[65,66]. Wool, feathers, hair, horns and nails are excellent source of Keratin. Aluigi *et al.* used Keratin extracted from Merino wool for the synthesis of Ce6 loaded Keratin NPs for the photodynamic treatment of U20S and U87 cancer cells[67]. Keratin can also be functionalized with different drugs simultaneously. The efficacy of the combination between DTX and Ce6 will be discussed in the paper III of this thesis where the two drugs are co-loaded in the same keratin NP.

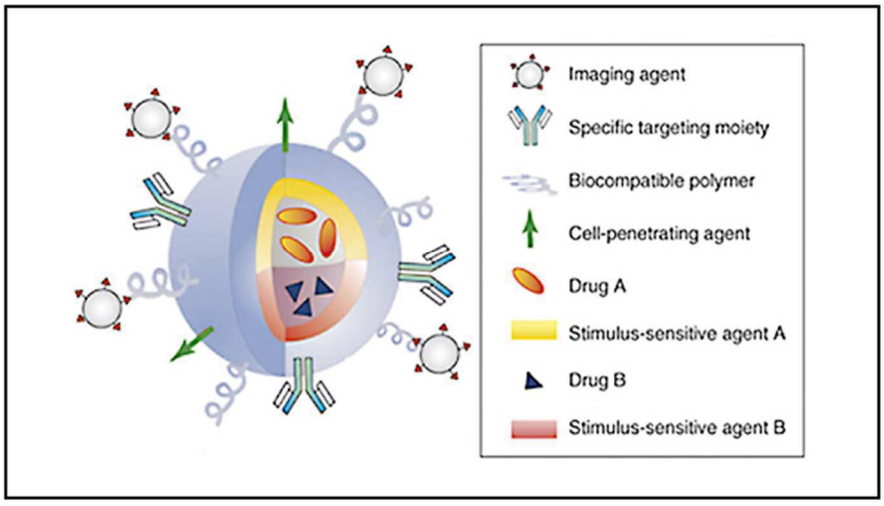

Figure 2: Example of multifunctional nanoparticle for drug delivery (figure from Sanvicens and Marco[7], 2008).

Combination therapy for cancer treatment

Conventional cancer treatments including surgery, chemotherapy and radiation therapy often result in non-efficacious tumor destruction and subsequent cancer recurrence. In particular, chemotherapy is the most common strategy to treat primary and metastatic cancers but the intrinsic toxicity toward normal cells and lack of selectivity of the chemotherapeutic agents represent limitations of its use. Moreover, especially when administered as single agent, chemotherapy often leads to the development of resistance. The major causes of resistance are the over expression of membrane efflux pumps (pump resistance), and the activation of anti-apoptotic factors (non-pump resistance)[3]. Three transporter proteins, belonging to the ATP binding cassette family and including P-glycoprotein (P-glyc), multidrug resistance-associated protein 1 (MRP1) and breast cancer resistance protein (BCRP) are the major resistance pumps over-expressed in different type of cancer cells[68]. Non-pump resistance acts instead avoiding cytochrome c release from the mitochondria because of BCL2 activation and inhibition of apoptosis. To overcome these problems therapeutic modalities are often combined. The simultaneous administration of methotrexate, 6-mercaptopurine, vincristine and prednisone (known as the POMP regimen) represents the first example of combination therapy used by Frei *et al*. for the efficacious treatment of acute leukemia in pediatric patients[69]. After this success, combination therapy has been widely investigated and has now a pivotal role in cancer therapy[70,71]. In recent years different type of combination therapy have been examined including the combination of chemotherapy with radiation therapy, photodynamic therapy, phototermal therapy, gene therapy and anti-angiogenic treatment[72-76]. Furthermore, combining different drugs and/or treatment modalities, acting through different mechanisms and on different cellular targets, gives the possibility to exert cytotoxic activity against different cancer cell sub-population as for example cancer stem cells (CSCs)[77]. Thus, the purpose of combination therapy is to improve cancer treatment efficacy avoiding the increase of systemic toxicity and bypassing at the same time drug resistance developed by cancer cells. This can be realized employing drugs that kill cancer cells by different mechanisms or acting on different cellular target. On these premises, when drugs are combined, each agent can be used at its optimal dose without intolerable unwanted toxicity obtaining a synergistic or additive effect[78]. In this context, the use of nanomaterials offers the opportunity to ameliorate the efficiency of drug delivery. Different therapeutic agents are often internalized by cancer cells through

different manner in term of amount and kinetics due to their different physico-chemical properties which affect the achievement of their correct spatiotemporal distribution. The inability of free drugs to reach the right place at the right time can be overcome through the encapsulation of drugs into efficient drug delivery systems[79]. The ability to exploit passive and active mechanisms of targeting, the protection of drugs that allows the escape from RES and the possibility to encapsulate drugs with low water-solubility, as discussed previously, are the main advantages of nanocarrier-based combination therapy. Moreover, the delivery of one or more drugs in nanocarriers allows maintaining the appropriate fixed drug concentration ratio that is crucial in order to obtain synergistic effects[80]. In fact, while the expectation for a successful combination therapy is the achievement of synergism, the interaction between different drugs can result also in additive or antagonistic effect. Drug ratio has a key role in determining this outcome. The combination of irinotecan/floxuridine, cytarabine/daunorubicin and cisplatin/daunorubicin were investigated in an in vitro study by Mayer and colleagues. They demonstrated that synergistic interaction occurred only when drugs were combined at specific drug ratios, 1:1, 5:1, and 10:1 respectively[81]. Many different nanoformulations including liposomes[82], dendrimers[83], carbon nanotubes[84] and polymeric nanoparticles[85] have been employed to accommodate drugs with different properties. Using nanocarriers drugs can be delivered with different strategies: one drug in free formulation combined with the other in nanoparticle, the two drugs can be delivered in separated nanoparticles or co-delivered in the same vehicle. While the first two strategies allow the sequential administration of the two agents used in combination, the last modality allows the simultaneous delivery of drugs. This last approach is considered the most useful for obtaining a synergistic combination therapy due to fixed concentration ratio of drugs loaded in the carrier[86,87]. The simultaneous tumor accumulation of drugs combined causes the improvement of treatment efficacy and the reduction of off-target toxicity. Despite most of the combination therapy reported in literature involve the co-delivery of two or more therapeutic agents in the same vehicle, recently, the attention has been directed also on the evaluation of the possible advantages offered by the delivery of drugs loaded in separated nanocarriers also known as dual nanomedicine[88]. In fact, co-encapsulation in a single NP shows great benefit when the two drugs must be directed to and act in the same site. On the other hand, dual nanomedicine is a more appropriate approach when the two agents act on separate targets or require a different dose, timing and way of administration. Gao and co-workers used two liposomes loaded with P-glycoprotein inhibitor

and DOX to target blood brain barrier (BBB) and glioma cells respectively[89]. In addition, using this method, possible drug-drug interaction can be avoided.

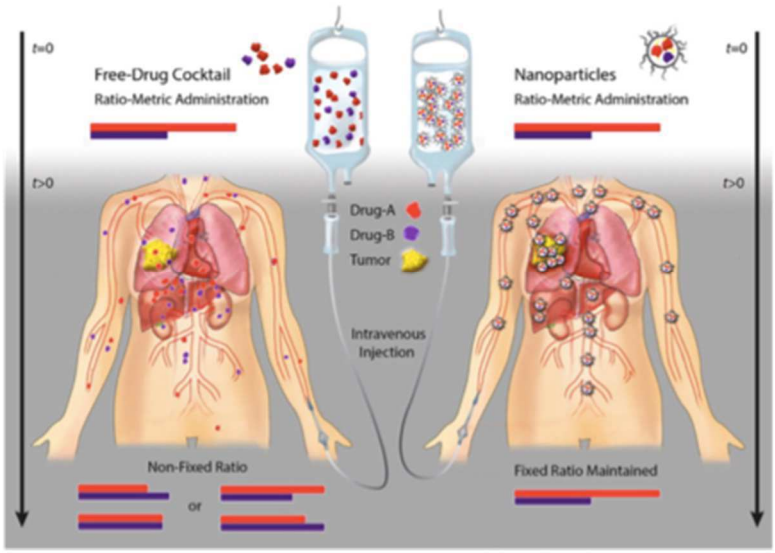

Figure 3: Comparison of pharmacokinetics and biodistribution of ratiometric drug combination delivered in free formulation and in NPs (figure from Zhang *et al*., 2016)[79].

Photodynamic therapy

Chemotherapy can be combined with other therapeutic modalities as for instance photodynamic therapy (PDT). To realize this combination, a chemotherapeutic agent and a photosensitizer for PDT have to be administered. PDT is less invasive and more selective when compared to conventional therapeutic modalities. It is approved for the treatment of several types of solid tumors and non-oncological diseases including macular degeneration, psoriasis and arteriosclerosis[90]. PDT is based on the use of three components: a photosensitizer, molecular oxygen and light, each one not toxic *per se.* After systemic administration and accumulation in the tumor, the PS is activated by visible light of a specific wavelength. Light activation promotes the PS from its ground state to an excited state in which PS reacts with molecular oxygen leading to production of reactive oxygen species (ROS), especially singlet oxygen ($^1O_2$), that cause oxidative damages of several cellular components and consequent cell death[91]. Three mechanisms contribute to tumor destruction by PDT which are equally important for long-term control of tumor progression[92] . The first is represented by the direct death of cancer cells caused by ROS, the second involves tumor vessels occlusion, causing indirect cell death

by oxygen and nutrient deprivation, and the last leads to potentiation of the immune system activation with reduction of cancer cell proliferation. PDT presents a series of advantages when compared to conventional cancer treatments because it is less invasive and treatment can be repeated more than one time if necessary. After administration, the PS is activated only in the tumor by local irradiation and this makes the treatment selective. Furthermore, the localization of PSs in the tumor site is facilitated by the intrinsic tumor microenvironment characteristics such as low extracellular pH value and high cell proliferation and vascularization that allow obtaining the increased of PS accumulation in tumor site compared to healthy tissue[93]. Despite this, some limitations are reported and cutaneous photosensitivity is the most important. Moreover, the hydrophobic nature of most of the PSs limits their solubility in the blood stream reducing their efficacy. Porphyrins, chlorins and phthalocyanins are the most common molecule employed as PDT PSs. The common characteristics of these compounds are a more or less intense absorption in the range 600 - 800 nm and a tetrapyrrolic structure. The red and far red region of the electromagnetic spectrum represent the so called therapeutic window. The use of red light source allows a deep tissue penetration (>1 cm) and at the same time limits light absorption by endogenous chromophores[94]. The ideal PS for PDT applications must possess several properties including the ability to trigger the photochemical reaction and the absence of toxicity without light activation together with the efficient absorption in the therapeutic optical window and high quantum yield of ROS. Moreover, ease of administration and rapid elimination from healthy tissue avoiding skin photosensitivity are required[90]. Many different molecules have entered the clinic as PDT photosensitizers and are usually classified in 1st, 2nd and 3rd generation PSs[95]. Hematoporphyrin derivative (HPD) known also with its commercial name Photofrin® is the first PS approved by FDA for photodynamic therapy. The low selectivity of HPD highlighted the need to develop PS molecules with improved chemical, photophysical and pharmacokinetic properties. Thus, in general, second generation photosensitizers, including mainly chlorins and phthalocyanines exhibit higher chemical purity and singlet oxygen quantum yields and optimized spectroscopic properties with more efficient light absorption in the red and near IR[96]. Among these PSs are included meso-tetraphenyl chlorin disulphonate (TPCS2a) and chlorin e6 (Ce6) used in the work of this thesis. TPCS2a is an amphiphilic chlorin approved for the treatment of cancer with photochemical internalization (PCI) in which the PS accumulates in endocytic vesicles where induces the release of drug macromolecules, after its activation by light[97]. The use of TPCS2a as PDT agent alone is less frequent but some works

are reported[98]. Ce6 is a PS synthesized from chlorophyll and has been employed for the treatment of several tumors including bladder[99] and colon cancers[100] and melanoma[101]. Among the second generation PSs also the so called pro-drugs are included. These are not PSs *per se* but are converted to photoactive molecules by metabolic reactions inside cells. The most common example is represented by 5- aminolevulinic acid (5-ALA)[102]. Attempting to further ameliorate the performances of the PSs, the encapsulation of these molecules in different nanostructures have been investigated to obtain the third generation photosensitizing agents. The encapsulation of the PSs in nanocarriers not only overcomes solubility problems, associated with most of these molecules, improving pharmacokinetics and biodistribution following intravenous administration, but gives also the possibility of co-delivering them with chemotherapeutics for combining PDT with chemotherapy.

Combination of PDT and chemotherapy

As described in a previous paragraph, performing combination therapy, synergistic effect is usually obtained using drugs/treatment modalities with non-overlapping toxicity or acting on different cellular targets. In this context, the use of PDT as adjuvant of chemotherapeutic agents has been widely reported in literature for the treatment of different type of solid tumors[103,104]. Photodynamic therapy can in fact significantly potentiate the toxicity of chemotherapeutic drugs and at the same time chemotherapy can enhance the effect of PDT[105,106]. It was reported that the alteration of the plasma membrane permeability caused by the photodynamic action enhances the uptake of cytotoxic drugs. On the other hand, combining low-dose chemotherapy with photosensitizing agent is possible to increase treatment efficacy compared to the effect elicited by high-dose chemotherapy alone. Nonaka *et al*. demonstrated the improvement of apoptotic response caused by the combination of PDT with cisplatin against lymphoma cancer cells[107]. The combination of etoposide (VP-16) and indocyanine green/PDT (ICG/PDT) was reported by Kasimova *et al.* as an effective strategy for the treatment of A549 human lung cancer cells[108]. Several papers have also been published about the use of nanoparticles as carriers for performing chemo/PDT combination therapy. In addition to the most common liposomes, other types of nanostructures have been investigated for obtaining more selective delivery to cancers of PSs, alone or in combination with other types of drugs, with the aim to increase treatment efficacy while reducing side effects. Nanoparticle-mediated combination therapy between doxorubicin and methylene blue showed efficacy in reducing tumor growth in

mammary adenocarcinoma tumor bearing mice[105]. Zhang and colleagues recently reported the synthesis of a Ce6 loaded RGD-NPs conjugated with DOX. Compared with the effect of the two drugs delivered alone in the free form, this drug delivery platform significantly enhanced the amount of drugs internalized by cancer cells that resulted in higher treatment efficacy[109]. Moreover, chemo/PDT treatment also offers the opportunity to bypass tumor hypoxia that represents one of the main obstacles to cancer therapy. Since oxygen is required to trigger the photodynamic reaction, in hypoxic condition efficacy of PDT is dramatically reduced. Xu and co-workers designed a drug complex that can generate oxygen to meet the demands of PDT process and alleviate the hypoxia producing at the same time a cytotoxic chemotherapeutic for a synergistic cancer therapy. This consisted of a Ce6-PEG-Pt(IV) complex co-assembled with an upconverting nanoparticles. Using this strategy, they demonstrated the *in vivo* complete tumor eradication in four different tumor models[110]. Even though the ideal combo therapy which include the co-delivery of a chemodrug and a PS has yet to be found, all these studies highlighted the promising role of PDT as useful treatment to be used in combination with more conventional therapies. The efficacy of the combination of docetaxel (DTX), a chemotherapeutic currently used for the treatment of breast, head and neck, prostate and non-small cell lung cancers[111] with TPCS2a and Ce6 will be discussed in paper I-II and III respectively.

Drug combination analysis

Dose-effect relationships in biological systems are governed by the principle of the mass-action law. Based on enzyme kinetics, followed the mathematical induction and deduction process, median effect principle (MEP) has been introduced in 1976 by Chou[112]. The mathematical evaluation of several inhibitors of different types and mechanisms of inhibition on enzyme kinetic models led to the so called combination index equation (CI equation)[113]. Grounded on this, the software Compusyn for the quantification of synergism, antagonism, and additivity has been developed by Chou and Talalay to evaluate the type of interaction between two treatments[114]. This relationship is described by the combination index plot (Fa-CI plot) in which CI is plotted *vs*. the fraction of affected cells (Fa). Practically, entering a series of dose and effect for each drug alone and their combinations, the software calculates the CI values for every drug concentration. CI values <1 indicate synergism; CI values ~1, additivity and CI

values >1 antagonism. Combination index can be calculated starting from the median-effect equation that is described by

$$\frac{fa}{fu} = \left(\frac{D}{D_m}\right)^m$$

where fa and fu are the fraction affected and unaffected (1-fa), respectively. D and D_m are the dose of drug and the dose required to inhibit the cell growth by 50%, respectively, while m indicates the shape of the dose-effect curve. The equation $y = ax + b$ where $x = \log(D)$ and $y = \log\left(\frac{fa}{fu}\right)$, m is the slope and D_m is the anti-log of the x-intercept represents the logarithmic form of the previous formula. The plot of x versus y is called median-effect plot.

$$\log\left(\frac{fa}{fu}\right) = mlog(D) - mlog(D_m)$$

Solving these equations the CI, that describes the interaction between two drugs, is calculated as follows:

$$CI = \frac{(D)_1}{(Dx)_1} + \frac{(D)_2}{(Dx)_2}$$

where $(Dx)_1$, $(Dx)_2$, $(D)_1$ and $(D)_2$ are the doses of drug1 and drug2 that inhibit x% alone or in combination respectively. From this last equation, it is also possible to derive the dose-reduction index (DRI) that describes how many times the dose of each drug in a synergistic combination can be reduced at a specific Fa level compared with the dose of each drug alone.

$$DRI = \frac{(Dx)_1}{(D)_1} + \frac{(Dx)_2}{(D)_2}$$

With the calculation of DRI is possible to obtain the reduction of drug toxicity against normal cells maintaining, at the same time, the desired therapeutic effect. The Compusyn software and the method on which it is based are widely used for the evaluation of the possible synergistic interaction in combination therapy[115-117]. Chou and Talalay algorithm has been recognized as one of the main method to assess the efficacy of a combined therapy and, as documented by the number of published papers, many research groups adopted this strategy to address this issue.

In vitro tumor models

Cell monolayers have been the gold standard model for *in vitro* experiments in cell biology. In this model cells are seeded on a plastic surface in culture flasks or dishes. Even now cell monolayers are currently used to investigate cancer cell growth mechanisms as well as cell response elicited by drug treatment. The ease of cell culture and maintenance modalities and the well established viability protocols are the main aspects that justify the widely employment of 2D culture strategy. Nevertheless, adherent cell cultures show several drawbacks. Changes of cell morphology, signaling, gene expression and the lack of interactions with other cells and components of the extracellular matrix, which lead to the loss of cell polarity, make this model far from the natural structure of a solid tumor[118-120]. Moreover, after cell transfer in 2D culture conditions, the gradient of oxygen and nutrient distribution, which characterize a solid tumor *in vivo*, is absent. All together these disadvantages point out the need to use alternative and more adequate *in vitro* tumor models for studying the drug/treatment efficacy whose results should be better reproduced in *in vivo* models in comparison to those obtained in cell monolayers.

3D tumor models

First studies on 3D tumor model have been conducted by Bissel and colleagues on spheroids generated by breast cancer cells[121]. Different types of 3D tumor models have been then developed due to advances in tumor cell biology, tissue engineering and the introduction of new materials. In general, these tridimensional models are classified in transwell-based, spheroid-based, hybrid platforms and tumor-microvessel models[122]. The first one is mainly used to study cell migration and invasion[123], multicellular tumor spheroids (MTSs) have been employed for

drug screening, to investigate the tumor interaction with the immune system and cell proliferation in avascular 3D tumor model[124,125]. The hybrid platforms and tumor-microvessel models combine the simplicity of an *in vitro* model with the interaction with the tumor environment and the vascular component, respectively[126,127]. Many advantages of the use of 3D tumor models have been reported together with some limitations, as for instance the difficulty to develop standardized models, but in any case these 3D tumor cell cultures are considered very useful as intermediate model between 2D cell monolayers and the animal models.

Spheroids

Spheroids are spherical cell aggregates and represent the most simple 3D culture models. After the first studies performed in 1970 by Sutherland *et al.*, multicellular tumor spheroids gradually became very utilized tools to evaluate the efficacy of chemotherapy, radiotherapy, immunotherapy and also PDT[128]. The use of these cell aggregates easily allow the formation of monocultures as well as of co-cultures of different cell types. Contrary to adherent cell monolayers, in spheroids oxygen and nutrient concentration gradient is established which modify cell metabolism and more in general cellular function and response to treatment[121]. For these reasons, spheroids mimic more closely the situation observed in a solid tumor *in vivo* and represent a useful tool to study tumor at their initial stage of development before blood vessels formation. One important observation is that many treatment protocols that exhibit a high efficacy in cell monolayers are ineffective when applied to 3D. As an example, chemotherapeutics often acting on proliferating cells, as the majority of cells cultured in 2D conditions, are highly cytotoxic toward tumor cells in monolayers. By contrast, in spheroids the efficacy can be strongly reduced because of limited drug diffusion into their more internal part and the presence of several quiescent cells, resistant to cytotoxic effect of treatment. In case of treatment failure in 3D models, the use of animals for *in vivo* tests can be avoided. In some cases, instead, drugs that failed to kill tumor cells in monolayers were able to kill cancer cells in spheroids. This is due to the presence of receptors or molecules, overexpressed only in 3D culture conditions, which represent specific targets for therapeutics[129]. It is more and more clear that spheroids reflect the *in vivo* tumor situation in term of antigen expression, pH value, oxygen gradient and proliferating and quiescent cells distribution[130]. Despite the advantages mentioned above, 3D spheroids show some limitations due to longer culture time and the more complex and often difficult to reproduce generation techniques. The use of different cell lines can lead

to the formation of spheroids with specific characteristics. These are classified in tight spheroids, compact aggregates and loose aggregates[131]. Different methods are employed to generate spheroids. Spontaneous aggregation is observed only for limited cell lines as for example MDA-MB-435. In the liquid overlay method, used in this work, cells are seeded in 96 well plate pre-coated with a non-adhesive substrate made of agar that allow cell aggregation. The same principle is used for spinner flask and gyratory rotation system methods in which cells are seeded and maintained in suspension in a liquid medium using a magnetic stirrer. In alternative, hanging drop method can be used. In this case, cells are seeded in a drop placed on the lid of a 96 well plate. Gravity drives cell aggregation at the bottom of the drop and, after some days, the formed spheroid is moved to the well previously coated with agar[132]. The liquid overlay and the hanging drop are the more appropriate techniques to perform studies on single spheroid. The other methods are instead suitable if a study with a high number of samples is required.

Mammospheres

It is well assessed that the failure of conventional anticancer therapies, very often represented by tumor recurrence following temporary disappearance of the disease, is due to several reasons including unwanted toxicity in healthy tissue, that can be dose-limiting, reduced accumulation of drug at the target site and the development of drug resistance. It is also clear that conventional drugs are unable to target and kill differentiated cancer cells and cancer stem cells (CSCs) simultaneously while the eradication of both cell type is necessary in order to avoid relapses[133]. In fact, in a solid tumor, in addition to the more abundant cancer differentiated cell fraction, a small subpopulation of stem-like cancer cells is present. As normal stem cells, these cells are slow proliferating, have the ability of self-renewal and the capacity to produce different phenotypical cell types. They have a crucial role in tumor development and recurrence in various types of tumor including breast cancer because, differently from normal stem cells, their proliferation occurs in an uncontrolled manner. Moreover, the lack of efficacy of conventional therapeutic modalities, in particular chemotherapy, is due to development of several adaptive mechanisms such as activation of DNA repair mechanisms and the expression of membrane efflux pumps and anti-apoptotic factors leading to high resistance[134,135]. CSCs were first identified in leukemia but subsequently were isolated also in several solid tumors. Al-Hajj and colleagues isolated and characterized for the first time cancer stem cells in breast cancer

(BCSCs)[136]. In a tumor mass CSCs represent generally a small percentage (0.05-1%) of the entire population[137]. However, culturing tumor cells, as breast cancer cells, under non-adherent non-differentiating conditions, is a useful strategy to isolate and enrich cancer stem cell population and lead to the formation of the so called mammospheres[138]. The sphere-forming assay is the most simple method to assess the presence and estimate the percentage of CSC in a cell population and allows evaluating the efficacy of drugs and/or treatment modalities with the ability to kill also CSCs in addition to other cancer cell types. Sphere forming cells are characterized by $CD44^{+}/CD24^{-/low}$ surface receptor profile that is exploited for the isolation of cancer stem cells by cell sorting. After the isolation of breast cancer cells and the development of well established assays to produce tumor spheres, several works have been performed to evaluate the efficacy of drugs administered alone or in combination to kill stem cell subpopulation. In particular, nanomedicine offers the possibility to ameliorate drug delivery of chemotherapeutics, photosensitizers for PDT or their combination also to target CSCs. MDA-MB-231, BT-474 and MCF-7 mammospheres were efficiently treated with doxorubicin loaded gold nanoparticles[44]. The encapsulation of methylene blue (MB) in a polymer-surfactant nanoparticles allows to kill MCF-7 mammospheres in normoxic as well as hypoxic conditions[139]. Wang *et al.* used hyaluronan-decorated fullerene-silica nanoparticles co-loaded with doxorubicin and indocyanine green (ICG) to target CSCs taking advantage of CD44 overexpression. They demonstrated the great potential of this multifunctional nanocarrier to perform combination therapy[140].

Aim of the thesis

The overall aim of the thesis was the *in vitro* evaluation of the cytotoxicity effects elicited by the combinatorial treatment between chemotherapy with docetaxel (DTX) and photodynamic therapy (PDT) with two different photosensitizers and the assessment that nanocarriers loaded with the chemotherapeutic drug and the PS for PDT are useful for increasing the synergic interaction of the two modalities of treating cancer. Thus, in the three papers forming the body of this thesis, the potentiality and limits of using PLGA-PEI layer-by-layer NPs (Paper I, II) and keratin NPs (Paper III) as nanocarriers for DTX in combination with meso-tetraphenyl chlorin disulphonate (TPCS2a) and chlorin e6 (Ce6), respectively, are discussed.

More specific aims of the studies on the efficacy of the combination of chemo- and photodynamic therapy were:

- evaluation of the NPs colloidal properties, stability and analysis of the kinetics of drug release from the nanoparticle (Paper I, II, III)

- evaluation of the cytotoxicity and ability to induce synergistic effects with the two drugs co-delivered in the same NPs compared to the effects of free drugs delivered in standard solvent or encapsulated in separate NPs (Paper I, II, III)

- determination of uptake and intracellular localization of PSs delivered by NPs compared to free PSs delivered in standard solvent (Paper I, II, III)

- analysis of cell death mechanisms elicited by monotherapies and combination therapies (Paper I)

- assessment of the ability of combination therapy to target and kill cancer stem cells (CSCs) using two drugs-loaded hyaluronic acid targeted nanoparticles (Paper II)

- evaluation of cell damages elicited by treatments in 3D tumor models using bright field microscopy (Paper II, III) and measure of tumor volume reduction (Paper III)

- assessment and comparison of optimal drug concentration ratios for synergism determined in 2D and 3D tumor cell cultures and evaluation of the most reliable *in vitro* model for identifying treatment condition that can be translated to *in vivo* models.

Paper I

molecular pharmaceutics

Article

Cite This: Mol. Pharmaceutics XXXX, XXX, XXX−XXX

pubs.acs.org/molecularpharmaceutics

Co-delivery of Docetaxel and Disulfonate Tetraphenyl Chlorin in One Nanoparticle Produces Strong Synergism between Chemo- and Photodynamic Therapy in Drug-Sensitive and -Resistant Cancer Cells

Elisa Gaio,[†] Claudia Conte,[‡] Diletta Esposito,[‡] Giovanni Miotto,[§] Fabiana Quaglia,[‡] Francesca Moret,*[,†] and Elena Reddi[†]

[†]Cell Biology Unit, Department of Biology, University of Padova, Padova, Italy

[‡]Drug Delivery Laboratory, Department of Pharmacy, University of Napoli Federico II, Napoli, Italy

[§]Department of Molecular Medicine, University of Padova, Padova, Italy

Supporting Information

ABSTRACT: Cancer therapies based on the combinations of different drugs and/or treatment modalities are emerging as important strategies for increasing efficacy and cure, decreasing unwanted toxicity, and overcoming drug resistance, provided that optimized drug concentration ratios are delivered into the target tissue. To these purposes, delivery systems such as nanoparticles (NPs) offer the unique opportunity to finely tune the drug loading and the release rate of drug combinations in the target tissues. Here, we propose double-layered polymeric NPs for the delivery of the chemotherapeutic docetaxel (DTX) and the photosensitizer disulfonate tetraphenyl chlorin (TPCS2a) coated with hyaluronic acid (HA), which allows cell targeting via CD44 receptors. The simultaneous delivery of the two drugs aims at killing DTX-sensitive (HeLa-P, MDA-MB-231) and DTX-resistant (HeLa-R) cancer cells by combining chemotherapy and photodynamic therapy (PDT). Using the Chou and Talalay method that analyses drug interactions and calculates combination index (CI) using the median-effect principle, we compared the efficiency of DTX chemotherapy combined with TPCS2a-PDT for drugs delivered in the standard solvents, coloaded in the same NP (DTX/TPCS2a-NP) or loaded in separate NPs (DTX-NPs + TPCS2a-NPs). Along with the drug interaction studies, we gained insight into cell death mechanisms after combo-therapy and into the extent of TPCS2a intracellular uptake and localization. In all cell lines considered, the analysis of the viability data revealed synergistic drug/treatment interaction especially when DTX and TPCS2a were delivered to cells coloaded in the same NPs despite the reduced PS uptake measured in the presence of the delivery systems. In fact, while the combinations of the free drugs or drugs in separate NPs gave slight synergism (CI < 1) only at doses killing more than 50% of the cells, the combination of drugs in one NPs gave high synergism also at doses killing 10−20% of the cells. Furthermore, the DTX dose in the combination DTX/TPCS2a-NPs could be reduced by ∼2.6- and 10.7-fold in HeLa-P and MDA-MB-231, respectively. Importantly, drug codelivery in NPs was very efficient in inducing cell mortality also in DTX resistant HeLa-R cells overexpressing P-glycoprotein 1 in which the dose of the chemotherapeutic can be reduced by more than 100 times using DTX/TPCS2a-NPs. Overall, our data demonstrate that the protocol for the preparation of HA-targeted double layer polymeric NPs allows to control the concentration ratio of coloaded drugs and the delivery of the transported drugs for obtaining a highly synergistic interaction combining DTX-chemotherapy and TPCS2a-PDT.

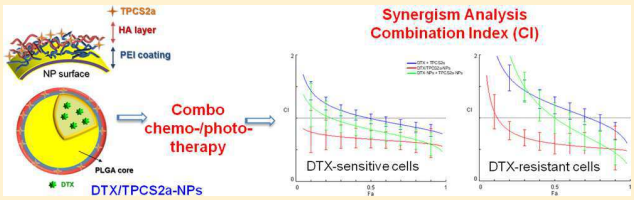

KEYWORDS: *combination therapy, combination index, nanoparticles, docetaxel, disulfonate tetraphenyl chlorin, photodynamic therapy*

INTRODUCTION

It is widely recognized that the treatments of aggressive tumors by one single modality, as for instance surgery, chemotherapy, radiotherapy, or, more recently, photodynamic and photothermal therapy, are not sufficient to completely eradicate and cure the disease.[1,2] Based on these observations, combinations of different chemotherapeutics and/or treatment modalities are increasingly considered as necessary strategies to improve the rate of tumor cure while decreasing systemic toxicity and circumventing drug-induced resistance.[3−6] Recently, the combination of chemotherapy and photodynamic therapy (PDT) is being intensively investigated for the treatment of various types of solid tumors,[7,8] being PDT minimally invasive

Received: June 8, 2018
Revised: July 31, 2018
Accepted: August 27, 2018
Published: August 27, 2018

ACS Publications © XXXX American Chemical Society

DOI: 10.1021/acs.molpharmaceut.8b00597
Mol. Pharmaceutics XXXX, XXX, XXX−XXX

Downloaded via UNIV OF PADOVA on September 28, 2018 at 12:50:50 (UTC).
See https://pubs.acs.org/sharingguidelines for options on how to legitimately share published articles.

and with reduced side effects compared with most of conventional therapies.[9] PDT induces tumor ablation through the production of reactive oxygen species (ROS), after the activation of a light-activated photosensitizer (PS). This treatment is *per se* selective because only the PS previously taken up by the tumor is activated by the local irradiation with light of wavelength absorbed by the PS.[10] PDT elicits a complex response in tumors, involving vascular damage, direct cancer cell killing, and the induction of innate and adaptive immune responses, whose relative contributions depend on the PDT treatment regimen.[11] The combination with chemotherapy can maximize the effect of PDT, and in turn, PDT can potentiate the drug that can be administered at lower doses without losing treatment efficacy.[12,13] The importance of delivering drugs at optimal concentration ratios for producing synergistic interactions has been repeatedly underlined for conventional chemotherapeutics, but this appears important also for the combination of chemotherapy and PDT. In fact, chemotherapeutics and PSs, because of their different physicochemical properties, exhibit different kinetics and efficiency of uptake in cancer cells both *in vitro* and *in vivo*. These differences highly complicate and make unlikely that the free drug combinations reach the target site at optimal ratios guaranteeing synergistic effects. However, the use of multifunctional nanocarriers that accommodate in their structure more than one drug at a fixed ratio appears a unique opportunity to overcome this problem.[14−18]

In the present work, we decided to investigate on the possibility to obtain synergistic cancer cells killing through the combination of docetaxel (DTX)-based chemotherapy with a PDT treatment based on the disulfonated tetraphenyl chlorin (TPCS2a) and to assess whether codelivery of the two molecules entrapped in a single nanoparticle (NP) could increase the synergism between the two treatment modalities. DTX is largely used for the treatments of several solid tumors including nonsmall cell lung, prostate, head and neck, and breast cancers.[19] However, its low water solubility heavily limits bioavailability that together with interpatient variability of pharmacokinetics and general toxicity suggests the need of DTX formulations providing more specific drug accumulation and cytotoxicity in cancer cells. Along this line, NP-based formulations of DTX are being investigated.[20−22] TPCS2a (Fimaporfin) is an amphiphilic negatively charged chlorin utilized in the photochemical internalization (PCI) technology for the light-triggered cytosolic delivery of endocytosed drugs/toxins that are unable to penetrate the cell plasma membrane.[23−25] Notably, the first phase 1 clinical trial in humans for the PCI of bleomycin showed that TPCS2a is safe and tolerable by the patients up to 1 mg/kg.[26] Here we explore the possibility of using suboptimal doses of DTX together with low doses of TPCS2a-PDT for efficient killing of DTX-sensitive and -resistant cells *in vitro*. A comparative study is carried out codelivering the two drugs in standard solvent formulations (free drugs) or loaded in double-layer nanoparticles (NPs) with a core−shell organization and ability to entrap and retain drugs of different solubility as already reported by us.[27] The hydrophobic core made of poly(lactide-*co*-glycolide) (PLGA) efficiently accommodate DTX and is surrounded by a layer of the cationic polymer polyethylenimine (PEI) that retains negatively charged PSs through electrostatic interactions and an external layer of hyaluronan (HA). Furthermore, adsorbed HA acts as a targeting coating since it binds specific receptors including CD44, RHAMM (receptor for hyaluronan-mediated motility), HARE (HA receptor for endocytosis), and Toll-like receptors-2 and -4 that are overexpressed by various solid tumors such as breast, cervical, lungs, gastric, pancreatic, and melanomas.[28,29] Thus, HA receptor-positive cell lines MDA-MB-231 and HeLa (DTX-sensitive as well as resistant) were used to assess (i) the occurrence of synergism when using DTX/TPCS2a-NPs vs free drugs by applying the method of Chou and Talalay[30] for the calculation of combination index (CI), (ii) the mechanisms of cell death after single or combined therapy, and (iii) the extent of intracellular uptake and localization of the PS free or loaded in NPs.

MATERIALS AND METHODS

Materials. Meso-tetraphenyl chlorin disulfonate (TPCS2a) was provided by PCI Biotech AS (Oslo, Norway). DTX was purchased from LC Laboratories (USA). TPCS2a and DTX solutions were prepared by dissolving known amounts of powder in ethanol and DMSO, respectively. Poly(D,L-lactide-*co*-glycolide) (PLGA) (50:50 Resomer RG 502H inherent viscosity 0.16−0.24 dL/g) was purchased from Boehringer Ingelheim (Ingelheim, Germany). PEI (MW = 10−25 kDa branched) and Poloxamer 188 (Pluronic F68) were purchased from Sigma-Aldrich. Acetonitrile and acetone were purchased from Carlo Erba Reagenti (Milan, Italy). HA (MW < 10 kDa) was a kind gift of Magaldi Life S.r.l. Dulbecco's modified Eagle's medium (DMEM) and fetal bovine serum (FBS) were purchased from Gibco Life Technologies (Milan, Italy). LysoTracker Green DND-26 was from Molecular Probes (Life Technologies). The CellTiter96 Aqueous One Solution Cell proliferation Assay (MTS) and the Colorimetric and CytoTox 96 Non-Radioactive Cytotoxicity Assay were from Promega Co. (Madison, USA). The Annexin V-FITC Apoptosis Detection Kit was from eBioscience (Wien, Austria). Ultrapure water was used throughout the study.

Preparation of NPs. DTX/TPCS2a-NPs were prepared by a layer-by-layer deposition method as previously described.[27] Briefly, DTX-loaded NPs were prepared by solvent diffusion of an organic phase (10 mg of PLGA and 7.5 μg of DTX in 2 mL of acetone) in an aqueous phase (4 mL of water with Pluronic F68 0.1%). After solvent evaporation, the dispersion was split into four Eppendorf tubes and centrifuged at 5000*g* for 15 min. NPs were first coated with 125 μL of a PEI water solution (1 mg/mL), centrifuged at 2800*g* for 15 min, and then 25 μL of a TPCS2a water solution (0.4 mg/mL) were added in order to reach a DTX/TPCS2a weight ratio 1:35. Thereafter, NPs were finally coated with a second layer of HA through the addition of 100 μL of a HA water solution (1 mg/mL) to each Eppendorf. The interval between each addition was kept constant at 15 min. NPs were finally freeze-dried for 24 h. Recovery yield of the production process was evaluated on an aliquot of NPs by weighting the solid residue after freeze-drying. Results are expressed as the ratio of the actual NP weight to the theoretical polymer + drug weight × 100. Control, unloaded NPs, DTX-loaded NPs, and TPCS2a-loaded NPs were prepared.

Characterization of NPs. Hydrodynamic diameter, polydispersity index (PI), and zeta potential of NPs after each preparation step were determined on a Zetasizer Nano Z (Malvern Instruments Ltd., UK). UV/vis absorption and fluorescence emission spectra of DTX/TPCS2a-NPs dispersed in water compared to the free TPCS2a (5 μg/mL) were recorded with a UV spectrophotometer (UV 1800, Shimadzu,

DOI: 10.1021/acs.molpharmaceut.8b00597
Mol. Pharmaceutics XXXX, XXX, XXX−XXX

Japan) and a RF-6000 spectrofluorophotometer (Shimadzu), respectively. All measurements were performed in a thermostated quartz cuvette (1 cm path length, 1 mL capacity). Emission fluorescence spectra were collected after excitation at 414 nm. Stability of NPs in water at room temperature was monitored until 10 days, in terms of size, zeta potential, and TPCS2a spectroscopic properties.

DTX loading inside NPs was assessed by placing 0.5 mg of freeze-dried NPs in 500 μL of DCM and overnight stirring until a film was formed at the bottom of the vial. Thereafter, 500 μL of water and 500 μL of acetonitrile were added, and the sample was filtered through a 0.45 μm filter (RC, Chemtek, Italy). DTX was analyzed by HPLC on a Shimadzu apparatus equipped with a LC-10ADvp pump, a SIL-10ADvp auto-injector, a SPD-10Avp UV−Vis detector, and a C-R6 integrator. The analysis was performed on a Juppiter 5 μm, C18 column (250 × 4.6 mm, 300 Å). The mobile phase was a 45:55 (v/v) mixture of water with TFA 0.1% and acetonitrile that was pumped at a flow rate of 1 mL/min. The UV detector was set at 227 nm. A calibration curve for DTX in ethanol was constructed in the concentration range 0.980−196 μg/mL. The limits of quantification (LOQ) and detection (LOD) were 1.29 and 0.39 μg/mL, respectively. TPCS2a loading inside NPs was evaluated by measuring its concentration, by UV spectrophotometry, in the supernatant after NP centrifugation at 17000*g* for 15 min. A calibration curve for TPCS2a in water was plotted at 414 nm (UV 1800, Shimadzu, Japan) in the concentration range 0.05−5 μg/mL.

The release of TPCS2a was followed at 37 °C on 1.25 mg of NPs dispersed in 1 mL of DMEM added with 10% FBS. At predetermined time intervals, the sample was centrifuged at 17000*g* for 20 min. TPCS2a release was assessed in the supernatant by spectrophotometry at maximum wavelength of 414 nm. A TPCS2a calibration curve in the range 0.05−5 μg/mL was constructed in the release medium.

Cell Lines. MDA-MB-231 human breast and HeLa human cervix cancer cells were purchased from American Type Tissue Culture Collection (ATCC, Rockville, USA). The cells were grown in DMEM with Glutamax supplemented with 10% heat-inactivated FBS, 100 U/mL streptomycin, and 100 μg/mL penicillin G (all from Life Technologies) and maintained at 37 °C under a humidified atmosphere containing 5% CO_2. A DTX-resistant HeLa cell line (HeLa-R) was obtained by cultivating HeLa parental (HeLa-P) cells in DMEM supplemented with 10% of FBS and intermittent low and increasing DTX concentrations (0.002−0.008 μg/mL) for seven months. Once a week, the cells were treated for 48 h with DTX; afterward, the chemotherapeutic was removed, and the cells were recovered and kept in DTX-free medium until the next treatment. The DTX concentration was increased every 4 weeks. The effective resistance to DTX of the HeLa-R cells was routinely measured, by the MTS assay, in terms of DTX cytotoxicity compared to HeLa-P cells.

Cytotoxicity Assays. HeLa-P, HeLa-R (6000 cells/well), and MDA-MB-231 (8000 cells/well) cells were seeded in 96-well plates in DMEM supplemented with 10% FBS. After 24 h of cell growth, the medium was replaced with fresh medium containing increasing concentrations of TPCS2a (0.05−2 μg/mL) or DTX (0.0014−0.057 μg/mL) or their combination delivered in the standard solvents or entrapped in NPs (DTX/TPCS2a ratio 1:35, w/w). Control experiments were performed in order to exclude unwanted cytotoxicity of corresponding doses of unloaded NPs (10−100 μg/mL). Cell viability was measured with the MTS assay after 24 h of drug incubation in the dark (time point 24 h) as well as after an additional 24 h in which the cells were kept in drug-free medium (time point 24 + 24 h). Instead, for phototoxicity experiments, cells were seeded as described above and treated in the dark for 24 h with TPCS2a alone or combined with DTX and delivered in the standard solvent (TPCS2a + DTX) or entrapped in the same (DTX/TPCS2a-NPs) or in separated NPs (e.g., TPCS2a-NPs + DTX-NPs). At the end of the dark incubation, cells were washed twice with PBS containing Ca^{2+} and Mg^{2+} and irradiated in PBS with a total light fluence of 1 J/cm^2 of red light (600−800 nm; irradiation time 67 s) emitted from a Waldmann PDT 1200 lamp (Waldmann Medizintechnik, Germany). The power density was 15 mW/cm^2 as measured with the radiometer IL 1700 (International Light, Newburyport, USA). Immediately after irradiation, the cells were brought back to the incubator after the replacement of PBS with fresh medium. Cell viability was measured using the MTS test after additional 24 h (phototoxicity; time point 24 + 24 h). In all cases, for the MTS assay, the cell medium was replaced with 100 μL of serum-free DMEM and 20 μL of CellTiter 96 Reagent, and the samples were incubated for 40−60 min at 37 °C in the dark. Afterward, the absorbance at 492 nm was measured with a Multiskan Go plate reader (Thermo Fisher Scientific, Waltham, USA), and the viability of treated cells was expressed as percentage of the absorbance of control cells that was taken as 100% viability.

Median-Effect Analysis and Determination of Combination Index (CI). In order to assess if the interaction of the two treatments resulted in a synergic effect, CI values were calculated from experimental data obtained from the cytotoxicity experiments using the CompuSyn software.[31] The software is based on Chou and Talalay method, which analyzes drug interactions and calculates CI using the median-effect principle.[32] The occurrence of drug synergisms for the selected drug ratio was determined by plotting the CI vs the fraction of affected cells (Fa). CI values < 1 indicate synergism; CI values ≈ 1, additivity; and CI values > 1, antagonism. The median-effect equation, derived from mass-action law principle

$$\frac{\mathrm{Fa}}{\mathrm{Fu}} = \left(\frac{D}{\mathrm{Dm}}\right)^m$$

describes dose−effect relationships where Fa and Fu are the fraction affected and unaffected (1 − Fa), respectively. D and Dm are the dose of drug and the dose required to inhibit the cell growth by 50%, respectively, while m indicates the shape of the dose−effect curve. The logarithmic conversion of this equation can be described in the form of $y = ax + b$ where $x = \log(D)$ and $y = \log\left(\frac{\mathrm{Fa}}{\mathrm{Fu}}\right)$ is the slope and D_m is the antilog of the x-intercept. The plot of x versus y is called the median-effect plot.

$$\log\left(\frac{\mathrm{Fa}}{\mathrm{FU}}\right) = m\log(D) - m\log(\mathrm{Dm})$$

Based on these equations we can evaluate the CI that describes the interaction between two drugs with the following formula:

$$\mathrm{CI} = \frac{(D)_1}{(Dx)_1} + \frac{(D)_2}{(Dx)_2}$$

DOI: 10.1021/acs.molpharmaceut.8b00597
Mol. Pharmaceutics XXXX, XXX, XXX−XXX

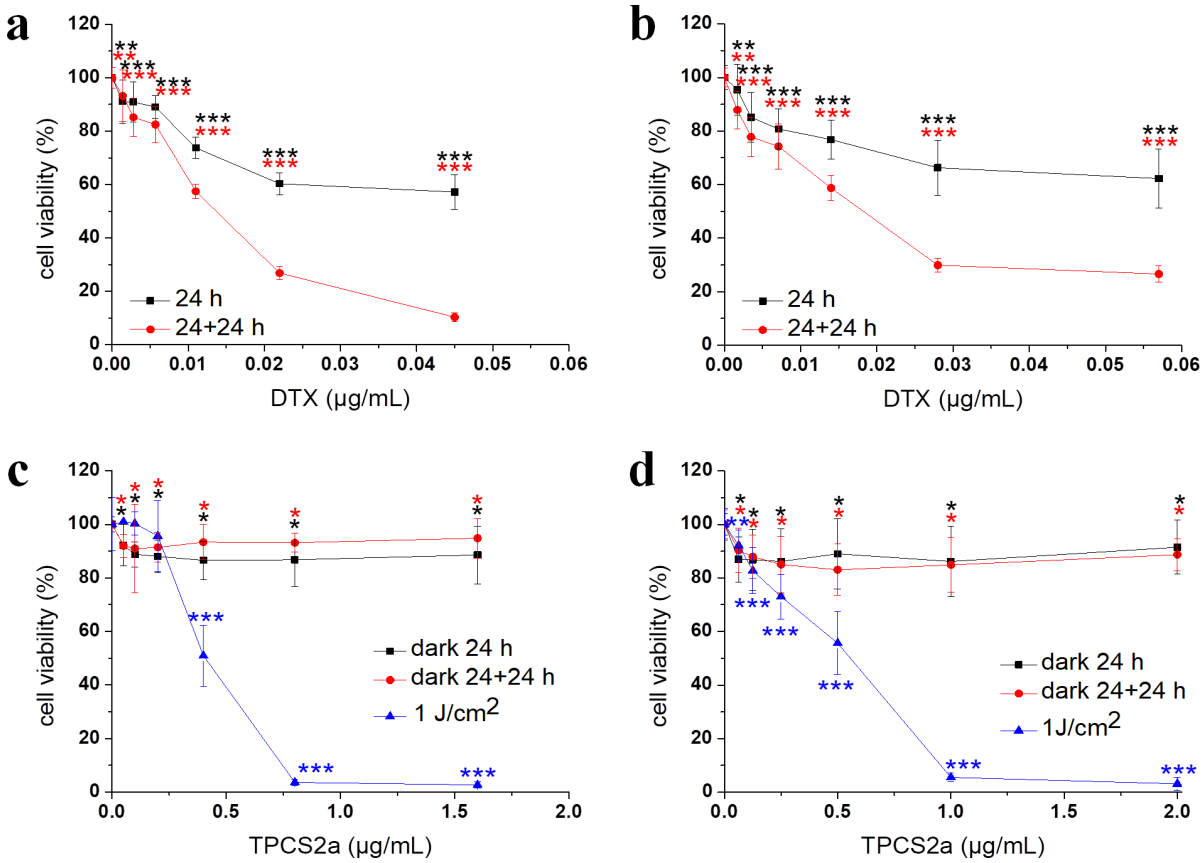

Figure 1. Viability of HeLa (a,c) and MDA-MB-231 (b,d) cells exposed to DTX (a,b) or TPCS2a (c,d) in dark and light conditions. Cytotoxicity of DTX was measured after 24 h of incubation with the drug (24 h) and after additional 24 h in drug-free medium (24 + 24 h). Cytotoxicity of TPCS2a was measured in the dark at 24 h and 24 + 24 h as well as after exposure to 1 J/cm^2 of red light. Data are expressed as mean percentage ± SD of at least three independent experiments, carried out in triplicate. *p < 0.05; **p < 0.01; ***p < 0.001 significantly different from control cells (Student's t test).

where $(Dx)_1$, $(Dx)_2$, $(D)_1$, and $(D)_2$ are the doses of drug1 and drug2 that inhibit x% alone or in combination, respectively. From this equation, it is also possible to derive the dose-reduction index (DRI) that describes how many folds the dose of each drug can be reduced in a synergistic combination compared with the dose of each drug alone.

$$\mathrm{DRI} = \frac{(Dx)_1}{(D)_1} + \frac{(Dx)_2}{(D)_2}$$

TPCS2a Uptake and Intracellular Localization Studies. For TPCS2a uptake measurement by flow cytometry, 5 × 10^4 HeLa and MDA-MB-231 cells were seeded in 24-well plates, and after 24 h of growth, the cells were incubated with fresh medium containing increasing concentrations of TPCS2a alone or in combination with DTX, delivered in the standard solvents as well as entrapped in NPs. After 24 h of drug incubation, the treatment solutions were removed, and the cells were washed with Versene solution, detached from the plates with trypsin that was neutralized with the addition of FBS. Cells were centrifuged and resuspended in Versene solution before measuring TPCS2a fluorescence using a BD FACSCanto II (Becton Dickinson, San Jose, USA) flow cytometer. The blue laser at 488 nm was used as the excitation source, and the TPCS2a fluorescence was detected at wavelengths longer than 670 nm (PerCP channel). Ten thousand events/samples were acquired and analyzed with the FACSDiva Software. For intracellular localization studies, 5 × 10^4 HeLa and 8 × 10^4 MDA-MB-231 cells were seeded in 35 mm cell imaging dishes (Eppendorf AG, Hamburg, Germany). After 24 h of growth, cells were incubated at 37 °C for additional 24 h with fresh medium containing 0.15 μg/mL TPCS2a in the standard solvent or in NPs. Fifteen minutes before completing the incubation, 100 nM LysoTracker Green DND-26, used as a marker for lysosomes, was added to the cells. Cells were then washed with HBSS and observed with a Nikon inverted fluorescence microscope equipped with a led excitation source. TPCS2a was detected with a 410/30 nm (excitation) and 630/90 nm (emission) filter, while for LysoTracker Green DND-26 we used 474/23 nm (excitation) and 527/42 (emission). The images were obtained with a 60× water immersion objective and analyzed with ImageJ software for the colocalization study.

Annexin-V/PI Staining. Cells (6 × 10^5) were seeded in 60 mm tissue culture dishes and, after 24 h of growth, were treated with DTX, TPCS2a, or DTX/TPCS2a delivered in the standard solvents or in NPs. At the end of the incubation time, cells were detached from the plates with trypsin, and 2 × 10^5 cells/sample were collected in flow cytometry tubes, washed with PBS and centrifuged. Annexin V, previously diluted in binding buffer, was added to each tube, and the cells were incubated in the dark for 10 min at room temperature, washed with the binding buffer, and then propidium iodide (20 μg/mL) was added before the flow cytometry analysis.

DOI: 10.1021/acs.molpharmaceut.8b00597
Mol. Pharmaceutics XXXX, XXX, XXX−XXX

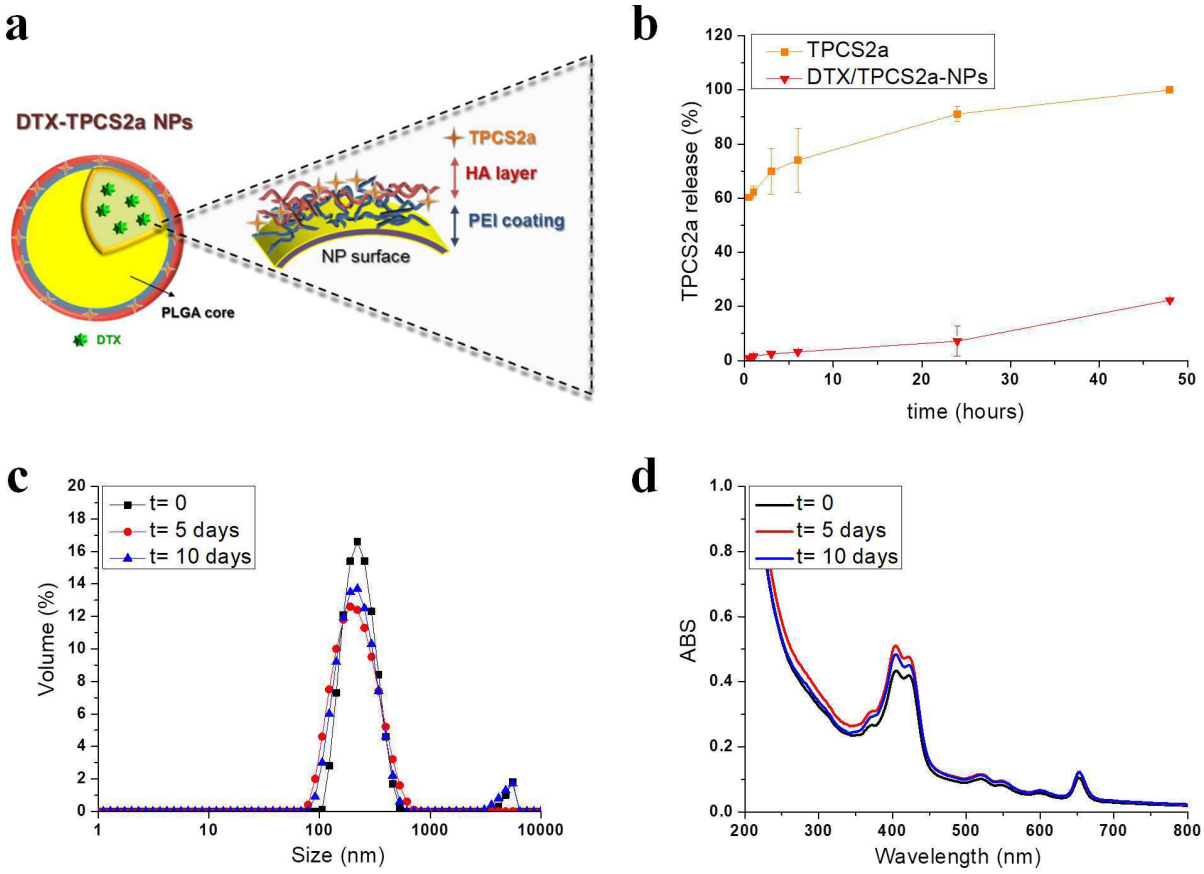

Figure 2. Overall properties of DTX/TPCS2a-NPs. (a) Schematic representation of NPs structure where DTX is contained in the core, while TPCS2a is embedded in the PEI/HA external coating; (b) release profile of TPCS2a from DTX/TPCS2a-NPs in DMEM with 10% FBS at 37 °C. Data are expressed as mean percentage ± SD of three independent experiments; (c) distribution curves and (d) UV spectra of DTX/TPCS2a-NPs in water kept at room temperature for 10 days.

Lactate Dehydrogenase (LDH) Release Assay. The release of LDH in the cell culture medium of HeLa and MDA-MB-231 cells was measured using the colorimetric CytoTox 96 Non-Radioactive Cytotoxicity Assay (Promega Co, Madison, WI, USA) according to the manufacturer's instructions. The assay quantitatively measures LDH, a small cytosolic enzyme, that is released in the culture medium of cells having damaged plasma membrane or lysis. The quantity of released LDH is proportional to the extent of cell damage/death. The activities of the total cellular LDH content and of that released in the cell culture medium were measured to calculate the percentage of LDH released during the exposure of the cells to the different drug formulations and treatments.

Statistical Analysis. The Primer software for biostatistics (McGraw-Hill, Columbus, USA) was used for statistical analysis of the data. The data are expressed as means ± standard deviations (SD) for at least three independent experiments. The difference between groups was evaluated using the Student's *t*-test and considered significant for $p < 0.05$.

■ RESULTS AND DISCUSSION

We have previously provided a proof of principle that the combination of chemotherapy and PDT could efficiently kill MDA-MB-231 breast cancer cell *in vitro* by delivering DTX and the PS $TPPS_4$ through HA-decorated double layer PLGA-based NPs.[27] The more efficient uptake of HA-decorated NPs in CD44 overexpressing MDA-MB-231 cells in comparison to MCF-7 cells with low expression was also reported, suggesting an active role of HA in the cell targeting. In this work, we have focused the attention on the optimal drug ratio to load in NPs and performed detailed analyses of cytotoxicity data to determine effective synergism of the combined treatment. An additional novelty is given by the use of TPCS2a as PS, which has a more favorable absorption in the PDT therapeutic window, with respect to the previously used $TPPS_4$, and is already in clinical trials for PCI application but not extensively studied for combination of PDT and chemotherapy. To exploit tumor active targeting mechanisms based on the HA-mediated NP internalization, HeLa (DTX-sensitive and -resistant) and MDA-MB-231 cells both overexpressing CD44-receptors were selected as model cancer cell lines for this study.

Assessment of Cytotoxicity of Monotherapies. The method of Chou and Talalay developed for determining the type of interaction between drugs/therapies *in vitro* and based on the median effect analysis demands that the cytotoxicity profiles of single drugs/therapies are assessed before proceeding with combination studies. For each single drug, the concentration that inhibits cell survival by 50% (IC_{50} or Dm) is assessed, and this allows to determine suitable concentration ratios of the two drugs to achieve synergism. Our standard protocols of treating cells with PDT alone or in combination include a 24 h incubation in the dark with the PS followed by irradiation after PS removal from the medium, and

DOI: 10.1021/acs.molpharmaceut.8b00597
Mol. Pharmaceutics XXXX, XXX, XXX−XXX

Table 1. Properties of NP Formulations[a]

formulation	size[a] (nm ± SD)	PI[b]	ZP[c] (mV ± SD)	DTX actual loading (μg DTX/mg NPs)	DTX entrap. eff. (%)	TPCS2a actual loading (μg TPCS2a/mg NPs)	TPCS2a entrap. eff. (%)
unloaded NPs	192 ± 3	0.2	−33 ± 3	-	-	-	-
DTX-NPs	184 ± 12	0.2	−30 ± 5	0.7 ± 0.01	93 ± 2	-	-
TPCS2a-NPs	208 ± 6	0.2	−32 ± 7	-	-	25 ± 1.2	97 ± 3
DTX/TPCS2a-NPs	202 ± 13	0.2	−31 ± 3	0.7 ± 0.03	98 ± 5	25 ± 0.8	98 ± 4

[a]Data are expressed as mean percentage ± SD of three independent experiments. [b]Polydispersity index. [c]Zeta potential.

measurements of cell viability after additional 24 h of culture in drug free medium. To match the timing of treatment also when treating cells with DTX, we measured the cytotoxicity in cells incubated with the drug for 24 h as well as after 24 h in drug free-medium (referred as dark cytotoxicity at 24 + 24 h). The cytotoxicity at these time points is measured also in cells exposed to TPCS2a without irradiation for excluding cytotoxic effects in the dark as required for an ideal PS.[9]

Exposure to DTX caused a significant reduction of cell viability already after 24 h of incubation in both cell lines that was, however, further reduced at 24 + 24 h (Figure 1a,b). At both time points, HeLa cells showed sensitivity to DTX higher than that of MDA-MB-231 cells. At 24 + 24 h, almost 100% of HeLa cells were killed after exposure to 0.045 μg/mL DTX, while approximately 25% of MDA-MB-231 cells survived also at the highest concentration tested (i.e., 0.057 μg/mL), demonstrating lower sensitivity to the treatment (Figure 1a,b). The Dm values extrapolated from the dose−response curves at 24 + 24 h were 0.019 and 0.013 μg/mL for MDA-MB-231 and HeLa cells, respectively. In the absence of light, TPCS2a showed negligible toxicity after 24 h and 24 + 24 h both in HeLa and in MDA-MB-231 cells confirming the safety of the drug and the absence of toxic effects in cells and tissues protected from light. However, when TPCS2a-incubated cells were irradiated with red light (600−800 nm), a concentration-dependent reduction of cell viability was measured, with Dm of 0.40 and 0.55 μg/mL in HeLa and MDA-MB-231 cells, respectively (Figure 1c,d), suggesting very similar sensitivity of the two cell lines toward PDT. Thus, considering the Dm values of each single drug/treatment and calculating the DTX/TPCS2a ratios in each cell line, it turned out that these values are 1:28 and 1:30 for MDA-MB-231 and HeLa cells, respectively. The two ratios are rather similar, and therefore, a DTX/TPCS2a ratio of 1:30 appears optimal for the combination therapy in both cell lines.

Preparation and Properties of NPs. TPCS2a and DTX were loaded in NPs (DTX/TPCS2a-NPs) following the formulation strategy previously described.[27] A schematic representation of the NP structure and surface composition is shown in Figure 2a. Not far from the suggested theoretical drug ratio, using the layer deposition method, we were able to prepare NPs containing DTX and TPCS2a at the 1:35 concentration ratio. As controls, we prepared also unloaded NPs and NPs loaded with each single drug (DTX-NPs and TPCS2a-NPs). The properties of all the formulations are reported in Table 1.

NPs showed a size around 200 nm, a low polydispersity index, and a high negative zeta potential, due to the external layer of negatively charged HA. These colloidal properties were not affected by the loading of the drugs alone or in combination. DTX was loaded with high efficiency in the PLGA core of NPs, in line with previous results,[27] whereas TPCS2a was adsorbed onto the PEI layer, covering the DTX-PLGA core of NPs, up to an amount of 25 μg/mg NPs. At this concentration, TPCS2a is completely adsorbed onto NPs as demonstrated by the fact that the supernatant does not give any appreciable absorption at the maximum wavelength of TPCS2a absorption (data not shown). UV−vis and emission spectra profiles of TPCS2a free in water or adsorbed on NP surface, with or without the presence of DTX in the formulation, are reported in Figure S1. In particular, in the UV−visible absorption spectra, typical of the chlorines, it is possible to note a broad Soret band with a maximum centered at 414 nm in a face-to face arrangement in H-type aggregates and a Q band with four additional minor absorption bands in the red region of the spectrum at ∼650 nm, which is important for use in PCI technology and PDT.[33] However, the Soret band of TPCS2a adsorbed on NP surface is split into three distinct peaks, located at, respectively, 367−373, 404−408, and 416−421 nm caused by the reduced mobility of the core electrons due to molecular twisting, compared to the free PS in water.[33]

The release of TPCS2a from NPs was performed in cell culture medium added with serum proteins in order to reproduce the experimental conditions of *in vitro* cell studies and to predict the behavior of the PS. In Figure 2b, it is evident that TPCS2a is strongly and stably adsorbed on NP surface, with only the 20% of the drug released after 48 h. If we compare these last data with those reported for $TPPS_4$ in our previous work,[27] in which we measured an immediate $TPPS_4$ release (20%) and an additional release (40%) in the following couple of hours of incubation reaching a 60% of total PS release after 6 h, we can conclude that TPCS2a affinity for this type of nanosystem is much higher and that the PS association clearly improved.

Stability studies of NPs were carried out monitoring both colloidal properties of the formulations (size, polydispersity index, and zeta potential), and the spectroscopic profile of the adsorbed PS along time. As shown in Figure 2c, distribution curves of NPs kept at room temperature for 10 days are completely overlapped, thus suggesting no modification of NP structure along time. Similarly, no significant changes in zeta potential values were found (data not shown). NPs demonstrated long-term stability also monitoring the spectroscopic properties of TPCS2a (Figure 2d). In fact, the absence of changes of the absorption spectrum confirms a great stability of the TPCS2a adsorbed on NP surface along time.

Unloaded NPs were shown to be safe and biocompatible since they induced no appreciable decrease of viability in HeLa and MDA-MB-231 cells incubated for 24 h and 24 + 24 h in dark and light conditions (Figure S2).

Combination Therapy with DTX/TPCS2a or DTX/TPCS2a-NPs and CI Analysis. To study whether synergism between DTX-chemotherapy and TPCS2a-PDT is realized at

DOI: 10.1021/acs.molpharmaceut.8b00597
Mol. Pharmaceutics XXXX, XXX, XXX−XXX

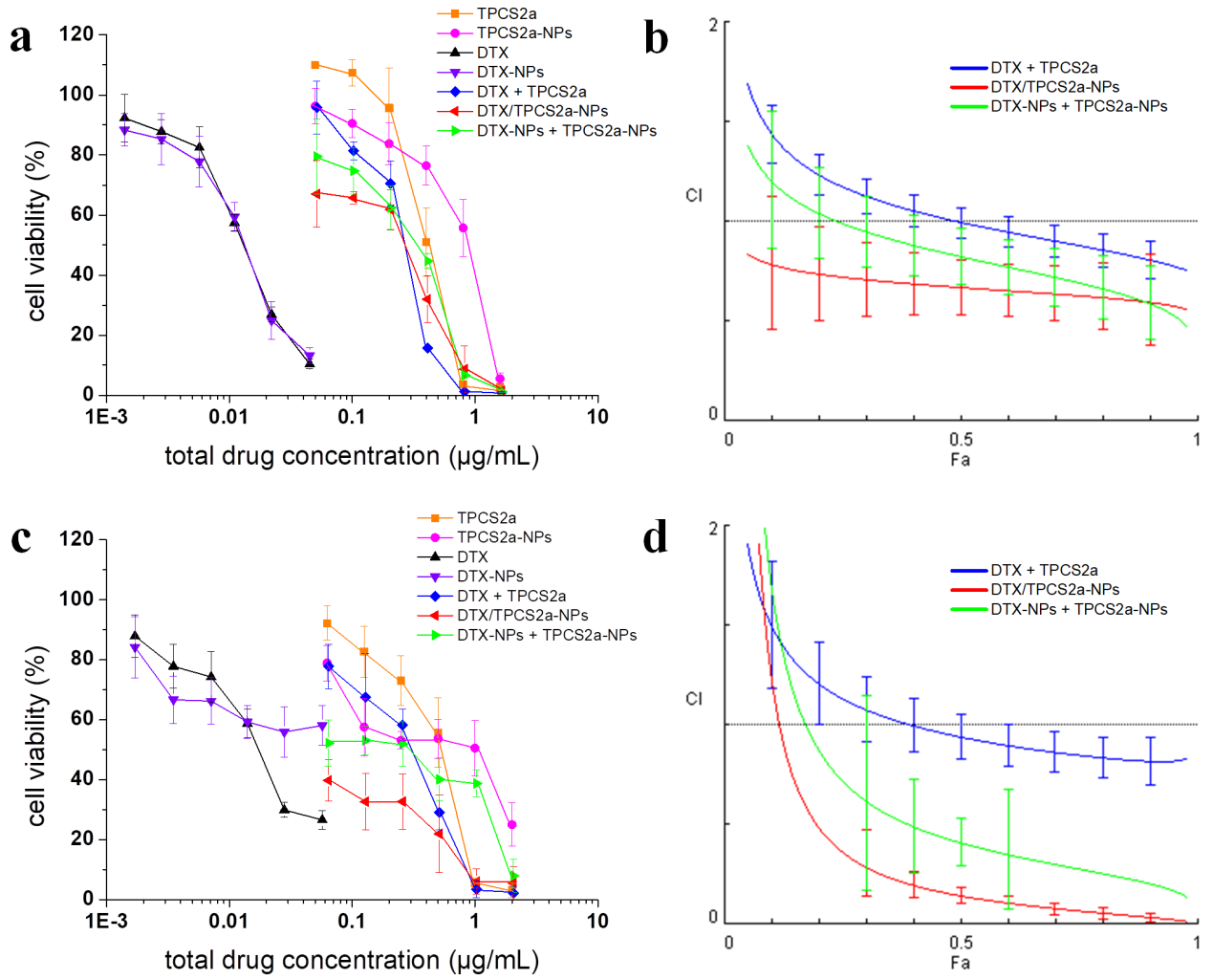

Figure 3. Dose−response curves and combination index plots (Fa vs CI plots) of HeLa (a,b) and MDA-MB-231 (c,d) cells treated with DTX-chemotherapy and/or TPCS2a-PDT with free or NP-loaded drugs. Total drug concentration is referred to DTX + TPCS2a concentration. Data are expressed as mean percentage ± SD of at least three independent experiments, carried out in triplicate.

Table 2. Dm Values and Dose-Reduction Index (DRI) Calculated by Compusyn Analysis in HeLa and MDA-MB-231[a]

			dose-reduction index (DRI)			
	Dm (μg/mL)		HeLa		MDA-MB-231	
treatment	HeLa	MDA-MB-231	DTX	TPCS2a	DTX	TPCS2a
TPCS2a	0.392	0.322	-	-	-	-
TPCS2a-NPs	0.528	0.455	-	-	-	-
DTX	0.011	0.016	-	-	-	-
DTX-NPs	0.011	0.067	-	-	-	-
DTX + TPCS2a	0.202	0.200	2.02	1.99	2.98	1.65
DTX/TPCS2a-NPs	0.154	0.055	2.66	2.62	10.76	5.96
DTX-NPs + TPCS2a-NPs	0.189	0.160	2.16	2.13	3.73	2.07

[a]Dm was calculated for cells exposed to DTX-chemotherapy and/or TPCS2a-PDT using free drugs as well as NP formulations. The DRI values were calculated for cells exposed to combination therapy and indicate how many folds the concentration of each single drug can be reduced to obtain a Fa value of 50%.

the coloaded 1:35 drug ratio, we determined dose−response curves with HeLa and MDA-MB-231 cells for calculating the CI values with the CompuSyn software by uploading a series of values of fraction affected (Fa) versus the drug dose for single and combination treatments. For assessing, whether the codelivery of DTX and TPCS2a loaded in separate NPs could bring an advantage with respect to coadministration of the drugs in the free forms, combination treatments were carried out also coadministering DTX-NPs + TPCS2a-NPs. The dose−response curves are shown in Figure 3a,c and report cell viability versus the total drug concentration (DTX dose + TPCS2a dose) while the relative Dm values are listed in Table 2. As concerns the single treatments, the entrapment of DTX and TPCS2a in NPs brings slight or no improvements of

DOI: 10.1021/acs.molpharmaceut.8b00597
Mol. Pharmaceutics XXXX, XXX, XXX−XXX

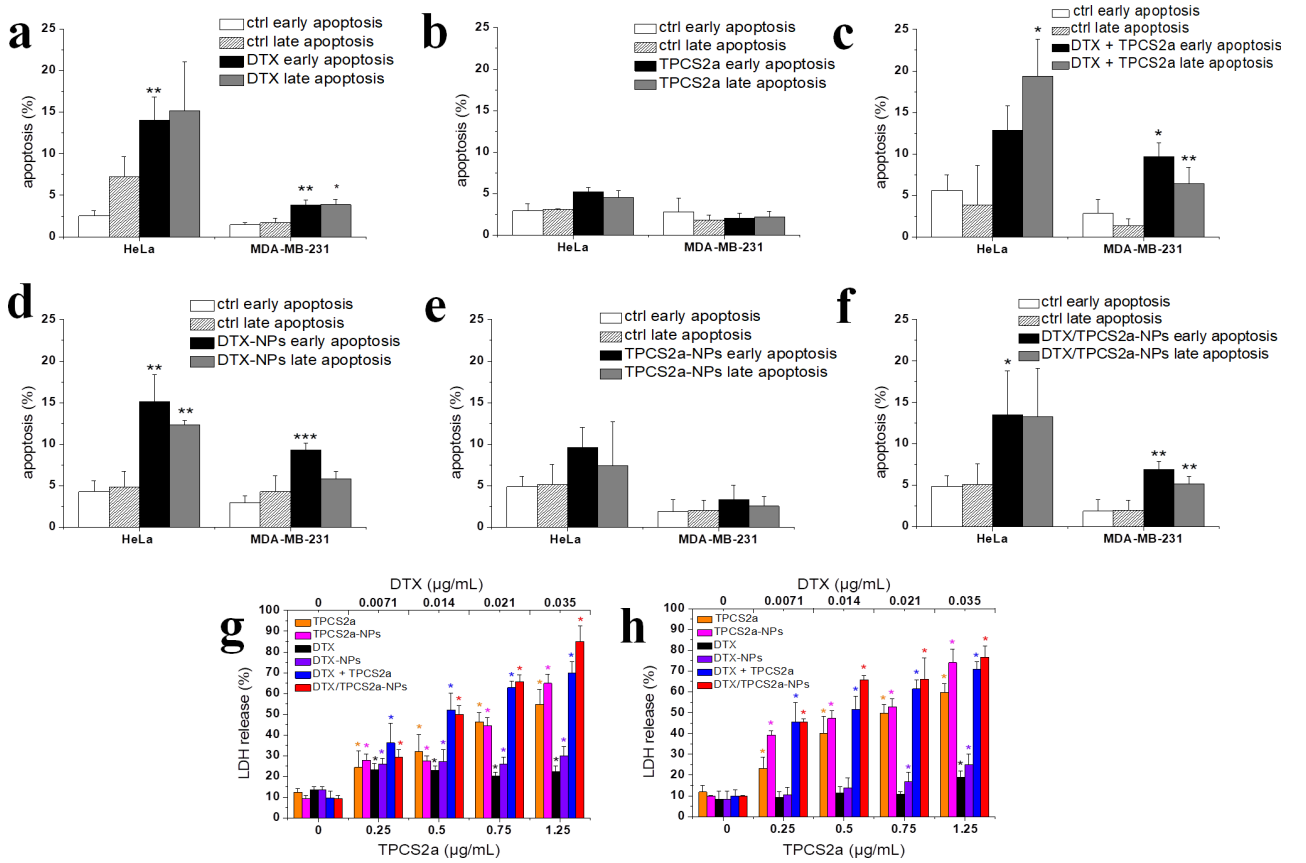

Figure 4. Cell death mechanisms: Annexin V/PI staining (a–f) and LDH release assay (g,h). Percentage of apoptotic cells in HeLa and MDA-MB-231 cells incubated for 24 + 24 h with DTX, exposed to TPCS2a-PDT or to combination therapy using the drugs delivered in the standard solvents (a–c) or in NP formulations (d–f). *$p < 0.05$; **$p < 0.01$; ***$p < 0.001$ significantly different from control cells (Student's t test). Percentage of LDH released in the culture medium of HeLa (g) and MDA-MB-231 (h) cells incubated for 24 + 24 h with the different drugs/therapies. Data are expressed as mean percentage ± SD of at least three independent experiments, carried out in triplicate. *$p < 0.001$ significantly different from control cells (Student's t test).

cytotoxicity, with respect to the free drugs, and the improvement is limited to the lower drug doses used in the experiments. On the contrary, the dose–response curves of the DTX/TPCS2a-NPs indicated that the entrapment of both drugs into NPs greatly enhanced the treatment efficacy with respect to the combination of free drugs, especially in MDA-MB231 cells. The Fa vs CI plots (Figure 3b,d), generated by the Compusyn software, clearly showed that the combination of DTX-chemotherapy and TPCS2a-PDT using the two drugs coloaded in the same NPs (DTX/TPCS2a-NPs) was significantly more potent (e.g., lower CI values) in inducing cytotoxicity in MDA-MB-231 and HeLa cells than the combination of the two drugs delivered in the standard solvents (DTX+TPCS2a) and, even more importantly, also the drugs delivered in separate NPs (DTX-NPs + TPCS2a-NPs).

In fact, the combination of DTX + TPCS2a showed slight synergism (CI not lower than 0.8) only when Fa exceeded 50–60%, while codelivery by NPs produced strong synergism in a wide range of Fa values, especially in MDA-MB-231 cells. As shown in Figure 3b,d, the CI values for DTX/TPCS2a-NPs in MDA-MB-231 cells were significantly lower than those measured in HeLa cells, while the CI values for DTX + TPCS2a were quite similar. In both cell lines, the combination of TPCS2a-NPs + DTX-NPs gave a synergism higher than that of the free drugs but lower than that of DTX/TPCS2a-NPs. As expected, in cells treated with the drug combinations but not exposed to red light the cytotoxic effects was exclusively due to DTX, and viability matched that measured after treatment with only DTX with no appreciable differences between the free and NP-loaded drug (Figure S3).

The experimental data were also analyzed to calculate the dose-reduction index (DRI, Table 2) for each type of combination (DRI > 1 and < 1 indicate favorable and not favorable dose-reduction, respectively, while DRI = 1 indicates no possibility of dose-reduction). The DRI value is very important since the reduction of the dose of a therapeutic agent allows the reduction also of its unwanted side effects. Thus, the possibility to reduce the dose of each single drug while preserving treatment efficacy is a key aspect associated with identification of conditions giving synergism. The DRI values show how many folds the concentration of each agent employed in the combination can be reduced to obtain a Fa value of 50% and were calculated by the Compusyn software using the doses of each single drug giving a Fa of 50% when delivered alone or in combination in standard solvent or in NPs (Table S1). The CompuSyn analysis indicated favorable DRI values (DRI > 1) for DTX and TPCS2a in both cell lines and with all combinations tested. As expected, on the basis of the CI analysis, the reduction dose is higher when the drugs are codelivered in the same NP compared to the coadministration in the standard solvents. In MDA-MB-231 we found DRI values of 10.76 and 3.73 for DTX and 5.96 and 2.07 for

DOI: 10.1021/acs.molpharmaceut.8b00597
Mol. Pharmaceutics XXXX, XXX, XXX–XXX

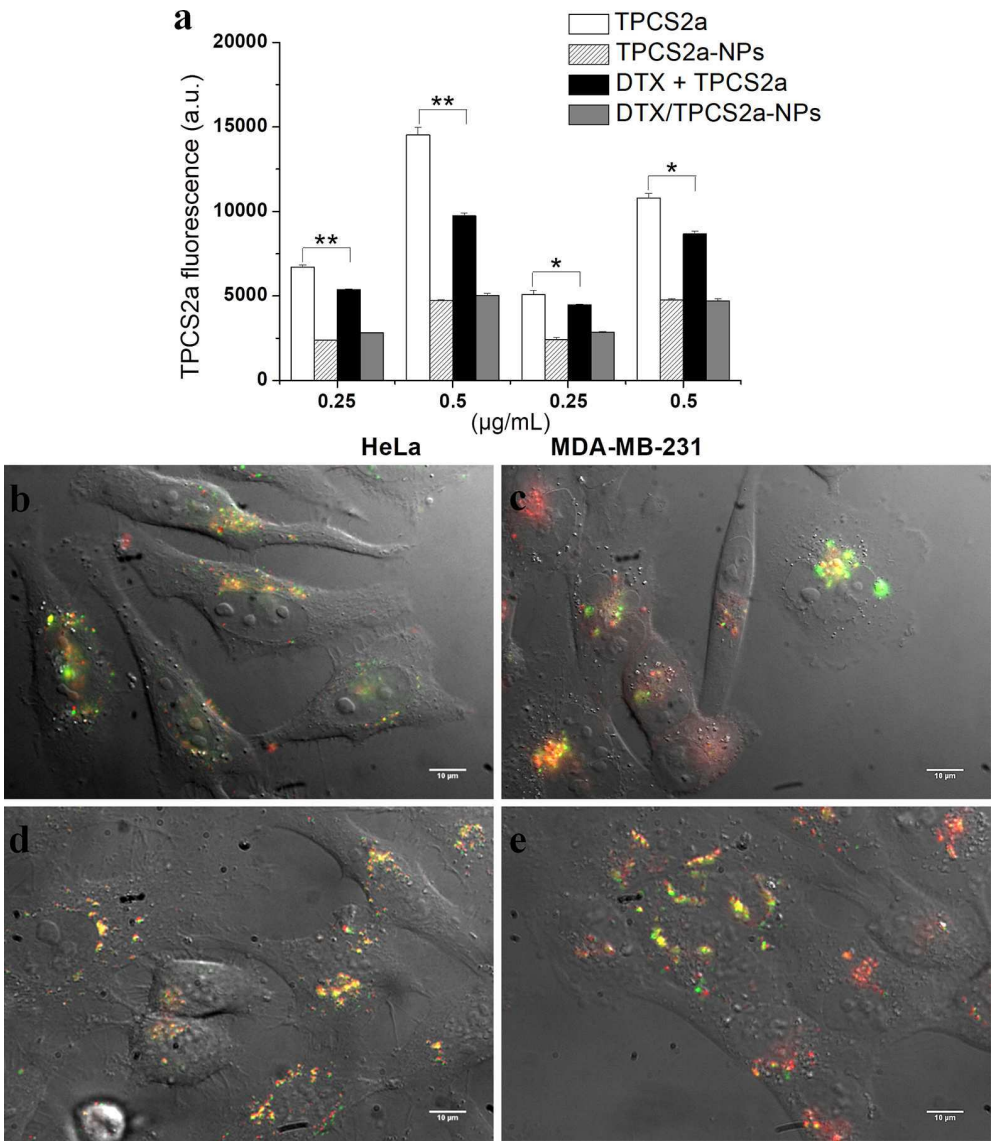

Figure 5. Uptake and intracellular localization of TPCS2a. Uptake (a) measured by flow cytometry after incubation for 24 h with 0.25 or 0.5 μg/mL TPCS2a in the absence/presence of, respectively, 0.0071 and 0.014 μg/mL DTX. Data are expressed as mean percentage ± SD of at least two independent experiments, carried out in triplicate; *$p < 0.01$; **$p < 0.001$; TPCS2a alone vs TPCS2a + DTX (Student's t test). Fluorescence microscopy images of HeLa (b,d) and MDA-MB-231 (c,e) cells showing the colocalization of the red fluorescence of free TPCS2a (b,c) or TPCS2a-NPs (d,e) with the green fluorescence of the endolysosome probe Lysotracker green.

TPCS2a when delivered respectively in DTX/TPCS2a-NPs or in separated NPs. The DRI values are in general lower with the combination of TPCS2a + DTX. Comparing the two cell lines, it is evident that for HeLa cells DRI values around 2 indicate only modest reduction of drug doses even with DTX/TPCS2a-NPs. These results are in perfect agreement with those reported in Fa vs CI plots showing much higher synergism produced by DTX/TPCS2a-NPs and DTX-NPs + TPCS2a-NPs compared to DTX + TPCS2a, in particular in MDA-MB-231 cells.

Analysis of Cell Death Mechanisms. The synergistic interaction between multiple drugs/treatment modalities is often achieved taking advantage of different cell death pathways activated by the individual treatment. Therefore, several combinations of chemotherapeutics acting with non-overlapping mechanisms on different cellular targets are shown to interact synergistically counteracting the drug resistance, caused by genetic heterogeneity of the cells in solid tumors, and limiting drug toxicity in normal cells because of the lowering of effective drug doses.[6,34] Thus, in order to gain more insight into the cell death mechanisms elicited by the combination of DTX chemotherapy and TPCS2a-PDT we performed: (i) Annexin V−PI assay to discriminate between apoptotic and necrotic cells simultaneously; (ii) Caspase-3 assay to evaluate the activation of the executioner caspase-3 involved in the apoptotic cascade; and (iii) LDH release assays as indirect measurement of cell death.[35]

Apoptosis is usually considered the predominant cell death mechanism caused by taxane chemotherapy.[36] In any case, the cell death modalities observed after a specific treatment are determined by several factors such as the mechanism of action of the drug, the dose and timing through which the treatment is administered, and the genetic profile of the cell line used. In our case, the Annexin V/PI staining of cells treated with 0.014

DOI: 10.1021/acs.molpharmaceut.8b00597
Mol. Pharmaceutics XXXX, XXX, XXX−XXX

μg/mL DTX (Figure 4a) or DTX-NPs (Figure 4d) for 24 + 24 h indicated a significant increase in the percentage of apoptotic cells, while the percentage of necrotic cells was comparable to that of untreated samples (data not shown). Accordingly, an increase of caspase-3 activity was measured (Figure S4a). In general, in HeLa cells the increase of the apoptotic population was more pronounced than in MDA-MB-231 cells, but it must be underlined that, in MDA-MB-231 cells, the exposure to DTX-NPs significantly increased ($p < 0.001$) apoptotic cell population with respect to exposure to DTX.

On the contrary, TPCS2a-PDT (0.5 μg/mL) performed by delivering the PS free or in NPs did not activate apoptotic response in neither of the two cell lines (Figures 4b,e and S4b), suggesting that a different cell death pathway was involved. Our observations are in agreement with those of Olsen et al. reporting the absence of activation of apoptotic factors, such as caspase-3, after TPCS2a-PDT in other cell lines.[37] In general, the combination of DTX-chemotherapy and TPCS2a-PDT did not increase the percentage of apoptotic cells (Figures 4c,f and S4c) with respect to DTX-chemotherapy alone (Figures 4a,d) with the exception of MDA-MB-231 cells exposed to DTX + TPCS2a. Overall, the results of the Annexin/PI and caspase-3 activation indicated that only a minor fraction of the HeLa and MDA-MB-231 cells undergo apoptosis following single and combination treatments. Thus, to gain more insight into the mechanism of cell death, we measured the release of the cytosolic LDH as an indicator of cell membrane damage and occurrence of death via necrosis. The percentage of LDH released from HeLa and MDA-MB-231 cells treated with PDT using TPCS2a or TPCS2a-NPs increased with the PS concentration and was higher when combination therapy was performed, irrespective of the drug delivery modality (Figure 4g,h). On the contrary, in agreement with the Annexin V/PI assay, a very low LDH release was detected after DTX or DTX-NPs treatment and only in HeLa cells (Figure 4g,h), confirming apoptosis as the predominant cell death mechanism induced by the chemotherapeutic. It is thus worth to note that the high synergism observed with the combination of DTX/TPCS2a-NPs is not associated with substantial changes in the mechanism of activation of cell death, indicating that the type/extent of cell death produced by the single treatment is not the main determinant for obtaining synergistic effects, especially in MDA-MB-231 cells.

Intracellular Uptake and Localization of TPCS2a and TPCS2a-NPs. It is well-known that, both the extent of the PS uptake and its intracellular localization plays an important role in determining the PDT efficacy. In this context, we investigated whether these parameters were affected by the delivery of TPCS2a through NPs. Thus, flow cytometry was used to comparatively measure the intracellular uptake of TPCS2a and TPCS2a-NPs after 24 h of incubation (Figure 5a). The TPCS2a uptake was concentration dependent irrespective of the delivery modality, but it was reduced to about one-third in the case of TPCS2a-NPs, in both cell lines. Notwithstanding, the reduced PS uptake, when using NPs, only slightly affected the photokilling efficiency (see Dm values in Table 2). The TPCS2a uptake was significantly higher in HeLa cells with respect to MDA-MB-231 cells when not included in NPs, but the increased internalization did not translate into an increased photoefficiency (Table 2) likely indicating a higher photosensitivity of MDA-MB-231 with respect to HeLa cells. We wondered whether the coadministration of the chemotherapeutic could affect the uptake of TPCS2a, and therefore, we measured also the internalization of DTX+TPCS2a and DTX/TPCS2a-NPs. The presence of DTX caused a decrease of the uptake of TPCS2a only when the drugs were delivered in the free forms, very likely due to DTX cytotoxic effects (Figure S3a,b). The decrease was more significant in HeLa with respect to MDA-MB-231 cells. The decrease of TPCS2a uptake was not observed when NPs were used for the delivery of the two drugs, and this underlines that by using combined NP we can control cell delivery of the two drugs in parallel. In fact, based on the drug release studies carried out in cell culture medium (Figure 2b) we can assume that the large fraction of TPCS2a and DTX delivered by NPs entered the cells still entrapped in the nanovehicle.

Fluorescence microscopy analysis of HeLa and MDA-MB-231 cells incubated for 24 h with TPCS2a or TPCS2a-NPs showed clear lysosomal accumulation of the PS as indicated by the colocalization of the red fluorescence of TPCS2a with the green fluorescence of LysoTracker Green (Figure 5b−e). A lysosomal accumulation of PS-loaded HA-targeted NPs in MDA-MB-231 cells was already reported by us,[27] indicating a CD44 receptor-mediated endocytic pathway as the preferential mechanism of NP entry. Moreover, these results are in agreement with literature data reporting TPCS2a localization in endocytic vesicles, as required for PCI applications.[38] These observations pose the questions whether PDT or PCI determines or contributes to the overall cytotoxic effects. In fact, a release of NPs and their contents from endosomes/lysosomes is very like to occur during irradiation, which, in the case of the combined treatment, may favor the interaction of DTX with microtubules. However, it is rather difficult to discriminate between PDT and/or PCI effects, and additional investigations based on light-induced drug relocalization might be useful to clarify this point.

Combination Therapy and CI Analysis in DTX-Resistant HeLa Cells. Combination therapies using nanoformulations of common chemotherapeutics appear as a promising strategy for treating cancers with innate or acquired drug resistance due to overexpression of multidrug transporters and/or altered apoptotic pathways.[39] We wanted to assess if combined NPs could be useful to fight acquired drug-resistance. To this end, we created a DTX-resistant HeLa cell line (Hela-R) that was about 8-fold more resistant to DTX as compared to parental HeLa cell line (HeLa-P) (Dm for DTX of 0.011 μg/mL for HeLa-P vs 0.093 μg/mL for HeLa-R) (Figure S5a). The overexpression of membrane efflux pumps has been identified as a key element causing drug resistance, leading to the reduction of the drug accumulation in cancer cells,[40] and among the various subtype of pumps, the P-glycoprotein 1 (P-gp), belonging to the ATP binding cassette family (ABC), is known to be responsible of taxane resistance.[41] Indeed, the Western blot analysis of Hela-R cell protein extracts showed a significant overexpression of P-gp compared to HeLa-P (Figure S5b).

As shown in Figure 6a, DTX-NPs were significantly more cytotoxic toward HeLa-R cells than DTX with a calculated Dm of 0.106 and 0.831 μg/mL, respectively, indicating that the use of the NPs to deliver DTX helps to circumvent P-gp efflux. On the contrary, when P-gp is not overexpressed in HeLa-P cells, comparable cytotoxicity was observed for DTX and DTX-NPs (Figure 2a). Similarly, Wang and Jia recently reported the improvement of PTX efficacy *in vitro* and *in vivo* using HA-conjugated PTX-loaded NPs against PTX-sensitive and -resistant SKOV-3 ovarian cancer cells.[42] For comparison, in

DOI: 10.1021/acs.molpharmaceut.8b00597
Mol. Pharmaceutics XXXX, XXX, XXX−XXX

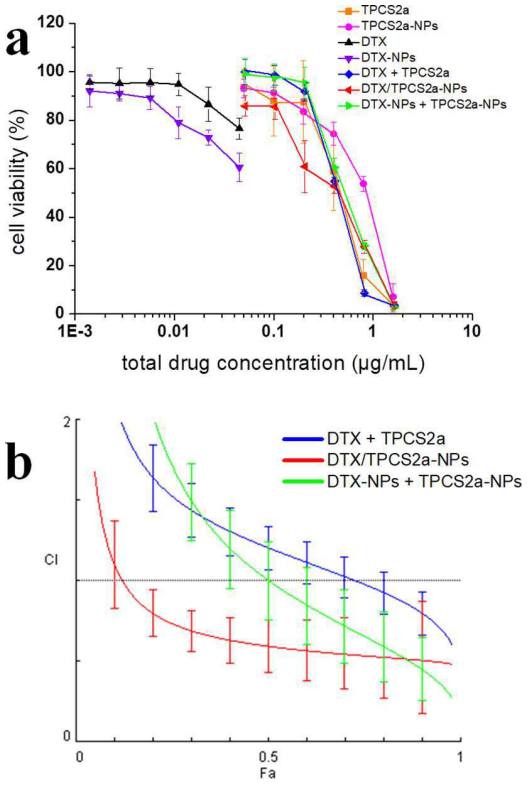

Figure 6. Viability of DTX-resistant HeLa cells (Hela-R) and CI analysis. Dose−response curves (a) of HeLa-R cells treated with DTX, TPCS2a-PDT, or their combination delivering the drugs in the standard solvent or in NPs. Fa vs CI plots (b) obtained from the viability data shown in (a). The data are means ± SD of at least three independent experiments, carried out in triplicates.

Figure S6, the dose−response curves of HeLa-R cells incubated with TPCS2a and DTX combination for 24 h or 24 + 24 h but not exposed to light are reported.

On the contrary, HeLa-R cells were sensitive to PDT as HeLa-P cells, and Dm values for TPCS2a and TPCS2a-NPs were comparable (Tables 2 and 3), but this was somehow expected because this PS is not a substrate of P-gp.[37] However, when combination therapy was performed, the CI analysis highlighted the increased synergism of DTX/TPCS2a-NPs compared to the other combination modalities (Figure 6b), where only slight synergism and at high Fa was observed. Notably, with DTX/TPCS2a-NPs in HeLa-R cells the CI values were quite lower than those calculated for HeLa-P. In addition, in HeLa-R cells the DRI values (Table 3) of DTX were impressive for all types of combinations when compared to those measured in HeLa-P cells (ca. 2), but the highest DRI value of 104.27 was calculated for DTX/TPCS2a-NPs. However, comparable DRI values of TPCS2a were found in DTX sensitive and resistant HeLa cells very likely because the two cell lines are equally sensitive to TPCS2a-PDT. All together, these findings on the HeLa-R cells corroborate the hypothesis that P-gp overexpression is responsible for the reduced DTX cytotoxicity since no reduced apoptotic activity was measured (data not shown) and suggest the possibility to overcome the drug resistance using well-conceived delivery systems as our HA-targeted layer-by-layer NPs. Our findings clearly demonstrate the advantage of the codelivery of DTX and PS in the same NP and strongly encourage the use of nanomaterials as important tools for the codelivery of drugs when combining chemotherapy and PDT, especially for the treatment of chemo-resistant cells.

Table 3. Dm Values and Dose-Reduction Index (DRI) Calculated by the Compusyn Analysis in HeLa-R[a]

		dose-reduction index (DRI)	
drug formulation	Dm (μg/mL)	DTX	TPCS2a
TPCS2a	0.345		
TPCS2a-NPs	0.537		
DTX	0.831		
DTX-NPs	0.106		
DTX + TPCS2a	0.423	70.73	0.83
DTX/TPCS2a-NPs	0.287	104.27	1.23
DTX-NPs + TPCS2a-NPs	0.485	61.71	0.73

[a]Dm were calculated for cells exposed to DTX-chemotherapy or/and TPCS2a-PDT using the drugs delivered in the standard formulations and NP formulations. The DRI values were calculated for cells exposed to combination therapy with the different drug formulations.

CONCLUSIONS

We have herein proposed for the first time the combination of TPCS2a-PDT and DTX-chemotherapy and shown that the efficient codelivery of the two drugs in HA-targeted PLGA-based layered NPs results in a strong synergism of the two therapeutic modalities. The particular NP architecture and synthesis methodology allow the control of the drug loading at the most appropriate concentration ratio to exploit synergistic effects. The CI analysis performed with the Compusyn software revealed that the strongest synergism between DTX cytotoxicity and TPCS2a-PDT occurred when the two drugs were codelivered simultaneously in the same NPs with respect to the coadministration of the free drugs or drugs loaded in separated NPs. Our data demonstrated that the codelivery in a single NP is particularly important for cancer cells showing innate or acquired resistance. The usefulness of HA-decorated layered NPs as drug delivery system to overcome chemotherapeutic resistance, mainly related to the P-gp protein overexpression, was confirmed with the DTX-resistant HeLa-R cells, in which the combination of DTX/TPCS2a-NPs exhibited a much higher synergism with respect to that of the DTX-sensitive parental cell line.

ASSOCIATED CONTENT

Supporting Information

The Supporting Information is available free of charge on the ACS Publications website at DOI: 10.1021/acs.molpharmaceut.8b00597.

Caspase-3 assay; Western blot analysis; UV and emission spectra of NPs compared to free TPCS2a in water; cytotoxicity of unloaded NPs; cell viability curves of HeLa and MDA-MB-231 cells exposed to single/combination therapy in the absence of light; results of Caspase-3 activation; characterization of DTX-resistant HeLa cells (Hela-R); cell viability curves of HeLa-R cells exposed to single/combination therapy in the absence of light; data for Fa = 0.5 of HeLa, MDA-MB-231, and HeLa-R (PDF)

DOI: 10.1021/acs.molpharmaceut.8b00597
Mol. Pharmaceutics XXXX, XXX, XXX−XXX

AUTHOR INFORMATION

Corresponding Author

*E-mail: francesca.moret@unipd.it. Tel: +39 049 8276282.

ORCID

Francesca Moret: 0000-0002-1534-3714

Notes

The authors declare no competing financial interest.

ACKNOWLEDGMENTS

The financial support of the University of Padova and Italian Association for Cancer Research (IG2014 #15764) are gratefully acknowledged. The authors are grateful to PCI Biotech, Oslo, Norway for providing the photosensitizer TPCS2a (Fimaporfin).

REFERENCES

(1) Siegel, R.; Ma, J.; Zou, Z.; Jemal, A. Cancer statistics, 2014. *Ca-Cancer J. Clin.* **2014**, *64*, 9−29.

(2) DeSantis, C. E.; Lin, C. C.; Mariotto, A. B.; Siegel, R. L.; Stein, K. D.; Kramer, J. L.; Alteri, R.; Robbins, A. S.; Jemal, A. Cancer treatment and survivorship statistics, 2014. *Ca-Cancer J. Clin.* **2014**, *64*, 252−271.

(3) Kennedy, A.; Brown, D. B.; Feilchenfeldt, J.; Marshall, J.; Wasan, H.; Fakih, M.; Gibbs, P.; Knuth, A.; Sangro, B.; Soulen, M. C.; Pittari, G.; Sharma, R. A. Safety of selective internal radiation therapy (SIRT) with yttrium-90 microspheres combined with systemic anticancer agents: expert consensus. *J. Gastrointest. Oncol.* **2017**, *8*, 1079−1099.

(4) Corn, P. G.; Agarwal, N.; Araujo, J. C.; Sonpavde, G. Taxane-based Combination Therapies for Metastatic Prostate Cancer. *Eur. Urol Focus.* **2017**, DOI: 10.1016/j.euf.2017.11.009.

(5) Lhuillier, C.; Vanpouille-Box, C.; Galluzzi, L.; Formenti, S. C.; Demaria, S. Emerging biomarkers for the combination of radiotherapy and immune checkpoint blockers. *Semin. Cancer Biol.* **2017**, DOI: 10.1016/j.semcancer.2017.12.007.

(6) Lee, A.; Djamgoz, M. B. A. Triple negative breast cancer: Emerging therapeutic modalities and novel combination therapies. *Cancer Treat. Rev.* **2018**, *62*, 110−122.

(7) Huang, H. C.; Mallidi, S.; Liu, J.; Chiang, C. T.; Mai, Z.; Goldschmidt, R.; Ebrahim-Zadeh, N.; Rizvi, I.; Hasan, T. Photodynamic Therapy Synergizes with Irinotecan to Overcome Compensatory Mechanisms and Improve Treatment Outcomes in Pancreatic Cancer. *Cancer Res.* **2016**, *76*, 1066−1077.

(8) Ali, S.; Muhammad, S.; Khurshid, A.; Ikram, M.; Maqsood, M.; Fisher, C.; Cathcart, J.; Lilge, L. Effective Phthalocyanines mediated Photodynamic Therapy with Doxorubicin or Methotrexate combination therapy at sub-micromolar concentrations in vitro. *Photodiagn. Photodyn. Ther.* **2018**, *22*, 51−64.

(9) Allison, R. R. Photodynamic therapy: oncologic horizons. *Future Oncol.* **2014**, *10*, 123−142.

(10) Agostinis, P.; Berg, K.; Cengel, K. A.; Foster, T. H.; Girotti, A. W.; Gollnick, S. O.; Hahn, S. M.; Hamblin, M. R.; Juzeniene, A.; Kessel, D.; Korbelik, M.; Moan, J.; Mroz, P.; Nowis, D.; Piette, J.; Wilson, B. C.; Golab, J. Photodynamic therapy of cancer: an update. *Ca-Cancer J. Clin.* **2011**, *61*, 250−281.

(11) Dolmans, D. E.; Fukumura, D.; Jain, R. K. Photodynamic therapy for cancer. *Nat. Rev. Cancer* **2003**, *3*, 380−387.

(12) Postiglione, I.; Chiaviello, A.; Palumbo, G. Enhancing photodynamic therapy efficacy by combination therapy: dated, current and oncoming strategies. *Cancers* **2011**, *3*, 2597−2629.

(13) Brodin, N. P.; Guha, C.; Tomé, W. A. Photodynamic Therapy and Its Role in Combined Modality Anticancer Treatment. *Technol. Cancer Res. Treat.* **2015**, *14*, 355−368.

(14) Koot, D.; Cromarty, D. Anticancer efficacy and toxicokinetics of a novel paclitaxel-clofazimine nanoparticulate co-formulation. *Drug Delivery Transl. Res.* **2015**, *5*, 257−267.

(15) Ramsay, E. C.; Dos Santos, N.; Dragowska, W. H.; Laskin, J. J.; Bally, M. B. The formulation of lipid-based nanotechnologies for the delivery of fixed dose anticancer drug combinations. *Curr. Drug Delivery* **2005**, *2*, 341−351.

(16) Conte, C.; Ungaro, F.; Maglio, G.; Tirino, P.; Siracusano, G.; Sciortino, M. T.; Leone, N.; Palma, G.; Barbieri, A.; Arra, C.; Mazzaglia, A.; Quaglia, F. Biodegradable core-shell nanoassemblies for the delivery of docetaxel and Zn(II)-phthalocyanine inspired by combination therapy for cancer. *J. Controlled Release* **2013**, *167*, 40−52.

(17) Conte, C.; Maiolino, S.; Pellosi, D. S.; Miro, A.; Ungaro, F.; Quaglia, F. Polymeric Nanoparticles for Cancer Photodynamic Therapy. *Top. Curr. Chem.* **2016**, *370*, 61−112.

(18) Conte, C.; Ungaro, F.; Mazzaglia, A.; Quaglia, F. Photodynamic Therapy for Cancer: Principles, Clinical Applications, and Nanotechnological Approaches. In *Nano-Oncologicals: New Targeting and Delivery Approaches*; Alonso, M. J., Garcia-Fuentes, M, Eds.; Cham Springer: 2014; pp 123−160.

(19) Nieuweboer, A. J.; de Morrée, E. S.; de Graan, A. J.; Sparreboom, A.; de Wit, R.; Mathijssen, R. H. Inter-patient variability in docetaxel pharmacokinetics: A review. *Cancer Treat. Rev.* **2015**, *41*, 605−613.

(20) Valicherla, G. R.; Dave, K. M.; Syed, A. A.; Riyazuddin, M.; Gupta, A. P.; Singh, A.; Wahajuddin; Mitra, K.; Datta, D.; Gayen, J. R. Formulation optimization of Docetaxel loaded self-emulsifying drug delivery system to enhance bioavailability and anti-tumor activity. *Sci. Rep.* **2016**, *6*, 26895.

(21) Conte, C.; Mastrotto, F.; Taresco, V.; Tchoryk, A.; Quaglia, F.; Stolnik, S.; Alexander, C. Enhanced uptake in 2D- and 3D lung cancer cell models of redox responsive PEGylated nanoparticles with sensitivity to reducing extra- and intracellular environments. *J. Controlled Release* **2018**, *277*, 126−141.

(22) Palma, G.; Conte, C.; Barbieri, A.; Bimonte, S.; Luciano, A.; Rea, D.; Ungaro, F.; Tirino, P.; Quaglia, F.; Arra, C. Antitumor activity of PEGylated biodegradable nanoparticles for sustained release of docetaxel in triple-negative breast cancer. *Int. J. Pharm.* **2014**, *473*, 55−63.

(23) Lund, K.; Bostad, M.; Skarpen, E.; Braunagel, M.; Kiprijanov, S.; Krauss, S.; Duncan, A.; Høgset, A.; Selbo, P. K. The novel EpCAM-targeting monoclonal antibody 3−17I linked to saporin is highly cytotoxic after photochemical internalization in breast, pancreas and colon cancer cell lines. *MAbs.* **2014**, *6*, 1038−1050.

(24) Bostad, M.; Olsen, C. E.; Peng, Q.; Berg, K.; Høgset, A.; Selbo, P. K. Light-controlled endosomal escape of the novel CD133-targeting immunotoxin AC133-saporin by photochemical internalization - A minimally invasive cancer stem cell-targeting strategy. *J. Controlled Release* **2015**, *206*, 37−48.

(25) Bostad, M.; Kausberg, M.; Weyergang, A.; Olsen, C. E.; Berg, K.; Høgset, A.; Selbo, P. K. Light-triggered, efficient cytosolic release of IM7-saporin targeting the putative cancer stem cell marker CD44 by photochemical internalization. *Mol. Pharmaceutics* **2014**, *11*, 2764−2776.

(26) Sultan, A. A.; Jerjes, W.; Berg, K.; Høgset, A.; Mosse, C. A.; Hamoudi, R.; Hamdoon, Z.; Simeon, C.; Carnell, D.; Forster, M.; Hopper, C. Disulfonated tetraphenyl chlorin (TPCS2a)-induced photochemical internalization of bleomycin in patients with solid malignancies: a phase 1, dose-escalation, first-in-man trial. *Lancet Oncol.* **2016**, *17*, 1217−1229.

(27) Maiolino, S.; Moret, F.; Conte, C.; Fraix, A.; Tirino, P.; Ungaro, F.; Sortino, S.; Reddi, E.; Quaglia, F. Hyaluronan-decorated polymer nanoparticles targeting the CD44 receptor for the combined photo/chemo-therapy of cancer. *Nanoscale* **2015**, *7*, 5643−5653.

(28) Hamilton, S. R.; Fard, S. F.; Paiwand, F. F.; Tolg, C.; Veiseh, M.; Wang, C.; McCarthy, J. B.; Bissell, M. J.; Koropatnick, J.; Turley, E. A. The hyaluronan receptors CD44 and RHAMM (CD168) form complexes with ERK1,2 which sustain high basal motility in breast cancer cells. *J. Biol. Chem.* **2007**, *282*, 16667−16680.

(29) Toole, B. P. Hyaluronan: from extracellular glue to pericellular cue. *Nat. Rev. Cancer* **2004**, *4*, 528−539.

DOI: 10.1021/acs.molpharmaceut.8b00597
Mol. Pharmaceutics XXXX, XXX, XXX−XXX

(30) Chou, T. C.; Talalay, P. Quantitative analysis of dose-effect relationships: the combined effects of multiple drugs or enzyme inhibitors. *Adv. Enzyme Regul.* **1984**, *22*, 27−55.
(31) Chou, T. C.; Martin, N. *CompuSyn for Drug Combinations: PC Software and User's Guide: A Computer Program for Quantitation of Synergism and Antagonism in Drug Combinations, and the Determination of IC50 and ED50 and LD50 Values*; ComboSyn Inc: Paramus, NJ, 2005.
(32) Chou, T. C. Theoretical basis, experimental design, and computerized simulation of synergism and antagonism in drug combination studies. *Pharmacol Rev.* **2006**, *58*, 621−681.
(33) Lilletvedt, M.; Tønnesen, H. H.; Høgset, A.; Sande, S. A.; Kristensen, S. Evaluation of physicochemical properties and aggregation of the photosensitizers TPCS2a and TPPS2a in aqueous media. *Pharmazie* **2011**, *66*, 325−333.
(34) Pinto, A. C.; Ângelo, S.; Moreira, J. N.; Simões, S. Schedule treatment design and quantitative in vitro evaluation of chemotherapeutic combinations for metastatic prostate cancer therapy. *Cancer Chemother. Pharmacol.* **2011**, *67*, 275−284.
(35) Cummings, B. S.; Schnellmann, R. G. Measurement of cell death in mammalian cells. *Curr. Protoc Pharmacol.* **2004**, 12.
(36) Wang, L. G.; Liu, X. M.; Kreis, W.; Budman, D. R. The effect of antimicrotubule agents on signal transduction pathways of apoptosis: a review. *Cancer Chemother. Pharmacol.* **1999**, *44*, 355−61.
(37) Olsen, C. E.; Berg, K.; Selbo, P. K.; Weyergang, A. Circumvention of resistance to photodynamic therapy in doxorubicin-resistant sarcoma by photochemical internalization of gelonin. *Free Radical Biol. Med.* **2013**, *65*, 1300−1309.
(38) Weyergang, A.; Cheung, L. H.; Rosenblum, M. G.; Mohamedali, K. A.; Peng, Q.; Waltenberger, J.; Berg, K. Photochemical internalization augments tumor vascular cytotoxicity and specificity of VEGF(121)/rGel fusion toxin. *J. Controlled Release* **2014**, *180*, 1−9.
(39) Hu, C. M.; Zhang, L. Nanoparticle-based combination therapy toward overcoming drug resistance in cancer. *Biochem. Pharmacol.* **2012**, *83*, 1104−1111.
(40) Brooks, T. A.; Minderman, H.; O'Loughlin, K. L.; Pera, P.; Ojima, I.; Baer, M. R.; Bernacki, R. J. Taxane-based reversal agents modulate drug resistance mediated by P-glycoprotein, multidrug resistance protein, and breast cancer resistance protein. *Mol. Cancer Ther.* **2003**, *2*, 1195−1205.
(41) Murray, S.; Briasoulis, E.; Linardou, H.; Bafaloukos, D.; Papadimitriou, C. Taxane resistance in breast cancer: Mechanisms, predictive biomarkers and circumvention strategies. *Cancer Treat. Rev.* **2012**, *38*, 890−903.
(42) Wang, L.; Jia, E. Ovarian cancer targeted hyaluronic acid-based nanoparticle system for paclitaxel delivery to overcome drug resistance. *Drug Delivery* **2016**, *23*, 1810−1817.

DOI: 10.1021/acs.molpharmaceut.8b00597
Mol. Pharmaceutics XXXX, XXX, XXX−XXX

Supporting Information

Co-delivery of docetaxel and disulphonate tetraphenyl chlorin in one nanoparticle produces strong synergism between chemo- and photodynamic therapy in drug-sensitive and -resistant cancer cells

Elisa Gaio[1], Claudia Conte[2], Diletta Esposito[2], Giovanni Miotto[3], Fabiana Quaglia[2], Francesca Moret[1*], Elena Reddi[1]

[1] Cell Biology Unit, Department of Biology, University of Padova, Padova, Italy
[2] Drug Delivery Laboratory, Department of Pharmacy, University of Napoli Federico II, Napoli, Italy
[3] Department of Molecular Medicine, University of Padova, Padova, Italy

*Corresponding Author: e-mail: francesca.moret@unipd.it; Address: Department of Biology, Via Ugo Bassi 58/B, 35121 Padova, Italy. Telephone: +39 049 8276282.

Materials and Methods

Caspase 3 assay

HeLa and MDA-MB-231 cells were seeded (3 x 10^5 and 5 x 10^5, respectively) in 100 mm dishes. After 24 h of growth, cells were incubated with DTX, TPCS2a or DTX + TPCS2a using the same conditions as in the cytotoxicity experiments. At the end of incubation time, cells were washed twice with PBS and then lysed in Cell Lysis Buffer (included in the CaspACE™ Assay System,) by performing a 3 freeze-thaw cycles. The cell lysates were centrifuged for 10 min at 15000 x g at 4 °C, and the supernatant was collected and stored at -80 °C. The protein content of each extract was determined using the Bradford method. Each untreated (control cells) and treated cell extract was combined with the appropriate amounts of Caspase Assay Buffer, DMSO, DTT, water and caspase-3 substrate as described in the CaspACE TM Technical Bulletin, (#TB270). Samples were incubated overnight at room temperature and then the enzymatic activity of caspase-3 was measured using a BioSpectrometer (Eppendorf) reading sample absorbance at 405 nm. The values of the specific caspase-3 activity were corrected for the incubation time of the assay and the amount of protein loaded for each sample (nmol tot/h/mg of protein).

Western blot analysis

HeLa-P and HeLa-R cells were grown in DMEM supplemented with 10% of FBS, then harvested and lysed in RIPA buffer (150 mM NaCl, 1% NP-40, 0.5% sodium deoxycholate, 0.1% SDS and 50 mM Tris) supplemented with protease inhibitor cocktail, sodium orthovanadate (1mM) and sodium fluoride (10mM). Whole cell lysates were normalized for protein content using the Bradford method. Forty µg of proteins were resolved by a Mini-PROTEAN TGX Precast Protein Gel (10%, Biorad, USA), transferred to a nitrocellulose membrane (Biorad) for 2 h at 4 °C at 200 milliA. Membrane was then blocked for 1 h in 2% milk, 0.1 % Tween 20 in PBS buffer. After washing twice for five min with 0.1 % Tween 20-PBS buffer, membrane was incubated overnight at 4 °C with anti-Pgp antibody (ab170904, Abcam, Cambridge, UK) and anti-β-actin antibody (Abcam, Cambridge, UK). The membrane was washed other four times for 5 min, and then incubated with the anti-mouse and anti-rabbit secondary antibodies (Abcam, Cambridge, UK) for 1 h at room temperature. At the end of incubation, membrane was washed and developed by enhanced chemi-luminescent detection reagent (Clarity™ Western ECL Substrate, Biorad). The quantitative analysis of the protein bands in the blots was performed using Image J software.

Supplementary Figures

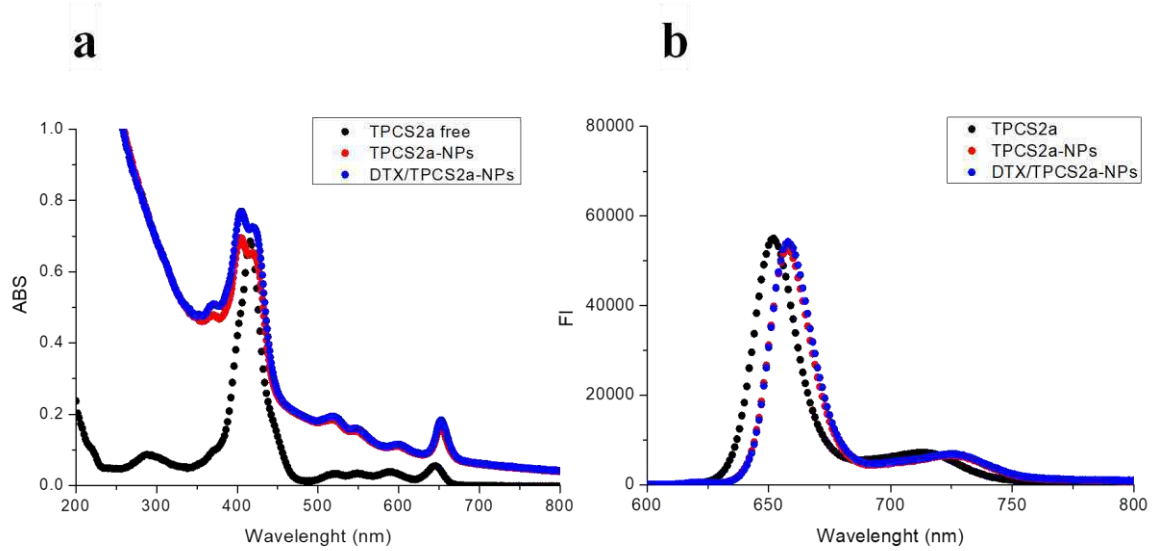

Figure S1. UV and emission spectra of NPs compared to free TPCS2a in water. TPCS2a concentration was 5 ug/mL.

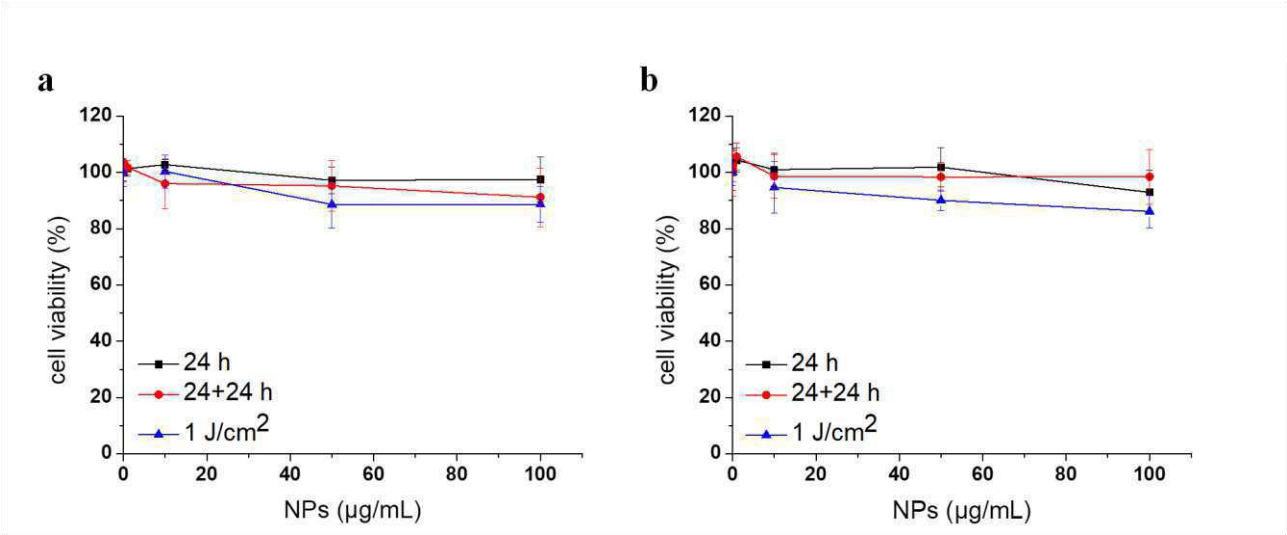

Figure S2. Cytotoxicity of unloaded NPs. Viability measured in HeLa (a) and MDA-MB-231 (b) cells exposed to increasing concentrations of empty NPs for 24 h as well as 24 + 24 h in the dark or exposed to NPs for 24 h and irradiated with 1 J/cm^2 of red light. Cell viability was measures with MTS assay and data are expressed as mean percentage ± S.D. of at least three independent experiments, carried out in triplicate.

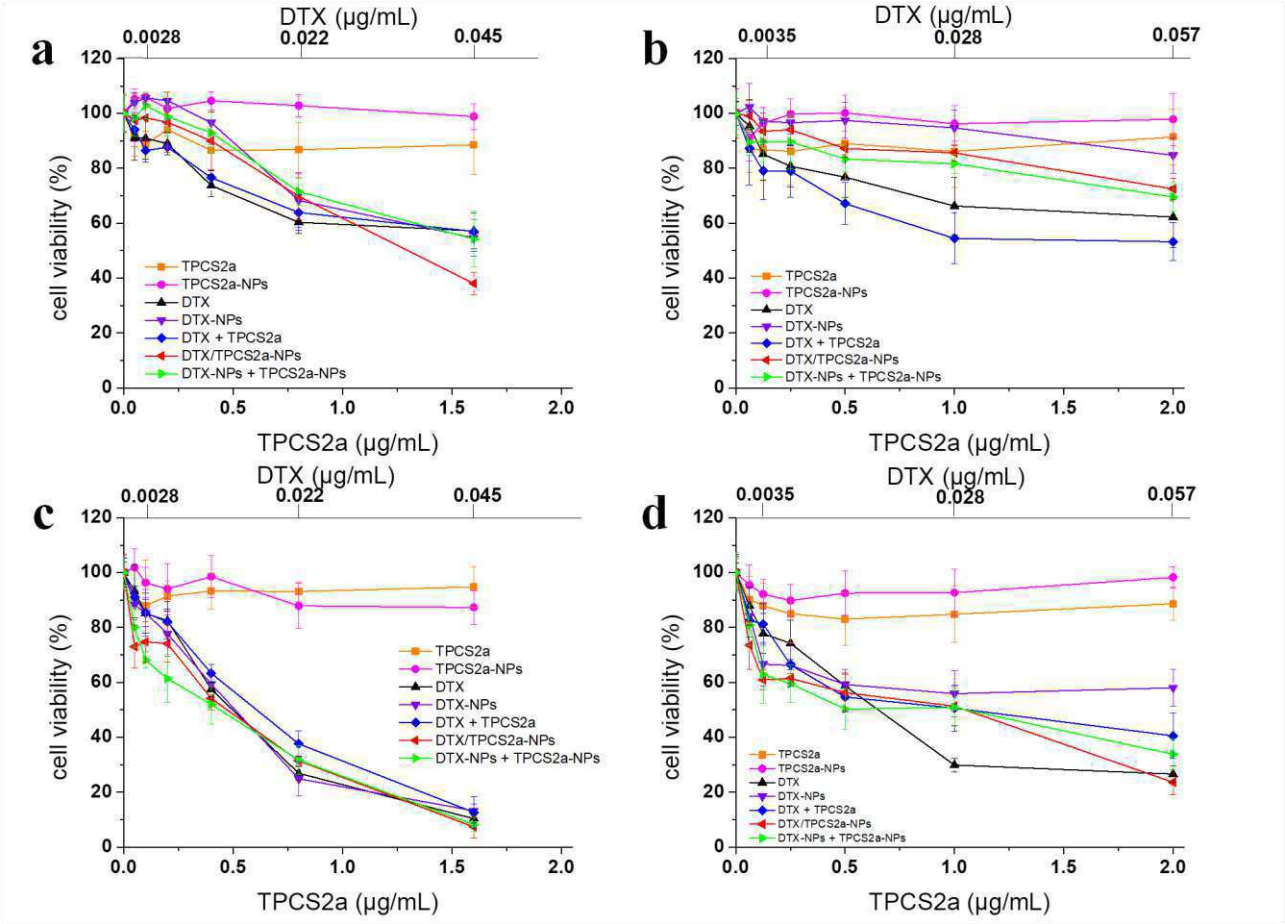

Figure S3. Dark Cytotoxicity. Viability of HeLa (a, c) and MDA-MB-231 (b, d) cells exposed to DTX, TPCS2a and their combination in the standard solvents or in NPs after 24 h (a, b) as well as 24 + 24 h (c, d) of drug incubation. Cell viability was measures with MTS assay and data are expressed as mean percentage ± S.D. of at least three independent experiments, carried out in triplicate.

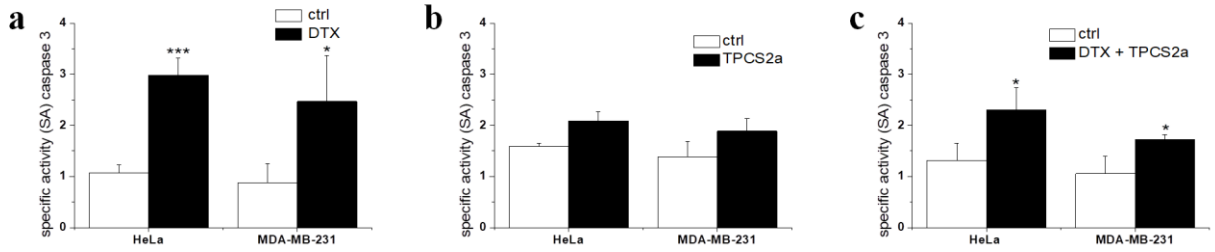

Figure S4. Caspase-3 activation in HeLa and MDA-MB-231 cells incubated for 24+24h with free DTX (a), exposed to TPCS2a-PDT (b) or to combination therapy (c). Data are expressed as mean percentage ± S.D. of at least three independent experiments. *: $p < 0.05$, **: $p < 0.01$; ***: $p < 0.001$ significantly different from control cells (Student's t-test).

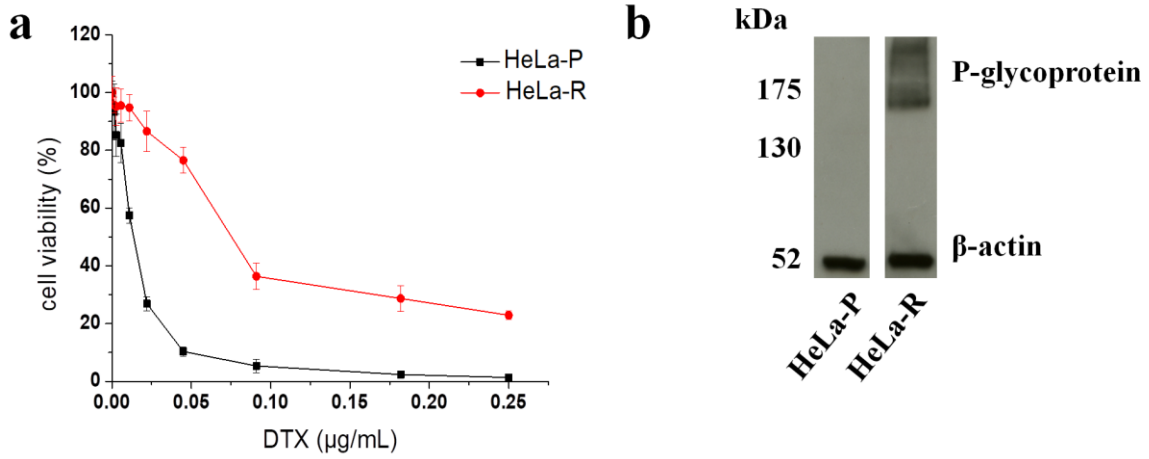

Figure S5. Characterization of DTX-resistant HeLa cells (Hela-R). Comparative dose-response curves (a) of HeLa-P and HeLa-R incubated with DTX for 24 h and assessed for cell viability with the MTS assay 24 h post the release in DTX-free medium (24 + 24 h). Western blot analysis (b) of P-glycoprotein 1 (P-gp) protein in cell lysates of HeLa-P and HeLa-R cells.

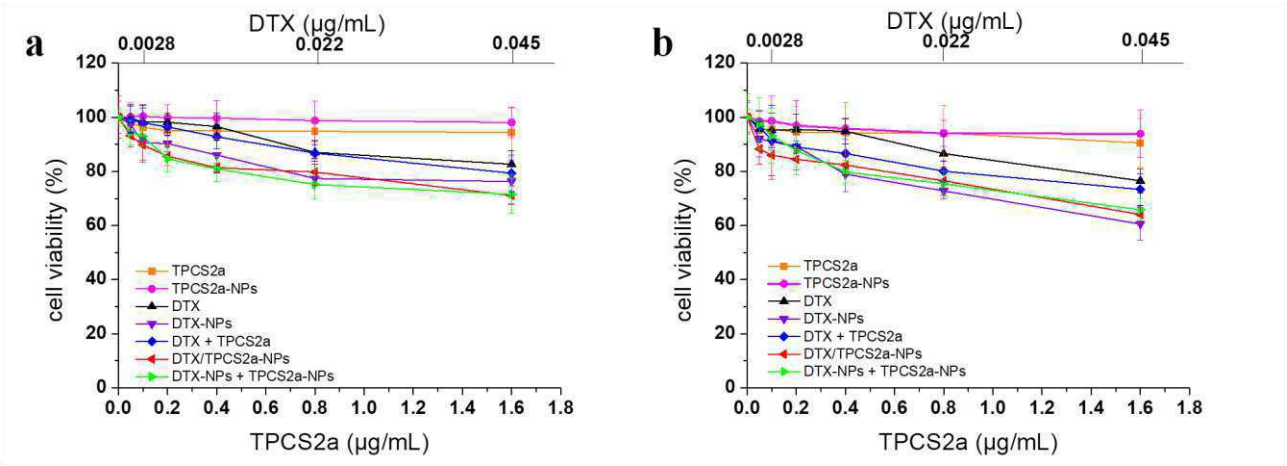

Figure S6. Dark Cytotoxicity in DTX-resistant HeLa cells (HeLa-R). Viability measured in cells exposed to DTX, TPCS2a and their combination in the standard formulations (free) or in NPs after 24 h (a) as well as 24 + 24 h (b) of drug incubation. Cell viability was measures with MTS assay and data are expressed as mean percentage ± S.D. of at least three independent experiments, carried out in triplicate.

Supplementary Table

Table S1. Data for Fa = 0.5 of HeLa, MDA-MB-231 and HeLa-R.

Data for Fa = 0.5	Drug dose (μg/mL)			
Drug Formulation	**TPCS2a**	**DTX**	**TPCS2a-NPs**	**DTX-NPs**
HeLa				
TPCS2a	0.39255			
DTX		0.01139		
TPCS2a-NPs			0.52872	
DTX-NPs				0.01108
DTX + TPCS2a	0.19695	0.00563		
DTX/TPCS2a-NPs	0.14972	0.00428		
DTX-NPs + TPCS2a-NPs	0.18419	0.00526		
MDA-MB-231				
TPCS2a	0.32248			
DTX		0.01661		
TPCS2a-NPs			0.45552	
DTX-NPs				0.06783
DTX + TPCS2a	0.19477	0.00556		
DTX/TPCS2a-NPs	0.05403	0.00154		
DTX-NPs + TPCS2a-NPs	0.15570	0.00445		
HeLa-R				
TPCS2a	0.34544			
DTX		0.83160		
TPCS2a-NPs			0.53780	
DTX-NPs				0.10678
DTX + TPCS2a	0.41150	0.01176		
DTX/TPCS2a-NPs	0.27912	0.00797		
DTX-NPs + TPCS2a-NPs	0.47159	0.01347		

Paper II

Synergic effects of chemo- and photodynamic therapy in 3D tumor cell models treated with nanoparticles co-delivering docetaxel and disulphonate tetraphenyl chlorin

Elisa Gaio[a], Claudia Conte[b], Fabiana Quaglia[b], Francesca Moret[a], Elena Reddi[a].

[a] Cell Biology Unit, Department of Biology, University of Padova, Padova, Italy

[b] Drug Delivery Laboratory, Department of Pharmacy, University of Napoli Federico II, Napoli, Italy

ABSTRACT: Layer-by-layer nanoparticles (NPs) are considered promising tools to realize combination therapy of cancer. In this study PLGA-based HA-targeted layer-by-layer NPs were successfully synthetized and co-loaded with the chemotherapeutic docetaxel (DTX) and the photosensitizer meso-tetraphenyl chlorin disulphonate (TPCS2a) at 3 different drug ratios. These nanoformulations (DTX/TPCS2a-NPs 1:35, 1:5 and 1:3) were tested in different 3D tumor models including the avascular multicellular tumor spheroids (HeLa and DTX –resistant HeLa cells) and mammospheres of MCF-7 and MDA-MB-231 cells as cultures enriched of cancer stem cells (CSCs) and overexpressing CD44 receptor. This aspect could allow to exploit the HA targeting of our nanosystem. In spheroids, DTX/TPCS2a 1:35 gave antagonism, while 1:5 and 1:3 ratios induced a synergistic effects. In particular, in DTX –resistant spheroids, we obtain the highest extent of synergism (CI<1) using NPs co-loaded with drugs at 1:3 ratio. Combinatorial treatments with DTX and TPCS2a co-encapsulated in the same vehicle demonstrated also some extent of efficacy in the suppression of sphere formation due to the presence of CSCs in both breast cancer cell lines considered. These results highlighted the advantages of using HA-targeted layer-by-layer NPs as delivery vehicle for DTX and TPCS2a at fixed drug ratios to combined chemo and photodynamic therapy of cancer.

INTRODUCTION

The combinations of different chemotherapeutic drugs and or modalities of treating cancer are increasingly recognized as valuable tools to potentiate the treatment efficacy while decreasing unwanted toxicity to normal cells and development of drug resistance at the same time. Thus, cocktails of drugs are already widely used in standard therapeutic protocols for the treatment of various types of cancer and chemotherapy is very often applied before or after surgical removal of tumors or is combined to radiotherapy[1,2]. In the recent years, more and more preclinical studies are being carried out on the combination of photodynamic therapy (PDT) with the well-established chemotherapy, largely utilized for the treatment of many types of solid tumors. PDT is an emerging modality of treating cancer based on the use of a photosensitizing drug (PS) that exhibits some preferential accumulation in the tumor tissue and, following activation with red/near-infrared light, generates reactive oxygen species that causes photooxidative damages in tumor cells and tumor vasculature[3]. In addition, PDT elicits inflammatory and immunity responses which are very important for long-term control of tumor growth [4]. The exclusive activation of the PS localized in the tumor guarantees selectivity of the PDT treatment but limits

effectiveness in metastatic tumors that can however be increased by the combination with chemotherapeutics exhibiting more systemic effects. A higher efficacy of the combination of PDT and chemotherapy with respect to the efficacy of the monotherapies, has been reported for several cancer cell lines *in vitro* and tumor models *in vivo*[5,6,7]. The studies, aimed at demonstrate the benefits of the combination, highlighted also that the best results could be obtained by delivering the chemotherapeutic and the PS encapsulated in nanocarriers[8,9]. It is in fact well established that for successful combination therapy an optimized drug concentration ratio has to be delivered into the tumor and this fixed ratio can be more easily controlled using nanoparticles (NPs), co-loaded with the two drugs, as delivery vehicles. Currently, the most employed *in vitro* models for screening the efficacy of monotherapies or combination therapies are tumor cell monolayers. However, this cell culture model does not reproduce at all the complexity and heterogeneity that characterize solid tumors *in vivo.* In fact, when grown attached to flat surfaces, cells show altered morphology, gene expression and signaling[10]. Thus, the results of drug toxicity obtained exclusively in cell monolayers may not adequately predict the effective potential of therapeutic agents *in vivo,* with consequent failure of clinical development, because of discovery of lack of efficacy and/or unacceptable toxicity, at late stages of the evaluation process[11]. On the contrary, cultivation of cancer cells in a tridimensional arrangement allows the establishment of cell-cell interactions, recreates the extracellular matrix and the oxygen and nutrient concentration gradients that are found *in vivo*. These characteristics of a solid tumor *in vivo* can be reproduced in multicellular tumor spheroids[12]. For instance, Sarisozen *et al.* reported a good correlation between tumor inhibition studies *in vivo* and 3D tumor spheroids when studying the efficacy of the combination of paclitaxel and curcumin co-delivered to drug resistant ovarian cancers by polymeric micelles[13]. On the contrary, Barros and colleagues reported different synergistic effects in 2D and 3D pancreatic tumor models using the doxorubicin-resveratrol combination administered at the same concentration ratios[14]. In fact, the doxorubicin-resveratrol 1:4 and 1:5 ratios showed a combination index (CI) of about 8 and 5 times lower in 2D models than in spheroids indicating higher synergistic interaction in cell monolayer. This observation confirms the risk to overestimate the treatment efficacy when only cell monolayers are used.

Tumors are formed by a rather heterogeneous population of cells exhibiting different sensitivity towards chemotherapeutics because characterized by different proliferation rate, expression of antiapoptotic mechanisms and multidrug resistant pumps, responsible for chemotherapeutic resistance. A small fraction of cells particularly resistant to chemotherapy is represented by cancer stem cells (CSCs) that are considered major responsible of the failure of conventional cancer therapies. CSCs are difficult to be eradicated because of slow proliferation, and consequently low sensitivity to antimitotic agents, activation of DNA repair mechanisms and overexpression of different membrane efflux pumps, leading to the development of resistance to chemotherapeutic agents[15]. Combinatorial therapy based on the use of therapeutics acting against different targets can help to overcome this problem and, in particular, the combination of chemotherapy with PDT appears a promising strategy to investigate toward the eradication of CSCs.

We have already demonstrated that the combination of the chemotherapeutic docetaxel (DTX) and the photosensitizer disulphonate tetraphenyl chlorin (TPCS2a), for PDT application, is more effective than monotherapies towards drug sensitive and resistant tumor cells grown in monolayers. In these culture conditions, we found the strongest synergism between chemotherapy and PDT by co-delivering DTX and TPCS2a at a 1:35 concentration ratio entrapped in polymeric hyaluronan (HA)-decorated double-layer NPs with a core-shell organization[16].

Here, we aimed at assessing whether the DTX/TPCS2a nanoformulation which exhibit strong cytotoxicity and synergism in the cell monolayers performs equally well in 3D cultures and in particular if the loaded drug

ratio is optimal or have to be modified for obtaining synergic interaction between chemotherapy and PDT. Thus, DTX and TPCS2a were co-loaded in the HA-NPs (DTX/TPCS2a-NPs) at different concentration ratios and tested in multicellular tumor spheroids of HeLa cells sensitive (HeLa-P) or resistant (HeLa-R) to DTX.

Furthermore, to assess the potential of our DTX/TPCS2a-NPs to kill also CSCs, we used the same nanoformulation to perform combination therapy in MCF-7 and MDA-MB-231 derived breast spheres cultures (mammospheres), differently enriched in CSCs[17]. Here, the rationale is that PDT can kill also CSCs because they are not resistant to PDT and HA, forming the surface coat of our NPs, is a ligand for the CD44-receptor overexpressed by CSCs, and therefore DTX/TPCS2a-NPs can target CSCs by exploiting active targeting mechanisms.

EXPERIMENTAL SECTION

Chemicals and Reagents. Meso-tetraphenyl chlorin disulphonate (TPCS2a) was provided by PCI Biotech AS (Norway). DTX was purchased from LC Laboratories (USA). TPCS2a and DTX solutions were prepared by dissolving known amounts of powder in ethanol and DMSO, respectively. Poly (D,L-lactide-*co*-glycolide) (PLGA) (50:50 Resomer RG 502H inherent viscosity 0.16-0.24 dl/g) was purchased from Boehringer Ingelheim (Ingelheim, Germany). PEI (MW= 10-25 kDa branched) and Poloxamer 188 (Pluronic® F68) were purchased from Sigma-Aldrich. Acetonitrile and acetone were purchased from Carlo Erba Reagenti (Milan, Italy). Hyaluronic acid (HA, MW <10 kDa) was a kind gift of Magaldi Life S.r.l. Dulbecco's modified Eagle's medium (DMEM), DMEM/F12 medium, fetal bovine serum (FBS) and B27 mix were purchased from Life Technologies (Milan, Italy). CellTiter-Glo® 3D Cell Viability Assay was from Promega Co. (Madison, USA).

Synthesis and characterization of NPs. DTX/TPCS2a-NPs co-loaded with DTX and TPCS2a starting from 3 different weight ratios (1:1, 1:5 and 1:35) were prepared by a layer-by-layer deposition method as previously described by us[18,16]. Briefly, DTX-NPs were prepared by solvent diffusion of an organic phase (10 mg of PLGA and 250 μg, 50 μg or 7.5 μg of DTX in 2 mL of acetone, for the ratio 1:1, 1:5 and 1:35 respectively) in an aqueous phase (4 mL of water added with Pluronic F68 0.1%). After solvent evaporation, the dispersion was centrifuged at 5000 *g* for 15 min and then NPs were firstly coated with 125 μL of a PEI water solution (1 mg/mL), re-centrifuged at 2800 *g* for 15 min and then 25 μL of a TPCS2a water solution (0.4 mg/mL) was added. Thereafter, NPs were finally coated with a second layer of HA through the addition of 100 μL of a HA water solution (1 mg/mL), maintaining constant the interval between each addition at 15 min. NPs were finally freeze-dried for 24 h and the recovery yield of the production process was evaluated on an aliquot of NPs by weighting the solid residue. Results of the quantification are expressed as the ratio of the actual NP weight to the theoretical polymer + drug weight × 100. As control, unloaded NPs, DTX-NPs (3 different formulation with the 3 corresponding DTX loading) and TPCS2a-NPs were prepared.

NP characterization was performed as described in our previous paper[16]. Briefly, hydrodynamic diameter, polydispersity index (PI) and zeta potential of NPs after each preparation step were determined on a Zetasizer Nano Z (Malvern Instruments Ltd., UK). UV/Vis absorption spectra of DTX/TPCS2a-NPs dispersed in water compared to the free TPCS2a (5 μg/mL) were recorded with a UV 1800 spectrophotometer (Shimadzu, Japan). DTX loading inside NPs was assessed by HPLC on a Shimadzu apparatus equipped with a LC-10ADvp pump, a SIL-10ADvp autoinjector, a SPD-10Avp UV–Vis detector and a C-R6 integrator. The analysis was performed on a Juppiter 5 μm, C18 column (250 × 4.6 mm, 300Å). TPCS2a loading inside NPs was evaluated by measuring its concentration, by UV spectrophotometry, in the supernatant after NP centrifugation at 17000 *g* for 15 min.

Cell lines. HeLa human cervix and MCF-7 and MDA-MB-231 human breast cancer cells were purchased from American Type Tissue Culture Collection (ATCC, Rockville, USA). The cells were grown in DMEM with Glutamax™ supplemented with 10% heat-inactivated FBS, 100 U/mL streptomycin and 100 µg/mL penicillin G (all from Life Technologies), and maintained at 37 °C under a humidified atmosphere containing 5% CO_2. A DTX-resistant HeLa cell line (HeLa-R) was obtained in our laboratory by cultivating HeLa parental (HeLa-P) cells in DMEM supplemented with intermittent low and increasing DTX concentrations (0.002-0.008 µg/mL) for seven months as described in[16].

Generation of multicellular tumor spheroids. Spheroids of HeLa and HeLa-R cells were generated using the liquid overlay method, as previously reported[19]. The cells were harvested from monolayer cultures by trypsinization and seeded in flat-bottomed 96-well plates (1000 cells/well) previously coated with 1% agarose in DMEM in order to prevent cell adhesion. Immediately after seeding, the plates were centrifuged at 200 g for 5 min in order to promote cell aggregation and then placed in the incubator.

Cytotoxicity assay in spheroids. Three day-old spheroids, that reached a mean diameter of 200 µm, were incubated with 100 µL of fresh medium containing 10% of heat-inactivated FBS and increasing concentration of TPCS2a-NPs, DTX-NPs or DTX/TPCS2a-NPs carrying the two drugs loaded at three different ratios. After 24 h of incubation, spheroids were washed with PBS containing Ca^{2+} and Mg^{2+} and irradiated in PBS with a total light fluence of 7.5 J/cm^2 of red light (power density 25 mW/cm^2). Immediately after irradiation, the cells were brought back to the incubator after the replacement of PBS with fresh medium. Cell viability was measured using the CellTiter-Glo® 3D Cell Viability Assay after additional 24 h of cell release in drug-free medium. For the assay, only 50 µl of cell medium were left in each well containing one spheroid, and 50 µl of CellTiter-Glo® 3D Reagent were added; the well content was mixed and shacked for 5 min, incubated at room temperature for 25 min and luminescence was measured using a Perkin Elmer Envision instrument. Viability of treated spheroids was expressed as percentage of the luminescence value of control cells that was taken as 100 % viability. Moreover, at established time-points during the experiment, the morphological changes induced by NPs treatments were monitored by acquisition of bright field images with a microscope (DMI6000B, Leica) equipped with a DCF365FX camera.

Median-effect analysis, determination of Combination Index (CI) and Drug Reduction Index (DRI). In order to assess if the interaction of DTX-chemotherapy and TPCS2a-PDT resulted in a synergic effect, CI and DRI values were calculated using the CompuSyn software (ComboSyn Inc., NJ, USA), based on the Chou and Talalay method[20]. From the experimental data obtained from the cell viability curves we calculated the Fraction affected (Fa) values for each drug concentration tested and analyzed the data on the Compusyn software as already described[16]. The program reported also for each drug/combination of drugs the value of the drug concentration that inhibits cell survival by 50% (IC_{50} or Dm value).

TPCS2a localization and diffusion into spheroids. Spheroids were generated as described above and treated for 24 h with 2 µg/mL of TPCS2a delivered in the standard solvent or loaded in TPCS2a-NPs or DTX/TPCS2a-NPs. The localization of TPCS2a was evaluated by confocal microscopy (Leica SP5) by transferring the spheroids from 96-well/plates to 35 mm cell imaging dishes and washing them twice with PBS before visualization. Images were acquired from the top to the bottom of the spheroid in about 20 different focal planes. For the comparison of penetration of TPCS2a in the spheroids, 15 radial lines (regions of interest, ROI) were randomly drawn in each image of the equatorial plane and fluorescence at each pixel was recorded with the LAS AF Lite software. Furthermore, a 3D

reconstruction of the distribution of the fluorescence signal in the equatorial plane of spheroids was obtained using the software ImageJ.

Generation of CSCs-enriched mammospheres. Single cells of MCF-7 and MDA-MB-231 lines were plated in 24-well ultralow attachment flat-bottom plates (Corning, USA) at a density of 5000 and 100000 viable cells/mL, respectively, in serum-free DMEM-F12 supplemented with B27 (1:50, Invitrogen), 20 ng/mL epidermal growth factor (EGF), 20 ng/mL basic fibroblast growth factor (bFGF) (Peprotech, UK), and 5 µg/mL insulin (Sigma Aldrich) and grown for 7 and 4 days respectively. To re-propagate the so-called second generation of mammospheres, the formed mammospheres were collected on day 7 or 4 from seed, gently centrifuged (123 x g, 10 min) and dissociated to single cells by using 0.25% trypsin/EDTA (Life Technologies). The dissociated cells were re-seeded as indicated for the first generation mammospheres in order to obtain the corresponding second generation. The number of mammospheres formed on each generation (day 7 or 4 from seed) was obtained by counting the numbers of spheres from bright field microscopy acquired images. The mean diameter of each mammosphere was calculated with the LAS AF Lite software and mammosphere having a diameter below 100 µm were excluded from the counting analysis.

Flow cytometry analysis of CSCs-marker in mammospheres. Mammospheres of MCF-7 and MDA-MB-231 (7 days from seed) were collected and enzymatically dissociated into a single cell suspension; 1 x 10^5 cells were collected, washed twice with cold PBS and maintained on ice. In parallel, the same number of cells was collected from MCF-7 and MDA-MB-231 cells routinely cultured on T-75 cm^2 flasks. After a second step of washing, a combination of monoclonal antibodies against human CD44 (FITC-conjugated) and CD24 (PE-conjugated) (BD Biosciences, San Diego, CA, USA) was added to the cell suspension and incubated at 4°C in dark for 30-40 minutes. Labeled cells were washed in PBS to eliminate unbounded antibodies, and then analyzed with a BD FACSCanto™ II (Becton Dickinson, San Jose, USA) flow cytometer.

Cytotoxicity assay in mammospheres (sphere forming assay). Mammospheres of MCF-7 and MDA-MB-231 were generated as described above and at day 7 or 4 from seed, spheres were treated directly in ultra low attachment plates with DTX or/and TPCS2a delivered in NPs for 24 h. At the end of the incubation time, spheres were irradiated with 1 J/cm^2 of red light and then dissociated and re-seeded in non-adherent condition to allow the formation of second-generation mammospheres. The number of spheres for each treatment condition was evaluated in bright-field microscopy after additional 7 or 4 days and comparing first and second generation. Mammosphere formation efficiency (MFE) was calculated as the number of spheres divided by the original number of cells seeded and expressed as percentage means ± SD. In alternative, MFE was calculated starting from cell seeded and treated in monolayer. Cells of both cell lines (5 x 10^5) were seeded in 60 mm tissue culture dishes and, after 24 h of growth, were treated with DTX or/and TPCS2a delivered in NPs. At the end of the incubation, cells were irradiated as described for the other protocol mentioned above. Immediately after irradiation, MCF-7 and MDA-MB-231 cells were detached and then 5000 and 100000 cells/mL respectively were re-seeded in ultralow attachment plate to allow sphere formation. Sphere formed for each treatment condition (diameter > 100 µm) were counted after 7 or 4 days from seeding.

Statistical analysis. The Primer software for biostatistics (McGraw-Hill, Columbus, USA) was used for statistical analysis of the data. The data are expressed as means ± standard deviations (SD) for at least 2 independent experiments in triplicate. The difference between groups was evaluated with the Student's t-test and was considered significant for $p < 0.05$.

RESULTS AND DISCUSSION

Recently, we have reported on the successful use of HA-decorated double-layer-NPs co-loaded with the chemotherapeutic DTX and the PS TPCS2a for the synergic killing of DTX –sensitive and –resistant cancer cell monolayers *in vitro*[16]. The optimal drug ratio between DTX/TPCS2a of 1:35 was efficiently loaded in NPs and the combination of chemotherapy and PDT using NPs was significantly more effective in inducing cytotoxicity in DTX-sensitive cells (HeLa and MDA-MB-231) than the combination of the free drugs delivered in the standard solvent. Moreover, the nanoformulation demonstrated to be particularly appealing for the treatment of cells with induced DTX-resistance (HeLa-R cells); in fact it allowed an impressive chemotherapeutic dose reduction (about 100 times) compared to the therapy with the conventional drugs. Based on these very promising results, the aim of the present study was to assess whether the extent of synergism produced by DTX/TPCS2a-NPs therapy and measured in cell monolayers was equally effective in more complex *in vitro* tumour models, as multicellular tumour spheroids. It is well known that drug accumulation in cells in 3D models is worse compared to cells in monolayers, and therefore we preliminarly assessed the efficacy of DTX-chemotherapy and TPCS2a-PDT monotherapy in HeLa spheroids (data not shown) in order to identify some suitable drug ratios to be loaded in NPs. Based on this, in addition to the drug ratio of 1:35 already explored in monolayer cultures, we prepared and studied the performances of DTX/TPCS2a NPs loaded with the drug ratios of 1:5 and 1:1.

NPs preparation. Leaving unaltered the synthesis procedure already described[16] for the preparation of DTX/TPCS2a-NPs with the drug ratio of 1:35 (formulation C), we were able to prepare also the nanoformulation containing DTX/TPCS2a in the ratio 1:5 (formulation B), with drug entrapment efficiencies higher than 95% (Table 1). Unfortunately, we were unable to prepare DTX/TPCS2a-NPs co-loading the drugs in the ratio 1:1 (formulation A), since starting from a theoretical loading of 2.5% respect to copolymer weight, we found an entrapment efficiency of 36%, thus suggesting the saturation of the polymeric matrix to accommodate the drug. In any case, the saturation was not related to the presence of the PS, since also for NPs loaded exclusively with the same amount of DTX we measured a comparable DTX entrapment efficiency (39%). Thus, when we refer to formulation A the real ratio between DTX and TPCS2a inside NPs is about 1:3.

The overall properties of all the formulations are reported in Table 1, that include as controls also unloaded NPs and NPs loaded with each single drug (DTX-NPs at the three different loading and TPCS2a-NPs).

Table 1. Properties of NP formulations[a].

Formulation	µg DTX (DTX/TPCS2a weight ratio)	Size[a] (nm ±SD)	PI[b]	ZP[c] (mV ±SD)	DTX Actual loading (µg DTX/mg NPs)	DTX Entrap. Eff. (%)	TPCS2a Actual loading (µg TPCS2a/mg NPs)	TPCS2a Entrap. Eff. (%)
Unloaded NPs	-	192 ± 3	0.2	-33 ± 3	-	-	-	-
DTX-NPs A	250	177 ± 12	0.2	-30 ± 5	7.9	39 ± 2	-	-
DTX-NPs B	50	163 ± 5	0.2	-33 ± 2	5.2	98 ± 3	-	-
DTX-NPs C	7.5	202 ± 13	0.2	-31 ± 3	0.8	100 ± 3	-	-
TPCS2a-NPs	-	208 ± 6	0.2	-32 ± 7	-	-	25	97 ± 3
DTX/TPCS2a-NPs A	250 (1:1)	189 ± 10	0.2	-36.4 ± 5	8.8	36 ± 8	24	92 ± 4
DTX/TPCS2a-NPs B	50 (1:5)	205 ± 3	0.2	-37.2 ± 3	4.8	96 ± 4	24	95 ± 3
DTX/TPCS2a-NPs C	7.5 (1:35)	196 ± 8	0.2	-28.3 ± 2	0.8	100 ± 2	25	98 ± 4

[a]Data are expressed as mean percentage ± S.D. of three independent experiments. [b] Polydispersity Index. [c] Zeta Potential.

All the formulations showed a size of 180-200 nm, a polydispersity index (PI) of 0.2 and a high negative zeta potential, due to the presence of the negatively charged HA external layer. TPCS2a was adsorbed by electrostatic interactions with the PEI layer, covering the DTX-PLGA core of NPs, up to an amount of 25 µg/mg NPs, in all the 3 different DTX/TPCS2a-NPs formulations. UV-vis profiles of TPCS2a free in water or adsorbed on NP surface in the presence of DTX in the three different drug ratios are reported in Figure S1. A slight difference in terms of absorption is evidenced. In fact, despite the complete adsorption of the PS on NP core, different intensities of the scattering were found, proportionally to the amount of DTX entrapped, probably due to a different arrangement of the PS on NP surface.

Cytotoxicity and CI analysis in multicellular tumor spheroids. Three day-old spheroids of HeLa-P and HeLa-R were exposed to drugs delivered in the different nanoformulations (TPCS2a-NPs, DTX-NPs and DTX/TPCS2a-NPs) loaded with the three different drug ratios for 24 h. At the end of the incubation, spheroids were irradiated with a total light fluence of 7.5 J/cm^2 and cell viability was assessed after additional 24 h of incubation in drug-free medium (24 + 24 h) using the 3D-Glo Assay, which is based on the measurement of ATP content of cells. The dose-response curves for HeLa-P spheroids are reported in Figure 1 (drug ratio 1:35 in a, 1:5 in b and 1:3 in c), while the relative values of the drug concentration that inhibit cell survival by 50% (Dm) are listed in Table 2. As shown in the graphs, which reported the total drug concentration (DTX+TPCS2a) *vs* cell viability calculated from ATP reduction values, the encapsulation of TPCS2a in NPs significantly reduced PS photo-toxicity compared to the standard formulation (Dm of 0.775 and 0.379 for TPCS2a-NPs and TPCS2a, respectively). As one can see from the Dm values (Table 2), the NPs loaded with only DTX but in the different amounts, showed quite comparable cytotoxicity and, only slightly improved cytotoxicity with respect to those of free DTX. On the contrary, great improvement of the treatment efficacy compared to the effects of each single agent was observed when the drugs are co-delivered in DTX/TPCS2a-NPs, especially in the drug ratio 1:5 and 1:3 with Dm of 0.204 (0.034 DTX + 0.170 TPCS2a) and 0.135 µg/ml (0.067 DTX + 0.067 TPCS2a, respectively) (Figure 1b, c, Table S1) while the ratio 1:35 demonstrated the worst performances (Figure 1a; Dm 0.562 µg/ml).

To support these data, bright-field microscopy was used to evaluate the alteration in spheroid morphology after NPs treatment and combination therapy (Figure 1d). As shown in the images, while untreated spheroid maintained almost unaltered spherical structure along the observation period of 5 days, increasing the DTX dose loaded in NPs and after the combination therapy, the extent of spheroid damage increased, as documented by shrinkage and loss of dead cells from the central core of the spheroids. Accordingly to cell viability results, the release of dead cells was particularly evident using DTX/TPCS2a-NPs in the drug ratio 1:3 and 1:5 (Figure 1d), while single drug loaded NPs (Figure S2) induced limited morphological alterations compared to DTX/TPCS2a-NPs.

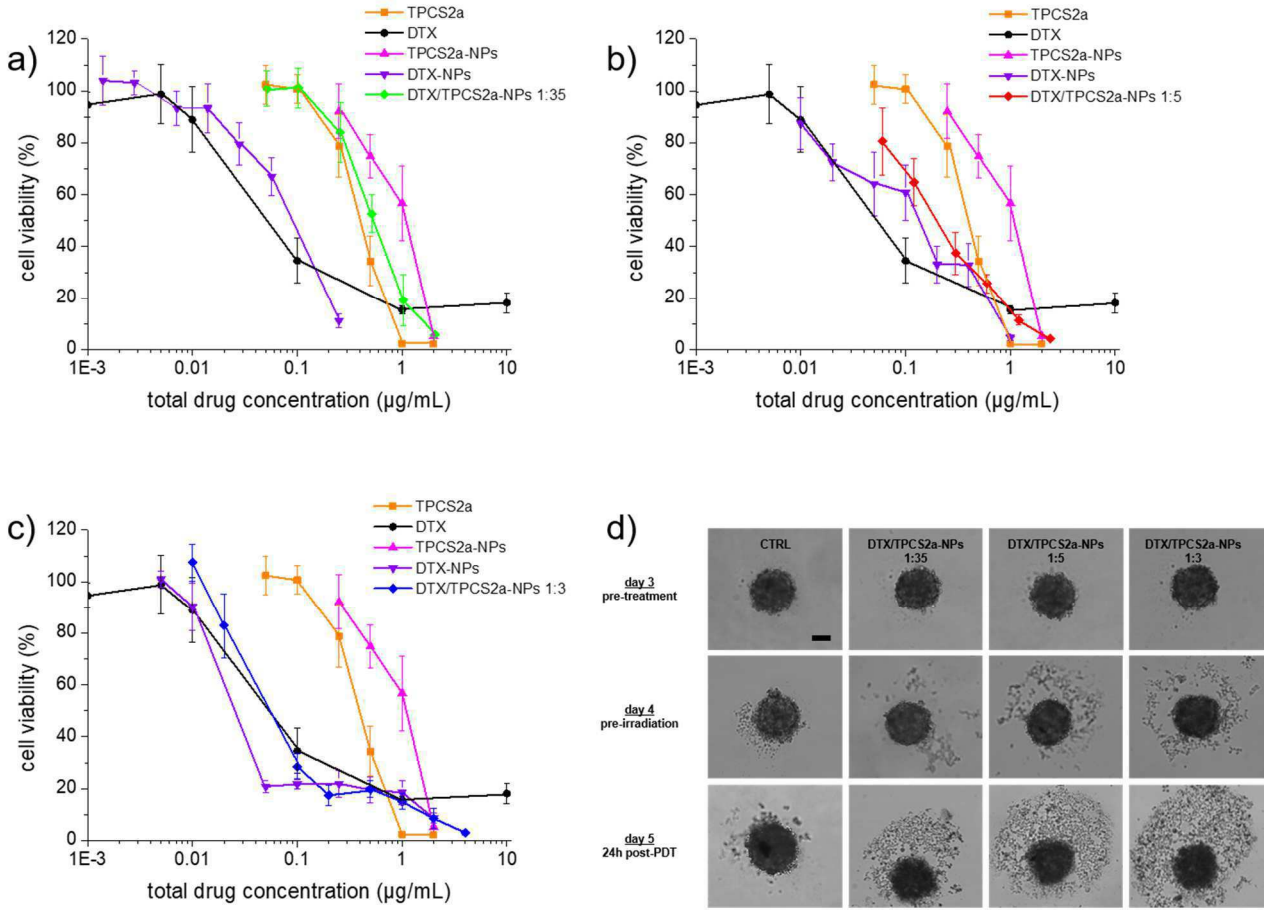

Figure 1. Combination therapy in HeLa-P spheroids. Dose-response curves of spheroids exposed to DTX-chemotherapy and/or TPCS2a-PDT with a DTX/TPCS2a concentration ratio 1:35 (a), 1:5 (b) and 1:3 (c) for 24 h. Cell viability was assessed using the 3D-Glo Assay. Data are expressed as mean percentage ± S.D. of at least two independent experiments in triplicate. d) Bright field images of: i) a representative untreated spheroid (CTRL) and ii) spheroids treated with DTX/TPCS2a-NPs drug ratios 1:35, 1:5, 1:3 monitored from day 3 (pre-treatment) to day 5 (24 h post-PDT). The spheroids incubated with the 3 different nanoformulations were exposed for 24 h to NPs on day 3, irradiated with 7.5 J/cm^2 of red light on day 4 and observed until 24 h post-PDT (day 5). The TPCS2a dose was 0.25 µg/ml while the DTX dose was 0.0071, 0.05 and 0.08 µg/ml respectively. Scale bar: 100 µm.

These results were supported by the CI analysis performed with Compusyn software. In Figure 2a is reported the combination index plot (Fa-CI plot) generated by the software in

which CI is plotted *versus* the fraction of cells affected (Fa). In this graph is clearly shown that the interaction of DTX and TPCS2a loaded in NPs in the drug ratio 1:35 was antagonistic (CI values >1). On the contrary, both the drug ratios of 1:5 and 1:3 showed the occurrence of a clear synergistic interaction (CI values < 1) between DTX-chemotherapy and TPCS2a-PDT. Comparing these latter results on CI analysis with those previously obtained by us in HeLa cell monolayers[16], in which the ratio 1:35 was sufficient to synergistically kill the cells, it is clear how introducing complexity in the cell culture models (i.e. tridimensional arrangement) may affect the overall NP performances.

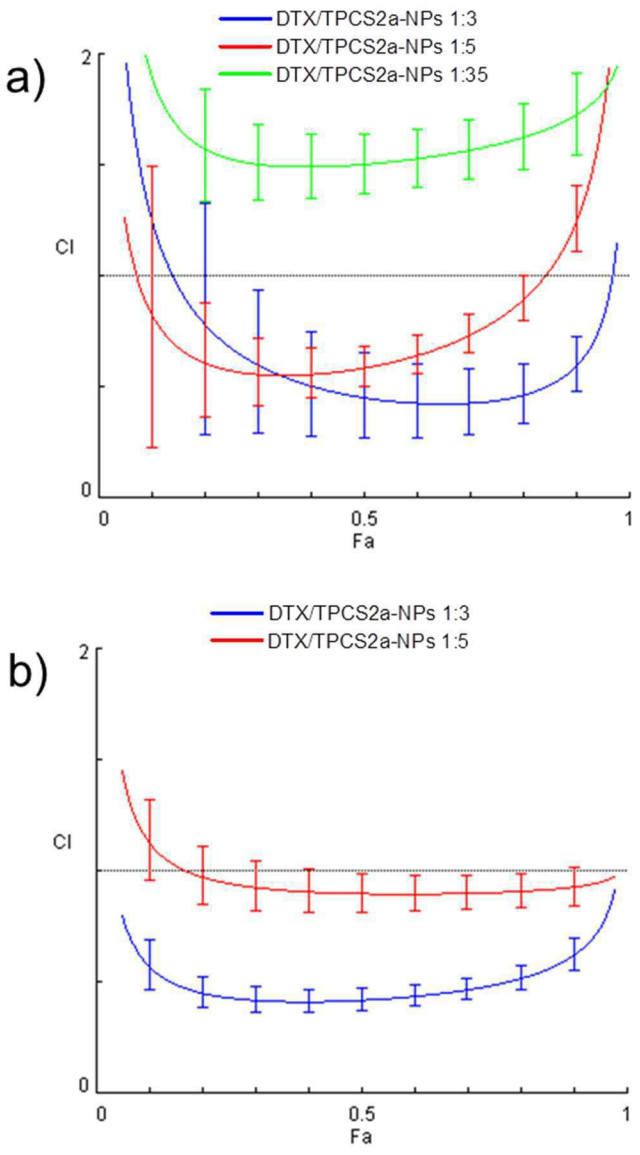

Figure 2. Combination Index Plots (Fa vs CI plots) of HeLa-P (a) and HeLa-R (b) spheroids exposed to combination therapy using the different drug ratios

The cell viability data were also analyzed to evaluate the dose reduction index (DRI) (Table 2), which indicates how many folds the concentration of each agent employed in the combination can be reduced to obtain a Fa value of 50% and, DRI > 1 and < 1 indicate favorable and not favorable dose-reduction, respectively, while DRI = 1 indicates no possibility of dose-reduction. DRI values were calculated by the Compusyn software using the doses of each single drug giving a Fa of 50% when delivered alone or in combination (Table S1). Since for 3D cell cultures higher doses of chemotherapeutic agents are required with respect to monolayers to obtained comparable Fa values, as it is expected when investigations are translated to *in vivo* models, the DRI analysis is particularly important. Moreover, reducing the dose of a therapeutic agent allows minimizing also its unwanted toxicity against normal cells and non-pathological tissue. As reported in Table 2, the Compusyn analysis underlined a favorable DRI values for anticancer drug (DRI > 1) using DTX/TPCS2a-NPs loaded with all the three drug ratios, with the possibility to reduce DTX dose of 6.33, 2.90 and 1.46 times using DTX/TPCS2a-NPs 1:35, 1:5 and 1:3 respectively compared to the use of the free chemotherapeutic. On the other hand, TPCS2a dose can be reduced of 2.23 and 5.61 times using DTX/TPCS2a-NPs with drugs loaded in the ratio 1:5 and 1:3, while no possibility of PS dose reduction is contemplated with the 1:35 drug ratio. This is probably due to the fact that in the latter case, where the dose of DTX is very low, the effect of combination is ascribable only to PS and the DTX contribution is quite negligible.

Drug formulation	Dm (µg/mL)		Dose-reduction index (DRI)			
	HeLa-P	HeLa-R	HeLa-P		HeLa-R	
			DTX	TPCS2a	DTX	TPCS2a
TPCS2a	0.379	0.473	-	-	-	-
TPCS2a-NPs	0.775	0.625	-	-	-	-
DTX	0.099	1.765	-	-	-	-
DTX-NPs 1:35	0.073		-	-	-	-
DTX-NPs 1:5	0.084	0.140	-	-	-	-
DTX-NPs 1:3	0.093	0.160	-	-	-	-
DTX/TPCS2a-NPs 1:35	0.562		6.33	0.69	-	-
DTX/TPCS2a-NPs 1:5	0.204	0.485	2.90	2.23	21.83	1.17
DTX/TPCS2a-NPs 1:3	**0.135**	0.313	1.46	5.61	11.27	3.02

Table 2. Dm (values of the drug concentration that inhibit cell survival by 50%) and dose-reduction index (DRI) calculated by Compusyn analysis in HeLa-P and HeLa-R spheroids. Dm was calculated for cells exposed to DTX-chemotherapy and/or TPCS2a-PDT using the drugs delivered in the standard formulations (free) as well as in NPs formulations. The DRI values were calculated for cells exposed to combination therapy with the different drug formulations and indicate how many folds the concentration of each single drug in combination therapy can be reduced to obtain a Fa value of 50%.

The studies described above on the combination of chemo and photodynamic therapy and analysis for synergism were performed also on HeLa-R spheroids, formed by cells that are DTX-resistant due to the overexpression of P-glycoprotein efflux pump[16]. Based on the fact that DTX and TPCS2a loaded in NPs in the drug ratio of 1:35 exhibited antagonistic effects in HeLa-P spheroids, we limited our studies to the drug ratios of 1:5 and 1:3. As reported in Figure 3a, b and similarly to that observed in HeLa-P spheroids, the encapsulation of TPCS2a in NPs did not caused improvement of photo-toxicity (Dm of 0.625 and 0.473, for TPCS2a-NPs and TPCS2a, respectively), while the delivery of DTX in NPs significantly enhanced the effect of chemotherapy. In fact, DTX-NPs enhanced more than 10 times the efficacy of the chemotherapy compared to the effect of free DTX with a calculated Dm of 0.140 µg/mL and 0.160 µg/mL for DTX-NPs 1:5 and 1:3 respectively and 1.765 µg/mL for free DTX (Table 2), indicating the ability of our nanoformulation to contrast DTX-resistance also in HeLa-R multicellular spheroids. More in details, the combination performed with the nanoformulation carrying the drug with ratio 1:3 was more effective than the nanoformulation 1:5, with measured Dm of 0.313 and 0.485 µg/mL, respectively (Figure 3b, Table 2). Bright field images showed HeLa-R spheroids alterations and cell release caused by combination therapy with DTX/TPCS2a-NPs 1:5 and 1:3 (Figure 3c). As expected based on the cell viability results, the CI analysis showed only slight synergism when DTX/TPCS2a-NPs 1:5 were used while a strong synergism was found in the entire range of Fa values using DTX/TPCS2a-NPs 1:3 (Figure 2b). The DRI calculation indicated a DTX dose reduction of 21.83 and 11.27 times, using DTX/TPCS2a-NPs 1:5 and DTX/TPCS2a-NPs 1:3, respectively. Interestingly, these values were significantly higher than those observed in HeLa-P

spheroids using the same nanoformulations reinforcing the idea of the great potential of this nanosystem for the treatment of chemo-resistant cancer cells (Table 2). On the other hand, comparable DRI values of TPCS2a were found in DTX -sensitive and -resistant HeLa cells very likely because the two cell lines are equally sensitive to TPCS2a-PDT.

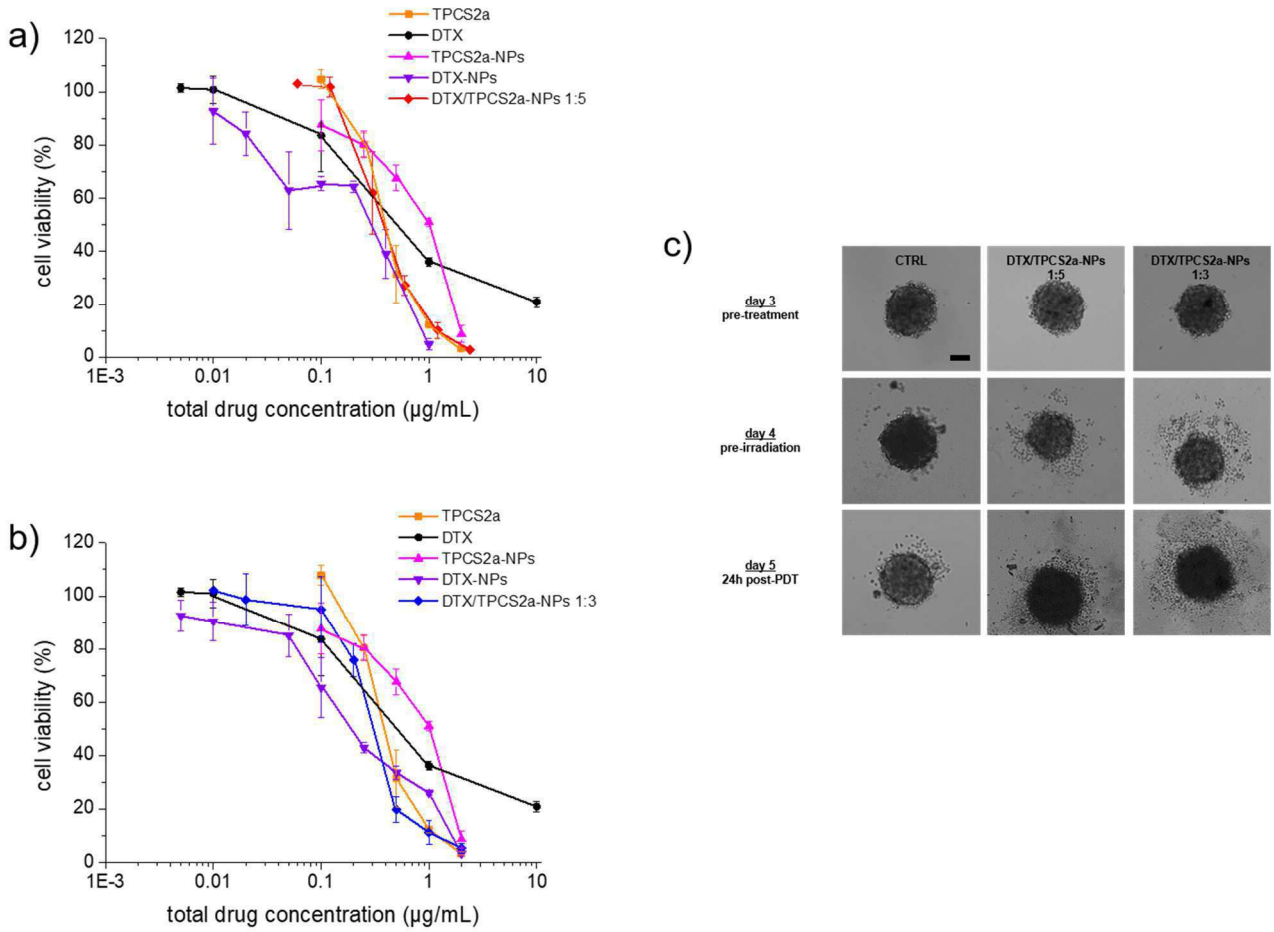

Figure 3. Combination therapy in HeLa-R spheroids. Dose-response curves of spheroids exposed to DTX-chemotherapy and/or TPCS2a-PDT with a DTX/TPCS2a concentration ratio 1:5 (a) and 1:3 (b) for 24 h. Cell viability was assessed using the 3D-Glo Assay. Data are expressed as mean percentage ± S.D. of at least two independent experiments in triplicate. c) Bright field images of: i) a representative untreated spheroid (CTRL) and ii) spheroids treated with DTX/TPCS2a-NPs drug ratios 1:5, 1:3 monitored from day 3 (pre-treatment) to day 5 (24 h post-PDT). The spheroids incubated with the different nanoformulations were exposed for 24 h to NPs on day 3, irradiated with 7.5 J/cm^2 of red light on day 4 and observed until 24 h post-PDT (day 5). The TPCS2a dose was 0.25 µg/ml while the DTX dose was 0.05 and 0.08 µg/ml respectively. Scale bar: 100 µm.

PS and NP penetration in multicellular tumor spheroids. Drug penetration inside the tumor mass is a fundamental requirement to efficiently eradicate differentiated cancer cells and CSCs, which generally are located in the most internal region of malignancies. This aspect must be considered also for PS penetration in cancer PDT. Multicellular spheroids represent the simplest 3D *in vitro* model reflecting more closely the *in vivo* tumor conditions[21] also for the screening of PS penetration. Thus, confocal microscopy was use to evaluate the accumulation/penetration of TPCS2a administered through the different delivery modalities (free TPCS2a, TPCS2a-NPs, DTX/TPCS2a-NPs 1:35) in HeLa spheroids incubated for 24 h. All the three TPCS2a formulations showed only limited penetration: TPCS2a fluorescence signal remained confined to the more external cell

layers, as documented by the images of the equatorial plane of spheroids (Figure 4a, d, g). Despite this, the intensity of the TPCS2a fluorescence signals appeared higher in the spheroid treated with the PS delivered in standard solvent or TPCS2a-NPs while the weaker signal was observed using DTX/TPCS2a-NPs. This observation was confirmed by the analysis of fluorescence intensity resulting from the signal of 15 ROIs traced in the equatorial plane of the spheroids. TPCS2a penetrates inside tumor up to 40, 20, and 20 µm when administered, respectively, in free formulation (Figure 4b), encapsulated alone in NPs (Figure 4e) and co-entrapped with DTX in NPs (Figure 4h). The same trend was observed also in the tridimensional reconstruction generated by the software ImageJ where yellow fluorescence picks, corresponding to high fluorescence intensity, were more in the case of free TPCS2a and TPCS2a-NPs (Figure 4c, f) compared to DTX/TPCS2a-NPs (Figure 4i) where they were almost absent. These data are also in agreement with the cytotoxicity studies performed in HeLa spheroids where TPCS2a-NPs and DTX/TPCS2a-NPs 1:35 were less efficient in inducing cell mortality compared to free TPCS2a (Figure 1a). The higher efficacy showed by the combination of the two drugs loaded in NPs at lower drug ratios was instead very likely ascribable to the higher dose of DTX leading to increased toxicity (Figure 1b, c).

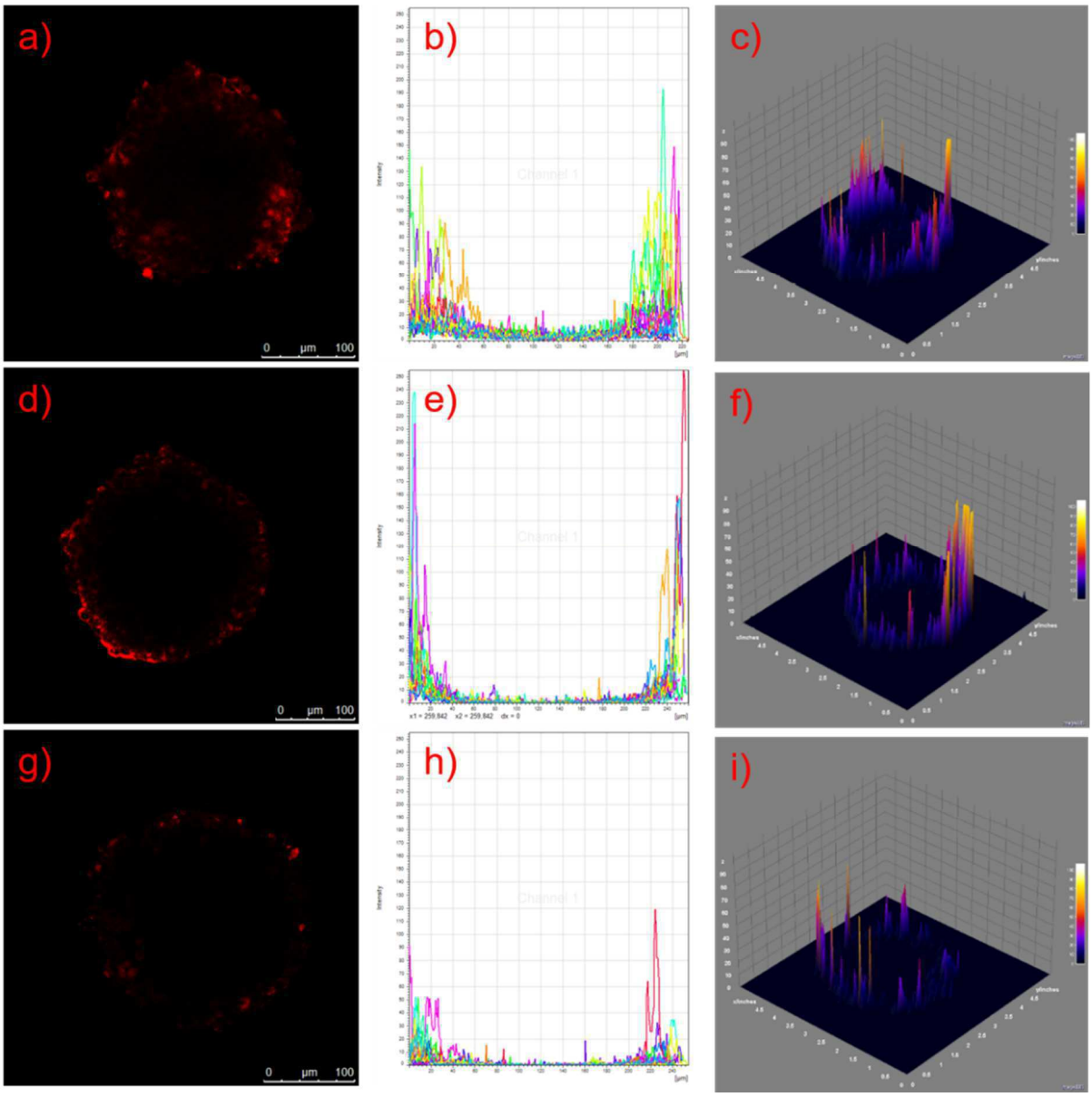

Figure 4. TPCS2a penetration in HeLa-P spheroids incubated for 24 h with 2 μg/mL free TPCS2a (a-c), TPCS2a-NPs (d-f) and DTX/TPCS2a-NPs (g-i). a,d,g) TPCS2a fluorescence at the equatorial plane of spheroids, scale bar: 100 μm; b,e,h) histograms representing the TPCS2a fluorescence signal intensities in 15 different randomly traced diameters in the equatorial planes; c,f,i) 3D reconstruction of TPCS2a fluorescence distribution in the equatorial plane of the spheroids.

Cytotoxicity assay in mammospheres. The tridimensional tumor models, in which the percentage of CSCs is enriched through well established culturing conditions (i.e. tumor spheres or mammospheres in the case of breast cancer cells) are used to evaluate the drugs therapeutic potential against this cancer cell sub-population[22-23]. This is justified by increasing evidences that successful cancer therapies require the simultaneous eradication of both differentiated and undifferentiated cancer cells to avoid tumor recurrence[24]. To assess whether DTX-chemotherapy and TPCS2a-PDT were effective in reducing tumor stemness, CSCs-enriched mammospheres were generated culturing breast cancer MCF-7 and MDA-MB-231 cells in non-adherent and serum-free conditions. These breast cancer cell lines were selected as models for these studies because they exhibit, when cultured as adherent cells, low and high expression of the CD44-receptor that is the target of HA forming the external coat of our NPs. Importantly, the CD44-receptor is overexpressed also by CSCs and is used as a marker for their identification. The strategy based on CD44-receptor targeting for killing CSCs has been previously reported by Wang and colleagues which demonstrated the successful eradication of breast CSCs using a hyaluronan-decorated fullerene-silica NPs loaded with Doxorubicin and Indocyanin Green for combination of chemo-, photodynamic and photo-thermal therapy[25].

The profile of CD44 expression in MDA-MB-231 and MCF-7 cells cultured in adherent and non-adherent conditions was analyzed by FACS after immunostaining (Table S2). The analysis performed with cells collected from monolayers and 7 day-old mammospheres, showed a slight increase of MCF-7 $CD44^{+/high}$ cells going from monolayer (5.4 %) to mammospheres culture (6.6 %) as well as a slight increase in the $CD24^{-/low}$ (8.4 and 8.8% for 2D and mammospheres, respectively). On the contrary, according to literature data[25], MDA-MB-231 cells showed CSC-like characteristics with almost all the cells with the phenotype $CD44^{+}/CD24^{-/low}$ both cultured in 2D and as mammospheres (Table S2).

The evaluation of mammosphere formation efficiency (MFE) after NPs treatments and combination therapy was used as a measure of the stemness and of CSC-self renewal capability of cells possessing different percentages of CSCs. This parameter was calculated using two different approaches. In the first case, already-formed mammospheres of MCF-7 and MDA-MB-231 cells were incubated for 24 h with the drugs in NPs (DTX/TPCS2a ratio 1:5), while in the second case, cell monolayers were incubated (DTX/TPCS2a ratio of 1:5 for MCF-7 and 1:35 for MDA-MB-231). For both protocols, at the end of the incubation time, the cells were irradiated with 1 J/cm^2 of red light and, after spheres dissociation and cell monolayer detachment, single cell suspensions were re-seeded in non-adherent condition to allow sphere formation.

For the choice of DTX/TPCS2a ratios co-loaded in the NPs used for treating monolayer-cultured cells we considered that: i) for MDA-MB-231, our previously published data[16] showed that the ratio 1:35 was the optimal to synergistically kill the cells, ii) for MCF-7 to cytotoxicity and CI analysis reported in Figure S3 highlighted antagonism for the ratio 1:35 and synergism for the ratio 1:5. Instead for treating mammospheres we decided to choose for both cell lines the 1:5 drug ratio based on the CI analysis reported above for HeLa spheroids, that indicated that to efficiently kill cells in the 3D condition the DTX dose must be increased.

As shown in Figure 5a, MFE percentages of treated *versus* untreated controls calculated for MCF-7 in which combination therapy was performed in monolayer-cultured cells showed not significantly enhanced ability of

DTX/TPCS2a-NPs in decreasing the capability of forming spheres with respect to DTX-NPs or TPCS2a-NPs. On the other hand, when first generation 7 day-old MCF-7 mammospheres were exposed to combination therapy (Figure 5b) using DTX/TPCS2a-NPs the numbers of mammospheres formed in the second generation was significantly reduced with respect to DTX-NPs or TPCS2a-NPs. The reduction of the number of formed spheres in each treatment condition was clearly observed also in the bright field microscopy images (Figure 5c). However, when the same analysis was extended to MDA-MB-231 cells, DTX/TPCS2a-NPs was significantly more potent than the single drug-loaded NPs in reducing the numbers of formed mammospheres exclusively when combination therapy was performed starting from 2D cultures (Figure 6a).

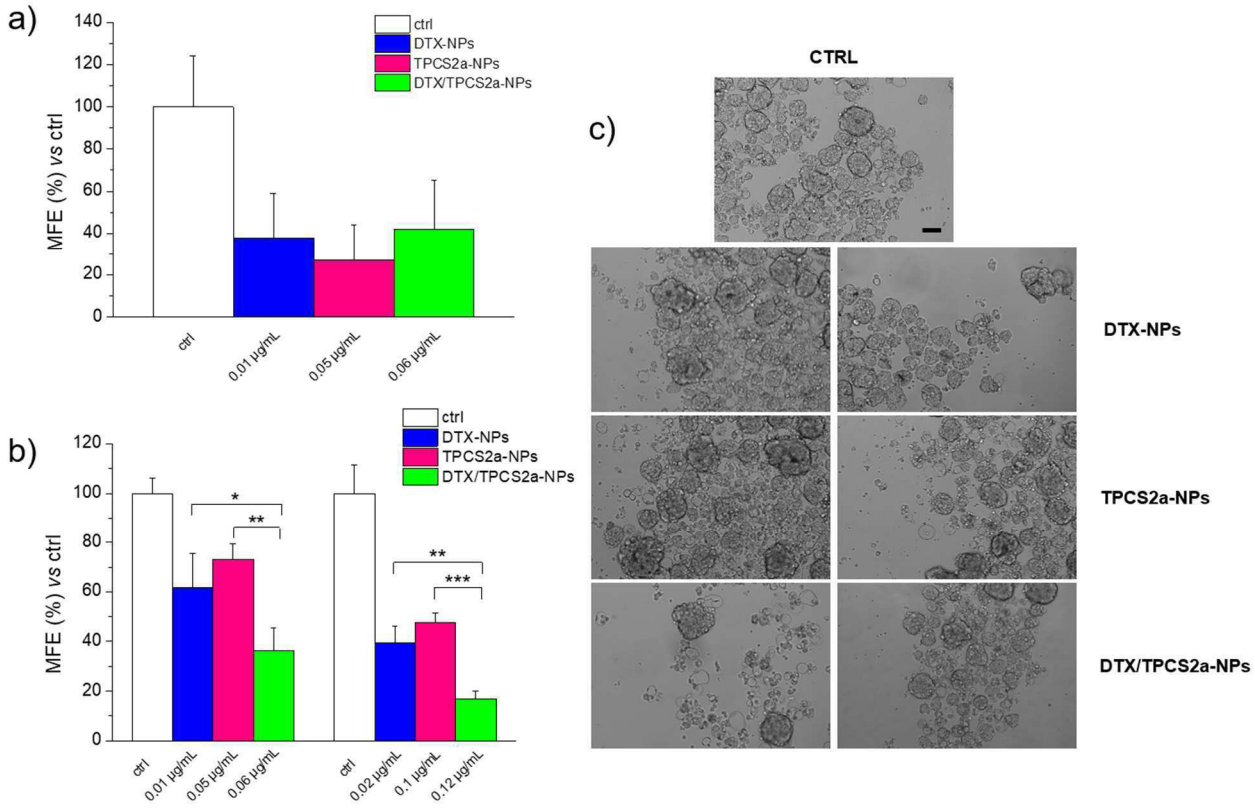

Figure 5. Mammosphere formation efficiency of MCF-7 cells. Mammosphere formation efficiency (MFE %) of MCF-7 cells incubated for 24 h with DTX-NPs, TPCS2a-NPs and DTX/TPCS2a-NPs 1:5, irradiated with 1 J/cm^2 and re-seeded in non-adherent condition to allow formation of spheres. MFE was evaluated treating cell monolayer (a) and first generation spheres (b) after 7 days from re-seeding. Data are expressed as mean ± S.D. of at least two independent experiments. *p < 0.05; **p < 0.01; ***p < 0.001 DTX/TPCS2a-NPs *vs* DTX-NPs and TPCS2a-NPs (Student's *t* test). c) Bright field microscopy of spheres untreated or incubated with the different NPs formulations starting from first generation mammospheres (left column) or from cell monolayer (right column). Scale bar: 100 µm.

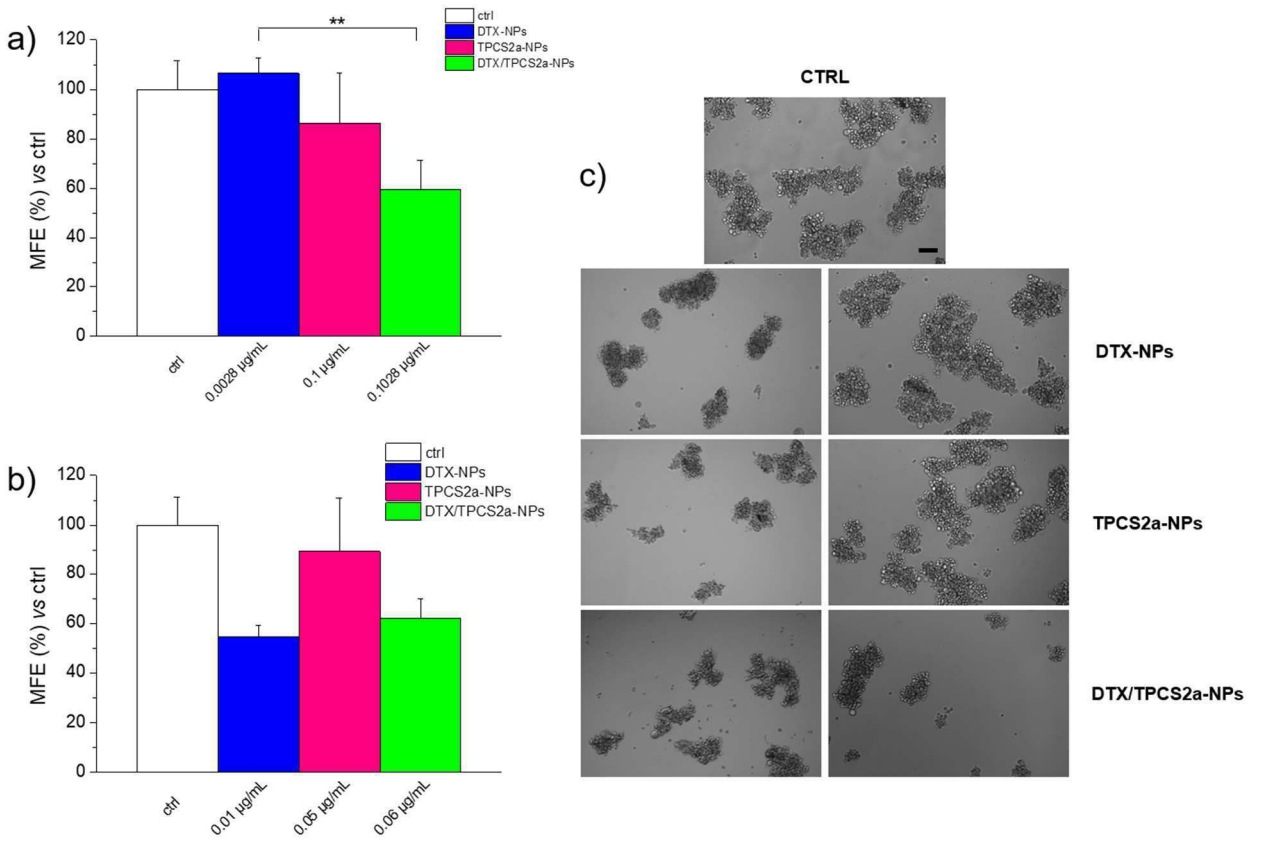

Figure 6. Mammosphere formation efficiency of MDA-MB-231 cells. Mammosphere formation efficiency (MFE %) of MDA-MB-231 cells incubated for 24 h with DTX-NPs, TPCS2a-NPs and DTX/TPCS2a-NPs 1:35 (a) or 1:5 (b), irradiated with 1 J/cm^2 and re-seeded in non-adherent condition to allow formation of spheres. MFE was evaluated treating cell monolayer (a) and first generation spheres (b) after 4 days from re-seeding. Data are expressed as mean ± S.D. of at least two independent experiments. *p < 0.05; **p < 0.01 DTX/TPCS2a-NPs *vs* DTX-NPs and TPCS2a-NPs (Student's *t* test). c) Bright field microscopy of spheres untreated or incubated with the different NPs formulations starting from first generation mammospheres (left column) or from cell monolayer (right column). Scale bar: 100 µm.

CONCLUSIONS

The results reported here have demonstrated that our PLGA NPs coated with hyaluronic acid can be loaded with various concentration ratios of DTX and TPCS2a without losing stability thus allowing studies on combination of chemo- and photodynamic therapy evaluating different treatment protocols. Our findings indicate that the determination of optimal drug ratio guaranteeing synergic interaction in combinatorial treatments is a difficult task to achieve and raise the question of the best *in vitro* tumor model to use for such studies. In fact, we have found that DTX and TPCS2a ratio giving strong synergism in monolayer cultures can give antagonism in 3D models as spheroids. In addition, for the same type of tumor cell models, the drug ratios giving synergism in one cell line does not function in others as for instance HeLa or MDA-MB 231 and MCF-7.

As regards CSCs, the results presented are somehow preliminary and additional experiments are necessary for concluding whether co-delivery of DTX and TPCS2a by these nanoaparticles can kill CSCs with the combination of chemotherapy and photodynamic therapy.

ACKNOWLEDGEMENTS

The financial support of the University of Padova and Italian Association for Cancer Research (IG2014 #15764) are gratefully acknowledged. The authors are gratefull to

PCI Biotech, Oslo, Norway for providing the photosensitizer TPCS2a (Amphinex®).

Appendix A. Supporting Information

REFERENCES

(1) Zhang, Q.; Chen, H.; Li, Q.; Zang, Y.; Chen, X.; Zou, W.; Wang, L.; Shen, Z. Combination Adjuvant Chemotherapy with Oxaliplatin, 5-Fluorouracil and Leucovorin after Liver Transplantation for Hepatocellular Carcinoma: A Preliminary Open-Label Study. *Invest. New Drugs* **2011**, *29* (6), 1360–1369.

(2) Crvenkova, S.; Pesevska, M. Important Prognostic Factors for the Long-Term Survival in Non-Small Cell Lung Cancer Patients Treated with Combination of Chemotherapy and Conformal Radiotherapy. *J. BUON. 20* (3), 775–781.

(3) Allison, R. R. Photodynamic Therapy: Oncologic Horizons. *Futur. Oncol.* **2014**, *10* (1), 123–124.

(4) Reginato, E.; Wolf, P.; Hamblin, M. R. Immune Response after Photodynamic Therapy Increases Anti-Cancer and Anti-Bacterial Effects. *World J. Immunol.* **2014**, *4* (1), 1–11.

(5) Lee, H.; Han, J.; Shin, H.; Han, H.; Na, K.; Kim, H. Combination of Chemotherapy and Photodynamic Therapy for Cancer Treatment with Sonoporation Effects. *J. Control. Release* **2018**, *283*, 190–199.

(6) Kim, D. H.; Hwang, H. S.; Na, K. Photoresponsive Micelle-Incorporated Doxorubicin for Chemo-Photodynamic Therapy to Achieve Synergistic Antitumor Effects. *Biomacromolecules* **2018**, *19* (8), 3301–3310.

(7) Xin, J.; Wang, S.; Zhang, L.; Xin, B.; He, Y.; Wang, J.; Wang, S.; Shen, L.; Zhang, Z.; Yao, C. Comparison of the Synergistic Anticancer Activity of AlPcS4 Photodynamic Therapy in Combination with Different Low-dose Chemotherapeutic Agents on Gastric Cancer Cells. *Oncol. Rep.* **2018**, *40* (1), 165–178.

(8) Nonaka, M.; Ikeda, H.; Inokuchi, T. Effect of Combined Photodynamic and Chemotherapeutic Treatment on Lymphoma Cells in Vitro. *Cancer Lett.* **2002**, *184* (2), 171–178.

(9) Khdair, A.; Handa, H.; Mao, G.; Panyam, J. Nanoparticle-Mediated Combination Chemotherapy and Photodynamic Therapy Overcomes Tumor Drug Resistance in Vitro. *Eur. J. Pharm. Biopharm.* **2009**, *71* (2), 214–222.

(10) Pampaloni, F.; Reynaud, E. G.; Stelzer, E. H. K. The Third Dimension Bridges the Gap between Cell Culture and Live Tissue. *Nat. Rev. Mol. Cell Biol.* **2007**, *8* (10), 839–845.

(11) Breslin, S.; O'Driscoll, L. Three-Dimensional Cell Culture: The Missing Link in Drug Discovery. *Drug Discov. Today* **2013**, *18* (5–6), 240–249.

(12) Leong, D. T.; Ng, K. W. Probing the Relevance of 3D Cancer Models in Nanomedicine Research. *Adv. Drug Deliv. Rev.* **2014**, *79–80*, 95–106.

(13) Sarisozen, C.; Abouzeid, A. H.; Torchilin, V. P. The Effect of Co-Delivery of Paclitaxel and Curcumin by Transferrin-Targeted PEG-PE-Based Mixed Micelles on Resistant Ovarian Cancer in 3-D Spheroids and in Vivo Tumors. *Eur. J. Pharm. Biopharm.* **2014**, *88* (2), 539–550.

(14) Barros, A. S.; Costa, E. C.; Nunes, A. S.; de Melo-Diogo, D.; Correia, I. J. Comparative Study of the Therapeutic Effect of Doxorubicin and Resveratrol Combination on 2D and 3D (Spheroids) Cell Culture Models. *Int. J. Pharm.* **2018**, *551* (1–2), 76–83.

(15) Choi, Y. H.; Yu, A.-M. ABC Transporters in Multidrug Resistance and Pharmacokinetics, and Strategies for Drug Development. *Curr. Pharm. Des.* **2014**, *20* (5), 793–807.

(16) Gaio, E.; Conte, C.; Esposito, D.; Miotto, G.; Quaglia, F.; Moret, F.; Reddi, E. Co-Delivery of Docetaxel and Disulfonate Tetraphenyl Chlorin in One Nanoparticle Produces Strong Synergism between Chemo- and Photodynamic Therapy in Drug-

Sensitive and -Resistant Cancer Cells. *Mol. Pharm.* **2018**, acs.molpharmaceut.8b00597.

(17) Wang, R.; Lv, Q.; Meng, W.; Tan, Q.; Zhang, S.; Mo, X.; Yang, X. Comparison of Mammosphere Formation from Breast Cancer Cell Lines and Primary Breast Tumors. *J. Thorac. Dis.* **2014**, *6* (6), 829–837.

(18) Maiolino, S.; Moret, F.; Conte, C.; Fraix, A.; Tirino, P.; Ungaro, F.; Sortino, S.; Reddi, E.; Quaglia, F. Hyaluronan-Decorated Polymer Nanoparticles Targeting the CD44 Receptor for the Combined Photo/Chemo-Therapy of Cancer. *Nanoscale* **2015**, *7* (13), 5643–5653.

(19) Gaio, E.; Scheglmann, D.; Reddi, E.; Moret, F. Uptake and Photo-Toxicity of Foscan®, Foslip® and Fospeg® in Multicellular Tumor Spheroids. *J. Photochem. Photobiol. B Biol.* **2016**, *161*.

(20) Chou, T.-C. Theoretical Basis, Experimental Design, and Computerized Simulation of Synergism and Antagonism in Drug Combination Studies. *Pharmacol. Rev.* **2006**, *58* (3), 621–681.

(21) Zanoni, M.; Piccinini, F.; Arienti, C.; Zamagni, A.; Santi, S.; Polico, R.; Bevilacqua, A.; Tesei, A. 3D Tumor Spheroid Models for in Vitro Therapeutic Screening: A Systematic Approach to Enhance the Biological Relevance of Data Obtained. *Sci. Rep.* **2016**, *6* (1), 19103.

(22) Sun, T.-M.; Wang, Y.-C.; Wang, F.; Du, J.-Z.; Mao, C.-Q.; Sun, C.-Y.; Tang, R.-Z.; Liu, Y.; Zhu, J.; Zhu, Y.-H.; et al. Cancer Stem Cell Therapy Using Doxorubicin Conjugated to Gold Nanoparticles via Hydrazone Bonds. *Biomaterials* **2014**, *35* (2), 836–845.

(23) Carrasco, E.; Álvarez, P. J.; Prados, J.; Melguizo, C.; Rama, A. R.; Aránega, A.; Rodríguez-Serrano, F. Cancer Stem Cells and Their Implication in Breast Cancer. *Eur. J. Clin. Invest.* **2014**, *44* (7), 678–687.

(24) Bao, B.; Ahmad, A.; Azmi, A. S.; Ali, S.; Sarkar, F. H. Overview of Cancer Stem Cells (CSCs) and Mechanisms of Their Regulation: Implications for Cancer Therapy. *Curr. Protoc. Pharmacol.* **2013**, *61* (1), 14.25.1-14.25.14.

(25) Wang, H.; Agarwal, P.; Zhao, S.; Yu, J.; Lu, X.; He, X. Combined Cancer Therapy with Hyaluronan-Decorated Fullerene-Silica Multifunctional Nanoparticles to Target Cancer Stem-like Cells. *Biomaterials* **2016**, *97*, 62–73.

Supporting Information

Synergic effects of chemo- and photodynamic therapy in 3D tumor cell models treated with nanoparticles co-delivering docetaxel and disulphonate tetraphenyl chlorin

Elisa Gaio[a], Claudia Conte[b], Fabiana Quaglia[b], Francesca Moret[a], Elena Reddi[a].

[a] Cell Biology Unit, Department of Biology, University of Padova, Padova, Italy

[b] Drug Delivery Laboratory, Department of Pharmacy, University of Napoli Federico II, Napoli, Italy

Supplementary Materials and Methods

Cell viability assays after treatments in cell monolayer. MCF-7 (8000 cells/well) cells were seeded in 96-well plates in DMEM supplemented with 10% FBS. After 24 h of cell growth, the medium was replaced with fresh medium containing increasing concentrations of DTX, TPCS2a or their combination (DTX/TPCS2a) delivered in the standard solvents or in NPs (DTX/TPCS2a ratio 1:35, 1:5). Cell viability was measured with the CellTiter 96 Aqueous One Solution Cell proliferation Assay (MTS) (Promega) after 24 h of drug incubation and an additional 24 h in which the cells were kept in drug-free medium (dark toxicity; time point 24 + 24 h). For photo-toxicity experiments, cells were seeded and treated as described above for 24 h. At the end of the incubation time, the cells were washed twice with PBS containing Ca^{2+} and Mg^{2+} and irradiated in PBS with a total light fluence of 1 J/cm^2 of red light (600-800 nm) emitted from a Waldmann PDT 1200 lamp (Waldmann Medizintechnik, Germany). The power density was 16 mW/cm^2 as measured with the radiometer IL 1700 (International Light, Newburyport, USA). Immediately after irradiation, the cells were brought back to the incubator after the replacement of PBS with fresh medium. Cell viability was measured with the MTS test after additional 24 h (photo-toxicity; time point 24 + 24 h). For the MTS assay, the cell medium was replaced with 100 µL of serum-free DMEM and 20 µL of CellTiter 96 Reagent and the samples were incubated for 40–60 min at 37 °C in the dark. Afterward, the absorbance at 492 nm was measured with a Multiskan Go plate reader (Thermo Fisher Scientific, Waltham, USA) and the viability of treated cells was expressed as percentage of the absorbance of control cells that was taken as 100% viability.

Supplementary Figures

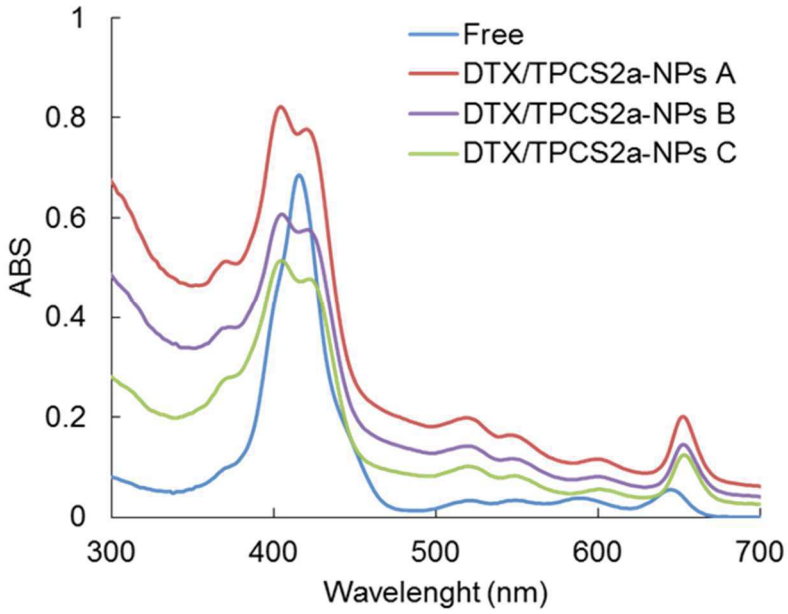

Figure S1. UV spectra of different TPCS2a formulations in water. Free TPCS2a and TPCS2a encapsulated with DTX in NPs at 1:3, 1:5 and 1:35 ratios (DTX/TPCS2a-NPs A, B, C respectively).

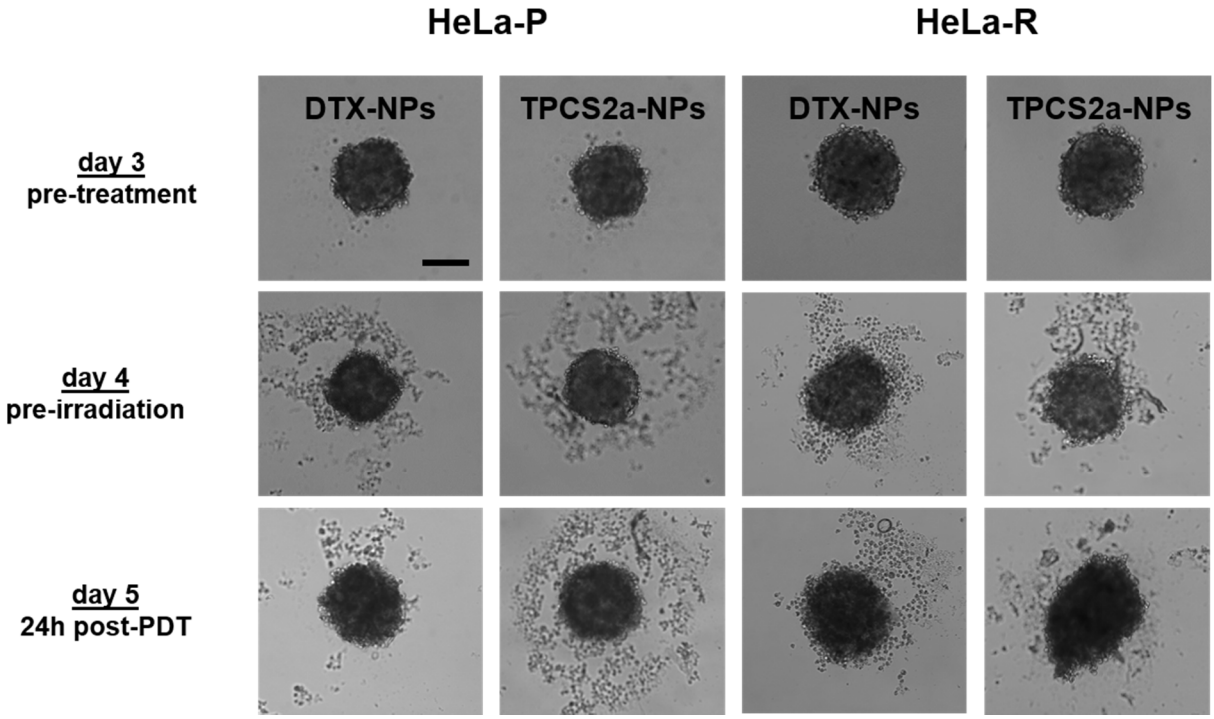

Figure S2. Bright field images of HeLa-P and HeLa-R spheroids treated with DTX-NPs or TPCS2a-NPs 1:3 monitored from day 3 (pre-treatment) to day 5 (24 h post-PDT). The spheroids incubated with the different nanoformulations were exposed for 24 h to NPs on day 3, irradiated with 7.5 J/cm^2 of red light on day 4 and

observed until 24 h post-PDT (day 5). The TPCS2a dose was 0.25 µg/ml and the DTX dose was 0.08 µg/ml. Scale bar: 100 µm.

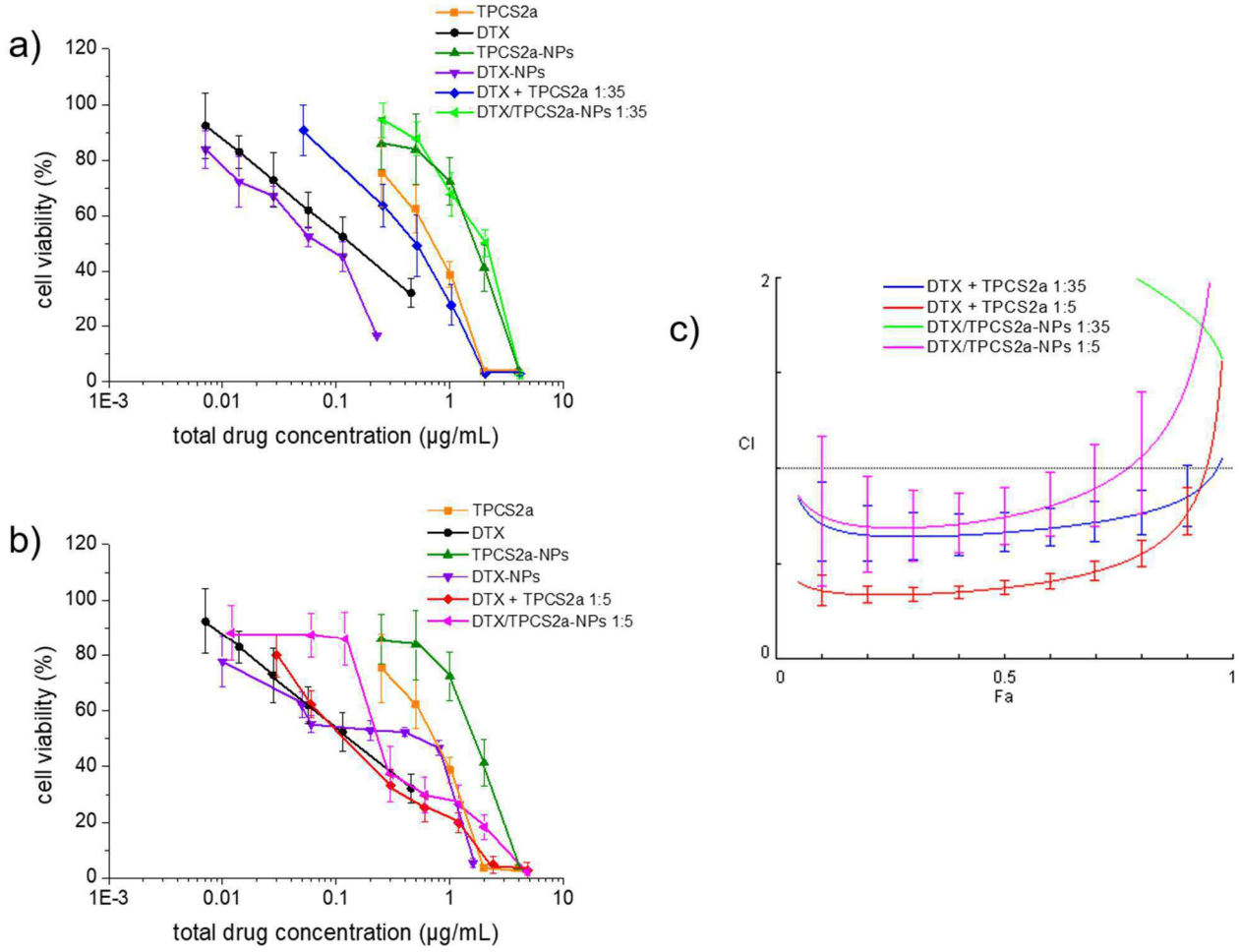

Figure S3. Dose-response curves (a, b) and Combination Index Plots (Fa vs CI plot) (c) of MCF-7 cells exposed to DTX-chemotherapy and/or TPCS2a-PDT with free or NP-loaded drugs. Cell viability was measures with MTS assay and data are expressed as mean percentage ± S.D. of at least two independent experiments in triplicate.

Supplementary Tables

Table S1. Data for Fa = 0.5 of HeLa-P and HeLa-R spheroids. The data were used to calculate the DRI values.

Data for Fa = 0.5	Drug dose (μg/mL)			
Drug Formulation	**TPCS2a**	**DTX**	**TPCS2a-NPs**	**DTX-NPs**
HeLa-P				
TPCS2a	0.37960			
DTX		0.099		
TPCS2a-NPs			0.77560	
DTX-NPs 1:35				0.07364
DTX-NPs 1:5				0.08414
DTX-NPs 1:3				0.09360
DTX/TPCS2a-NPs 1:3	0.06759	0.06759		
DTX/TPCS2a-NPs 1:5	0.17022	0.03404		
DTX/TPCS2a-NPs 1:35	0.54710	0.01563		
HeLa-R				
TPCS2a	0.47397			
DTX		1.76594		
TPCS2a-NPs			0.62596	
DTX-NPs 1:5				0.14041
DTX-NPs 1:3				0.16036
DTX/TPCS2a-NPs 1:5	0.40443	0.08089		
DTX/TPCS2a-NPs 1:3	0.15664	0.15664		

Table S2. Receptor profile of MDA-MB-231 and MCF-7 cultured in adherent and non-adherent conditions.

	$CD44^{+}$		$CD24^{-/low}$	
cell line	**2D**	**3D**	**2D**	**3D**
MDA-MB-231	93.5	94.9	99.8	93.5
MCF-7	5.4	6.6	8.4	8.8

Paper III

Keratin nanoparticles co-delivering Docetaxel and Chlorin e6 for synergic chemo- and photodynamic anticancer effect

Elisa Gaio[a#], Andrea Guerrini[b#], Marco Ballestri[b], Greta Varchi[b], Claudia Ferroni[b], Annalisa Aluigi[b], Francesca Moret[a*], Elena Reddi[a]

[a]Cell Biology Unit, Department of Biology, University of Padova, Padova, Italy

[b]Institute of Organic Synthesis and Photoreactivity, Italian National Research Council, Bologna, Italy

[#]Contributed equally

*Corresponding author

Abstract

Several strategies to improve the therapeutic outcome of cancer diseases are currently under investigation and, among them, the combination of chemotherapy with photodynamic therapy (PDT) seems to offer the possibility of limit the unwanted chemo-drug toxicity by reducing the administered dose and by contrasting acquired drug-resistance phenomena. Moreover, the re-formulation of clinically approved pharmaceuticals in biocompatible nanoparticles (NPs), in order to improve tumor delivery efficiency, appeared particularly appealing also for the co-loading of drugs with different solubility, as chemotherapeutics and photosensitizers (PSs). Here, we report on the facile and organic solvent-free synthesis of merino wool-extracted keratin NPs for the co-delivery of the antimitotic drug Docetaxel (DTX) and of the PS Chlorin e6 for the combination of chemo- and photo-therapy of DTX –sensitive and –resistant cancer cells. By using the aggregation method, which allowed the formation of bimodal NPs (DTX/Ce6-KNPs) in aqueous environment by exploiting the interactions between hydrophobic DTX and amphiphilic keratin residues, we obtained monodisperse NPs with an average diameter of 133 nm and with a drug ratio of 1:1.8 of Ce6 *vs* DTX. Combination therapy performed *in vitro* in monolayer cell cultures showed that the cytotoxic performances of DTX/Ce6-KNPs were not worsened with respect to those of DTX + Ce6 delivered in the standard clinical formulation in DTX -sensitive HeLa (HeLa-P) cells. Interestingly, the cooperation between the two drugs was synergistic in DTX -resistant HeLa (HeLa-R) cells exclusively when delivered in the bimodal nanosystem. Moreover, when combination therapy was assessed in tridimensional arranged tumor multicellular spheroids, obtained from HeLa-P and HeLa-R cells by liquid-overlay method, DTX/Ce6-KNPs demonstrated to be capable of inducing higher extent of cytotoxicity than the single drug loaded nanoformulations (i.e. DTX-KNPs and Ce6-KNPs) and to reduce significantly spheroid volumes, notwithstanding KNP penetration was confined to the outer rim of cells of the entire spheroid mass.

Keywords: combination therapy, keratin nanoparticles, Docetaxel, Chlorin e6, synergism, spheroids.

1. Introduction

The 2018 American Cancer Society report stated that, notwithstanding the widespread cancer diffusion, the death rates are continuously decreasing with respect to the 1990s, very likely for preventive interventions and early diagnosis but also significant improvements of tumor therapies in terms of efficacy [1]. As a matter of fact, the introduction in the clinic of new molecules with improved anticancer activity, the rather established strategy to associate different principles in chemotherapeutic drug cocktails as well as the amelioration of the pre-existing drug formulations, significantly increase the rates of cancer cure and patient survival. In particular, the application of recent nanotechnological approaches in medicine, and specifically in the anticancer drug delivery field, led to the reformulation of many pre-existing chemotherapeutics that enhanced therapeutic efficacy of drugs by improving bioavailability with effective possibility of dose reduction, which correlates with the decrease of the risk related to systemic side effects [2]. The majority of the nanoformulations on the market, even if based on delivery systems with highly different physic-chemical characteristics such as liposomes, inorganic nanoparticles (NPs), dendrimers, polymer-based micelles, have been developed for the transport of already clinically approved pharmaceuticals. A successful example is represented by the antimitotic drug Paclitaxel (PTX) which has been marketed formulated in three different types of nanosystems, namely polymeric micelles (Genexol®, Nanoxel®, Paclical®), albumin-based NPs (Abraxane®) and liposomes (Lipusu®) [3], and approved for the treatment of several types of tumors, including breast, pancreatic and non-small cell lung cancers [4]. On the contrary, clinically nanoformulations of its analog Docetaxel (DTX) have been still approved, even if tens of papers reported on its efficient encapsulation in several types of nanomaterials [5], sometimes in combination with others drugs [6][7][8]. Having the complete eradication of malignancies and avoidance of the recurrences as goals, DTX-chemotherapy is being proposed in association with other treatment modalities, such as photo-thermal [9] or photodynamic therapy (PDT) [10][11][12]; consequently properly engineered nanoformulations with the ability to carry two or more different drug molecules, at concentrations guaranteeing synergic interactions between drugs/therapies, were developed and are increasingly investigated [13].

As concerns PDT, the strength of this treatment modality relays on its intrinsic selectivity derived from the capability of the photosensitizer (PS) to be light-activated exclusively in the site of its preferential accumulation, e.g. tumor tissue. The reactive oxygen species (ROS), mainly singlet oxygen, produced following the localized PS excitation, remain confined and exert oxidative type of damages almost exclusively in the cancer cells where they are generated, contributing to realize selective killing of tumor tissues resulting from direct damages of cancer cells concomitant with tumor microvasculature destruction and to the activation of a prompt immunological response, that is very important for long term control of tumor growth [14]. In PDT, the use of nanocarriers helps to circumvent one major drawback caused by the high hydrophobicity of most PSs that highly impairs their delivery and photodynamic efficiency [15] and, the association in the same nanovehicle of a chemotherapeutic drug, may enhance the overall treatment efficacy by controlling the drug timing and the delivery rates.

The present study aims at evaluating a quite novel protein-based nanomaterial, namely keratin NPs (KNPs), for the bimodal co-delivery of DTX and the PS Chlorin e6 (Ce6) to cancer cells (DTX -sensitive and -resistant) cultured *in vitro* as classic monolayers as well as in a tridimensional arrangement (multicellular tumor spheroids).

The choice of keratin extracted from wool to fabricate NPs for drug delivery purpose is receiving increasing attention because it is a natural product with excellent biocompatibility and biodegradability and can be easily functionalized due to the specific structure of

the protein, which allows various possibilities of covalent and non-covalent modification for drug encapsulation [16]. Moreover, the presence on keratin backbone of cell adhesion sequences, as for example arginine-glycine-aspartic acid (RGD) and leucine-aspartic acid-valine (LDV) [17], able to bind integrins, overexpressed on the endothelium of the tumor neo-vasculature and on many types of cancer cells [18], offers the possibility of exploiting these sequences as intrinsic targeting elements to actively target tumor tissues.

We have already reported on the successful synthesis methodologies developed for the covalent delivery of Ce6 in KNPs, and demonstrated *in vitro* the capability of the nanoformulation to photo-kill osteosarcoma cells more efficiently than the standard free PS formulation [19]. Moreover, we have ascertained that the presence of chemotherapeutics like Doxorubicin (DOX) or PTX during KNP synthesis promotes the aggregation of the protein hydrophobic residues without the use of organic solvents (e.g. aggregation method in water) and the formation of stable NPs able to efficiently load and transport the drugs [20], in 2D and 3D cell cultures [21]. Based on these acquired expertise, here we explore the suitability of the aggregation method for the production of bimodal KNPs (DTX/Ce6-KNPs) and we evaluate whether the two drugs, co-loaded at a certain concentration ratio, are able to cooperate synergistically in inducing cancer cell mortality.

2. Materials and methods

2.1. Chemicals and Reagents

Chlorin e6 (Ce6) was provided by Livchem Logistics GmbH (Germany); DTX was purchased from LC Laboratories (USA). Ce6 and DTX standard solutions were prepared by dissolving known amounts of powder in DMSO. Cariaggi Fine Yarns, S.p.a. kindly supplied Australian Merino wool, while all other chemicals used for the nanoparticles characterization were purchased from Sigma-Aldrich (Italy). Keratin was extracted from Merino wool (21 μm fineness) by sulphitolysis reaction as previously reported [19]. Dulbecco's modified Eagle's medium (DMEM) and fetal bovine serum (FBS) were purchased from Gibco Life Technologies (Milan, Italy). The CellTiter96® Aqueous One Solution Cell proliferation Assay (MTS) and CellTiter-Glo® 3D Cell Viability Assay were from Promega Co. (Madison, USA).

2.2. Synthesis of DTX/Ce6-KNPs

For Ce6-KNPs and DTX/Ce6-KNPs nanoparticles synthesis, keratin was covalently functionalized with Ce6 as previously reported (Ker-Ce6) [19]. DTX/Ce6-KNPs were prepared as follows: a solution of DTX in EtOH (20 mg/mL) was slowly added (0.3 mL/min) to a PBS solution of Ker-Ce6 (5 mg/mL; Ce6 content = 70 $\mu g/mg_{ker}$) under vigorous stirring (600 rpm) at room temperature. The amount of DTX solution to be added was calculated in order to have a final DTX concentration of 13% (w/w) as respect to the final formulation, e.g. DTX/Ce6-KNPs. The solution was continuously stirred for 1 h becoming slightly opalescent; at this time 70 μl of the solution were withdrawn and diluted in cuvette with 1.9 mL of milliQ water for performing dynamic light scattering (DLS) analysis. The solution was then freeze-dried affording a white powder of DTX/Ce6-KNPs.

DTX-KNPs were prepared by means of the same procedure starting from pure keratin powder, while Ce6-KNPs were prepared by desolvation method [19] and used as controls for all experiments.

2.3. Characterization of DTX/Ce6-KNPs

The Ce6 loading on KNPs was evaluated by recording the absorption spectra of the Ker-Ce6 suspension with an UV-Vis spectrophotometer Cary 100 (Agilent Technologies). For Ce6 quantification, a calibration curve of Ce6 dissolved in $NaHCO_3$ buffer (pH = 9.2) in the 0 - 5 mg/mL concentration range was determined. NPs hydrodynamic diameter in aqueous solutions (0.5 mg/mL) was determined by photon correlation spectroscopy (PCS) at 25 °C using a NanoBrook Omni Particle Size Analyser (Brookhaven Instruments Corporation, USA)

equipped with a 35 mW red diode laser (nominal 640 nm wavelength). As far as the electrophoretic mobility is concerned, zeta-potential was measured at 25 °C by means of the same system.
DTX/Ce6-KNPs stability in physiological conditions was determined by dissolving 500 µg of NPs, containing 57.5 µg of DTX and 31 µg of Ce6, in 2 mL of PBS and maintaining them at 37°C. KNPs size and polydispersity over time was checked by dynamic light scattering analysis at pre-determined time intervals.

2.4. DTX release from KNPs

The evaluation of DTX release from DTX/Ce6-KNPs nanoparticles was performed as follows: 6.5 mg of DTX/Ce6-KNPs (lyophilized powder) containing 750 µg of DTX were solubilized in 2 mL of milliQ water, inserted in a dialysis bag (cut-off 12 kDa) and dialyzed against a solution of PBS/EtOH (10 mL; 2% EtOH). The system was heated at 37°C under stirring for 1 h (3x) and for 2 h (x2) until reaching 24 h. At predetermined time points, the outer solution was withdrawn and replaced with fresh buffer solution. At each time point the PBS/EtOH solution was extracted with CH_2Cl_2 (3x) and the collected organic phases were dried over Na_2SO_4 and concentrated under vacuum. The residue was dissolved in absolute EtOH (1 mL) and analyzed by UV-Vis spectroscopy (230 nm) and compared with a DTX calibration curve previously recorded.

2.5. Cell lines

MDA-MB-231 human breast and HeLa human cervix cancer cells were purchased from American Type Tissue Culture Collection (ATCC, Rockville, USA). The cells were grown in DMEM with Glutamax™ supplemented with 10% heat-inactivated FBS, 100 U/mL streptomycin and 100 µg/mL penicillin G (all from Life Technologies), and maintained at 37 °C under a humidified atmosphere containing 5% CO_2. A DTX-resistant HeLa cell line (HeLa-R) was obtained by cultivating HeLa parental (HeLa-P) cells in DMEM supplemented with 10% of FBS and intermittent low and increasing DTX concentrations (0.002-0.008 µg/mL) for seven months. Once a week the cells were treated for 48 h with DTX afterward the chemotherapeutic was removed, the cells were recovered and kept in DTX-free medium until the next treatment. The DTX concentration was increased every four weeks. The effective resistance to DTX of the HeLa-R cells was evaluated by the MTS assay to determine the value of the drug concentration that inhibits cell survival by 50% (Dm) for DTX in comparison to HeLa-P cells [13].

Monolayer cell cultures

2.6. Cell viability assays after treatments

HeLa, HeLa-R (6000 cells/well) and MDA-MB-231 (8000 cells/well) cells were seeded in 96-well plates in DMEM supplemented with 10% FBS. After 24 h of cell growth, the medium was replaced with fresh medium containing increasing concentrations of Ce6, DTX or their combination (Ce6/DTX) delivered in the standard solvents or in KNPs for 3 or 24 h. Cell viability was measured with the MTS assay after 24 h of drug incubation in the dark (time point 24 h) as well as after an additional 24 h in which the cells were kept in drug-free medium (time point 3 + 24 h, 24 + 24 h). For photo-toxicity experiments, cells were seeded and treated as described above for 3 or 24 h. At the end of the incubation time, the cells were washed twice with PBS containing Ca^{2+} and Mg^{2+} and irradiated in PBS with a total light fluence of 15.3 J/cm^2 of red light (600-800 nm) emitted from a Waldmann PDT 1200 lamp (Waldmann Medizintechnik, Germany). The power density was 25 mW/cm^2 as measured with the radiometer IL 1700 (International Light, Newburyport, USA). Immediately after irradiation, the cells were brought back to the incubator after the replacement of PBS with fresh medium. Cell viability was measured with the MTS test after additional 24 h (photo-toxicity; time points 3 + 24 h or 24 + 24 h). As controls, also the cytotoxicity in cells incubated with empty KNPs for 24 h and exposed to light was measured. For the MTS assay, the cell medium was replaced with 100 µL of serum-free DMEM and 20 µL of CellTiter 96 Reagent and the samples were

incubated for 40–60 min at 37 °C in the dark. Afterward, the absorbance at 492 nm was measured with a Multiskan Go plate reader (Thermo Fisher Scientific, Waltham, USA) and the viability of treated cells was expressed as percentage of the absorbance of control cells that was taken as 100% viability.

2.7. Ce6 uptake and intracellular localization studies

For measuring Ce6 cell uptake by flow cytometry, $5x10^4$ HeLa cells were seeded in 24-well plates and after 24 h of growth, the cells were incubated with fresh medium containing 1 μg/mL of Ce6 alone or in combination with DTX (1.8 μg/mL), delivered as free drugs in the standard solvents or loaded in KNPs. After 3 h of incubation, the treatment solutions were removed, the cells were washed with Versene solution and detached from the plates with trypsin that was neutralized with the addition of FBS. Cells were centrifuged and re-suspended in Versene solution before measuring Ce6 fluorescence using a BD FACSCanto™ II (Becton Dickinson, San Jose, USA) flow cytometer. The blue laser at 488 nm was used as the excitation source and Ce6 fluorescence was detected at wavelengths longer than 670 nm (PerCP channel). Ten thousand events/samples were acquired and analyzed with the FACSDiva Software. Moreover, confocal microscopy was used to determine the intracellular localization of Ce6. Cells (10^5) were seeded in 35 mm cell imaging dishes (Eppendorf AG, Hamburg, Germany) and, after 24 h of growth, were incubated at 37 °C for 3 h with fresh medium supplemented with 10 % FBS and 5 μg/mL of Ce6 delivered by standard solvent or NP formulations. Before visualization with a SP5 confocal microscope (Leica Microsystems, Milan, Italy), the cells were washed with PBS containing Ca^{2+} and $Mg^{2+}$and incubated for 15 min with Mito-Tracker Green (100 nM) or ER-Tracker Green (1μM), used as markers for mitocondra and endoplasmic reticulum, respectively.

3D cell cultures

2.8. Generation of tumor spheroids

Multicellular spheroids of HeLa and HeLa-R cells were generated using the liquid overlay method, as previously reported [22]. Briefly, the cells were harvested from monolayer cultures by trypsinization and seeded in flat-bottomed 96-well plates (1000 cells/well) previously coated with 1% agarose in DMEM in order to prevent cell adhesion. Immediately after seeding the plates were centrifuged at 200 g for 5 min in order to promote cell aggregation and then placed in the incubator. After 3 days the spheroids had reached a diameter of about 200 μm and were used for the following experiments.

2.9. Cytotoxicity Assays in spheroids

Three day-old spheroids were incubated with 100 μL of fresh medium containing 10 % FBS and increasing concentration of Ce6-KNPs, DTX-KNPs or DTX/Ce6-KNPs. After 3 h of incubation, spheroids were washed with PBS containing Ca^{2+} and Mg^{2+} and irradiated in PBS with a total light fluence of 30 J/cm^2 of red light (power density 50 mW/cm^2). Immediately after irradiation, the cells were brought back to the incubator after the replacement of PBS with fresh medium. Cell viability was measured using the CellTiter-Glo® 3D Cell Viability Assay after additional 24 h. Briefly, only 50 μl of cell medium were left in each spheroid well and 50 μl of CellTiter-Glo® 3D Reagent were added; the well content was mixed by shaking for 5 min, incubated at room temperature for 25 min and luminescence was measured immediately after with a Perkin Elmer Envision instrument. Moreover, for established data points during the experiment, a bright field microscope (DMI6000B, Leica) equipped with a DCF365FX camera was used to monitor the morphological changes induced by the treatments. The software LAS AF Lite (Leica Microsystems) was used to measure in each single spheroid image the minimum diameter (dmin) and maximum diameter (dmax) in order to measure the spheroid volume using the formula:

$$V = \frac{\Pi \times dmin \times dmax}{6}$$

as reported in [23]. The tumor spheroid volume ratio (R) was then calculated using the formula:

$$R = \frac{V_i}{V_0} x100\%$$

where V*i* is the tumor spheroid volume measured at the 3 + 24 h time-point, and V_0 is the spheroid volume prior to the treatment.

2.10. Ce6 localization and diffusion into spheroids

Spheroids were generated as described above and treated for 3 h with 5 µg/mL of Ce6 free or in KNPs. The localization of Ce6 was evaluated by confocal microscopy (Leica SP5) by transferring the spheroids from 96-well/plates to 35 mm cell imaging dishes and washing them twice with PBS before visualization. Images of about 20 different focal planes were acquired from the top to the bottom of the spheroid. Maximum projection images were obtained with the software LAS AF Lite by superimposing the images of the 20 acquired focal planes. For the comparison of penetration of Ce6 in the spheroids, 10 radial lines (regions of interest, ROI) were randomly drawn in each image of the equatorial plane and fluorescence at each pixel was recorded with the LAS AF Lite software. Furthermore, a 3D reconstruction of the distribution of the fluorescence signal in the equatorial plane of spheroids was obtained using the software ImageJ.

2.11. Calculation of Combination Index (CI) and Drug Reduction Index (DRI)

In order to assess if the interaction of DTX chemotherapy and Ce6-PDT resulted in a synergic effect, CI and DRI values were calculated using the CompuSyn software (ComboSyn Inc., NJ, USA), based on Chou and Talalay method [24]. From the experimental data obtained from the cell viability curves (for monolayers and spheroids) we calculated the Fraction affected (Fa) values for each drug concentration tested and we analyzed the data on the Compusyn software as already described [13]. For each monotherapy and combination therapy, the program calculated also the drug concentration that inhibits cell survival by 50% (IC_{50} or Dm value).

2.12. Statistical analysis

The Primer software for biostatistics (McGraw-Hill, Columbus, USA) was used for statistical analysis of the data. The data are expressed as means ± standard deviations (SD) for at least 2 independent experiments in triplicate. The difference between groups was evaluated with the Student's t-test and was considered significant for $p < 0.05$.

3. Results and discussion

3.1. KNPs synthesis and characterization

DTX/Ce6-KNPs (Fig. 1a) were fabricated with drug-induced aggregation exploiting the DTX hydrophobicity and affinity to the protein. This methodology afforded NPs with an average hydrodynamic diameter of 133 nm and a polydispersity index (PDI) of 0.35, indicating the presence of a single nanoparticles' population (Fig. 1b). After lyophilization, particles were resuspended in milliQ water or PBS in order to verify their solubility, indeed, DLS analysis of resuspended KNPs confirmed that particles maintain a size around 142 nm and a polydispersity of 0.38 (Fig. 1b). DTX/Ce6-KNPs have a negative zeta potential of -29 mV due to the negative charges present on the protein backbone.

Stability studies were performed in PBS at 37°C, indicating that neither nanoparticles hydrodynamic diameter and polydispersity index were significantly affected during the observation time (Fig. 1c), in agreement with a satisfactory stability index of DTX/Ce6-KNPs under these conditions. Due to the specific preparation procedure, we assume that DTX loading on DTX/Ce6-KNPs is 100% as respect to the DTX used for the aggregating process.

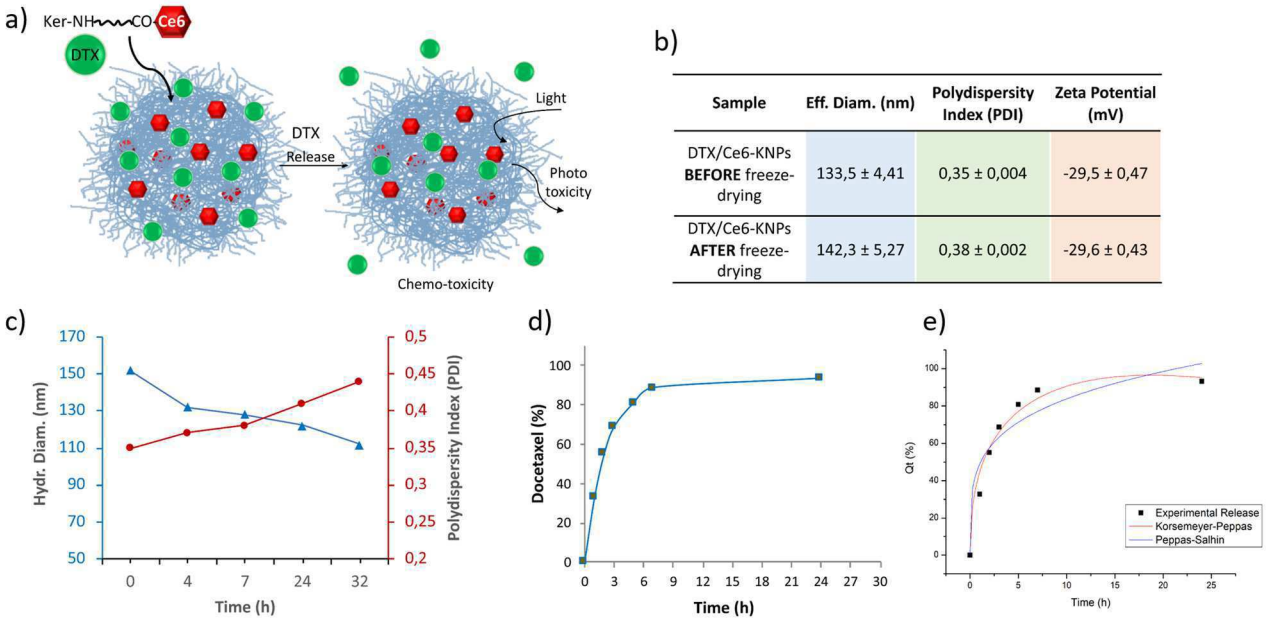

Sample	Eff. Diam. (nm)	Polydispersity Index (PDI)	Zeta Potential (mV)
DTX/Ce6-KNPs **BEFORE** freeze-drying	133,5 ± 4,41	0,35 ± 0,004	-29,5 ± 0,47
DTX/Ce6-KNPs **AFTER** freeze-drying	142,3 ± 5,27	0,38 ± 0,002	-29,6 ± 0,43

Figure 1. DTX/Ce6-KNPs characterization. a) Schematic representation of DTX/Ce6-KNPs design and structure. b) Values of DTX/Ce6-KNPs diameter, polydispersity index (PDI) and zeta potential measured in samples before and after the freeze-drying process. c) Stability of DTX/Ce6-KNPs measured up to 32 h of NP incubation in PBS at 37 °C checked by measuring diameter and PDI variations. d) Release profiles of DTX from DTX/Ce6-KNPs performed at 37 °C in PBS/EtOH and measured up to 24 h. e) Fitting models for the analysis of DTX release kinetic.

DTX release from DTX/Ce6-KNPs is shown in Fig. 1d, displaying a monophasic release trend, which includes an initial burst during the first 5 h, followed by a slower release in the following 24 h of observation up to approximately 90 %.

To better elucidate the type of release mechanism, data were analyzed by different semi-empirical models, i.e. Korsmeyer-Peppas and Peppas-Sahlin [25]. In particular, these models are useful to understand if the release mechanism is controlled by Fickian diffusion, matrix swelling or a combination of the two. As shown in Fig. 1e, DTX release from KNPs is exclusively controlled by diffusion mechanism.

3.2. Cytotoxicity and CI analysis in monolayer cell cultures

Before proceeding with the analysis of combination therapy using the bimodal keratin NPs as drug delivery system for DTX and Ce6, the cytotoxicity of the single therapeutic agents was evaluated by measuring the reduction of cancer cell viability by the MTS assay after 24 h of cell exposure.

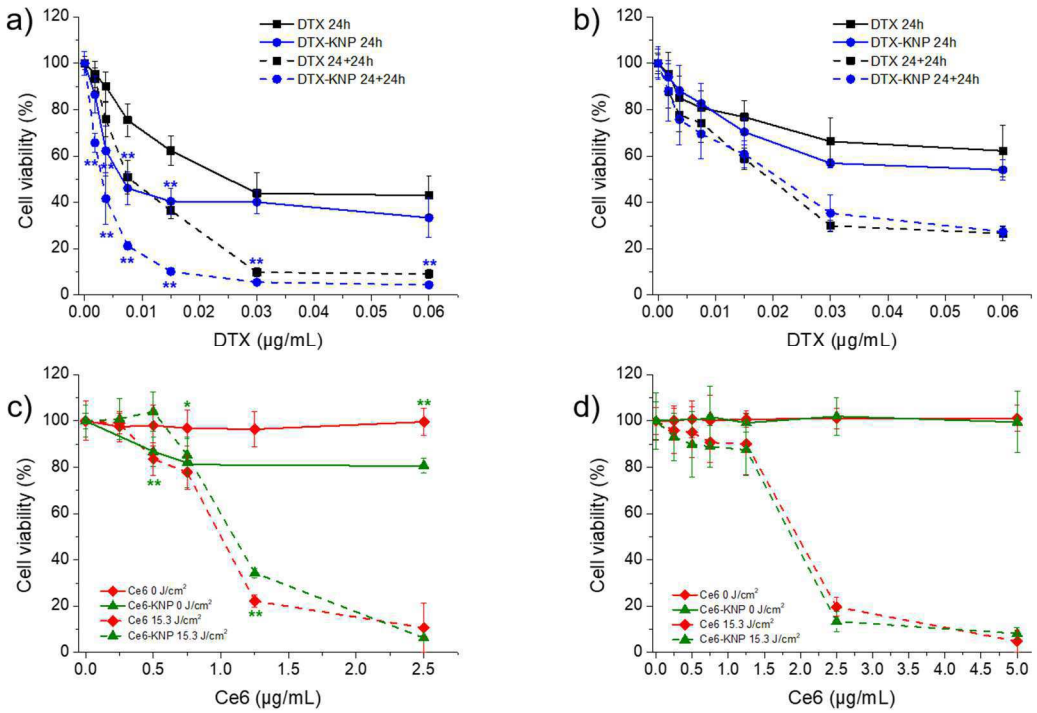

Figure 2. Cell viability measured with MTS assay in HeLa and MDA-MB-231 cells exposed to DTX-chemotherapy or Ce6-PDT. Cytotoxicity profiles of HeLa (a) and MDA-MB-231 cells (b) exposed for 24 h to free DTX or DTX-KNPs as well as treated for 24 h with the drug and release for additional 24 h in DTX-free medium (24 + 24 h). Viability of HeLa (c) and MDA-MB-231 cells (d) incubated for 24 with free Ce6 or Ce6-KNPs, not exposed or exposed to 15.3 J/cm^2 of red light. Cytotoxicity was measured 24 h post-PDT. Data are expressed as mean ± S.D. of at least two independent experiments in triplicate. *p < 0.05; **p < 0.001 free drug *vs* drug in NPs (Student's *t* test).

We compared the cytotoxicity of DTX loaded in KNPs with that of free DTX delivered in the standard solvent (DTX) in MDA-MB-231 and HeLa cells. As shown in Fig. 2, in MDA-MB-231 (b) the two DTX formulations produced comparable cytotoxic effects, while in HeLa cells (a) the use of DTX-KNPs significantly increased cell death, especially at very low drug concentrations (Dm 0.024 and 0.007 µg/ml for DTX and DTX-KNPs, respectively). Notably, cell death further increased after the release of both types of cells for additional 24 h in DTX-free medium (time point 24 + 24 h, Fig. 2a, b); also at this time point, KNPs were significantly more potent in inducing cytotoxicity in HeLa cells (Dm 0.0081 and 0.0029 µg/ml for DTX and DTX-KNPs, respectively). As a control, unloaded KNPs demonstrated to be absolutely safe at both time points considered (Fig. S1a and b). To the best of our knowledge, this is the first time that DTX was efficiently loaded in keratin-based NPs in water solution and that the nanoformulation demonstrated at least comparable efficacy to the standard clinical formulation.

As observed for DTX, the covalent link of Ce6 to KNPs did not affect negatively the PDT effects, in comparison to the free PS, in HeLa (Fig. 2c) and MDA-MB-231 (Fig. 2d) cells irradiated with 15.3 J/cm^2 of red light. Ce6-KNPs without light irradiation showed negligible cytotoxicity to both cell types. These results are not in agreement with those of a previous paper in which, for the synthesis of Ce6-KNPs, glutaraldehyde was used as crosslinking agent to promote NP aggregation, and PDT efficiency was significantly improved with respect to free Ce6 in osteosarcoma cells *in vitro* [19]. In the present paper, we completely avoided the use of crosslinking agents for NP formation, but the pure NP water suspension did not bring an increase of the phototoxic efficiency of the PS. The differences may be attributed to different

photophysical properties of Ce6 loaded in the two types of KNPs as well as to the different cell lines used. As for the single drug-loaded NPs, also bimodal NPs (DTX/Ce6-KNPs) were synthetized using the aggregation method in aqueous solution and in the absence of promoters of protein aggregation. Unfortunately, this synthesis procedure does not give the possibility of exploiting and co-loading a wide range of drug ratios within the NPs, thus limiting the capability of screening for optimal drug ratio with maximum extent of synergism. In fact, it is well known that to obtain synergism when combining different drugs or therapeutic modalities is of fundamental importance to choose the optimal drug ratio to be loaded inside the NPs [26], generally considering as starting point ratios calculated around the Dm values of each single treatment. Regarding this, and considering that we were able to obtain stable bimodal NPs with a drug ratio of 1:1.8 for Ce6 *versus* DTX, it is clear that combination therapy with bimodal KNPs could not be performed using the above mentioned treatment protocol (i.e. drug incubation for 24 h before PDT). In fact, as it can be deduced from Fig. 2, the Dm of DTX was significantly lower than that of Ce6-PDT in both cell lines considered, and the optimal drug ratio for that experimental setting must be in favor of Ce6 and not of DTX, as happens instead in bimodal KNPs prepared with the aggregation method. Thus, we modified the cell incubation protocol by reducing the time of drug exposure to 3 h in order to reduce DTX cytotoxicity, which, in the latter condition, became comparable with that of Ce6. All subsequent experiments were carried out only with HeLa cells (sensitive and resistant to DTX) since in MDA-MB-231 we did not observe appreciable therapeutic improvement using DTX-KNPs.

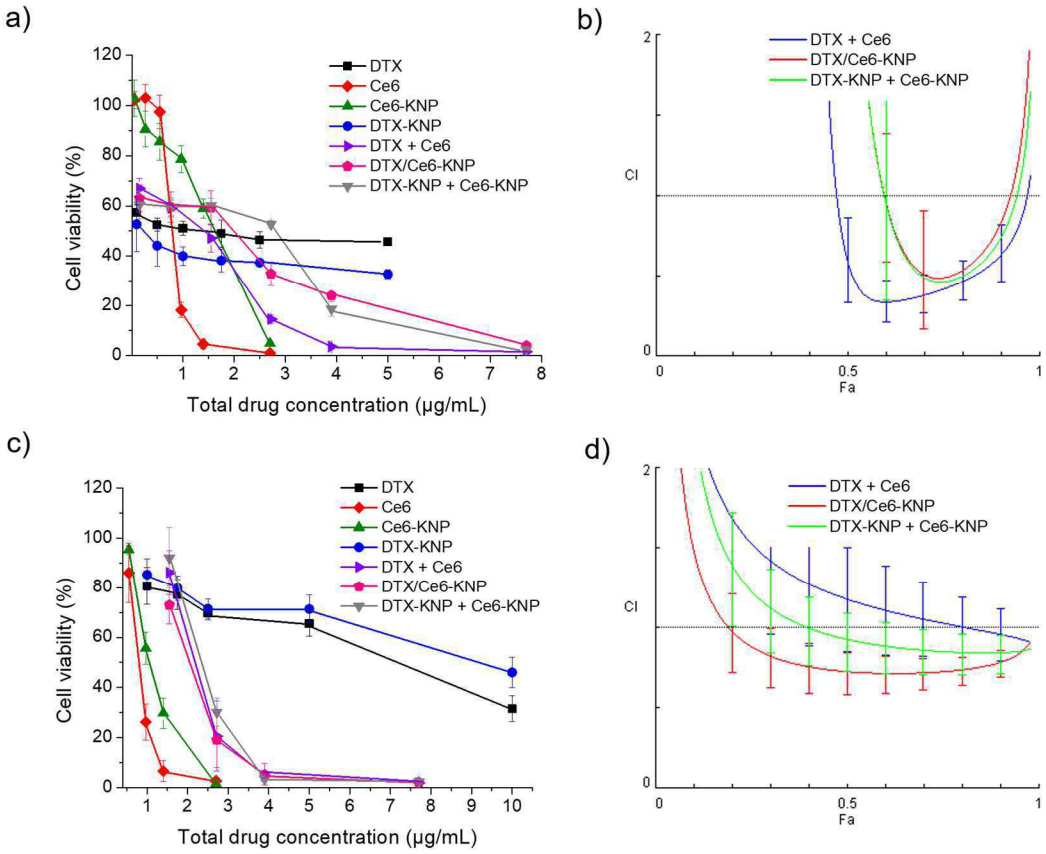

Figure 3. Dose-response curves and Combination Index Plots (Fa vs CI plots) of HeLa-P (a, b) and HeLa-R (c, d) cells exposed to DTX-chemotherapy and/or Ce6-PDT. For cell viability curves, data are expressed as mean percentage ± S.D. of at least two independent experiments carried out in triplicate.

As shown in Fig. S2a and Table 1, parental HeLa cells incubated in the dark for 3 h with increasing concentrations of DTX or DTX-KNPs showed a rapid decrease of cell viability at very low drug concentrations (Dm of 1.149 and 0.163 μg/ml for DTX and DTX-KNP, respectively) but the percentages of cell death only slightly increased by increasing the dose up to 5 μg/ml. Notably, even after a 3 h cell incubation, the advantage of using KNPs remain impressive, with a ~7-fold possibility of drug dose reduction with respect to free DTX.

Table 1. Dm values and Dose Reduction Index (DRI) calculated by Compusyn in DTX-sensitive HeLa (HeLa-P) and DTX-resistant HeLa (HeLa-R) cells. Dm was calculated for cells exposed to DTX-chemotherapy and/or Ce6-PDT (time point 3 + 24 h) using free drugs or KNP formulations. The DRI values were calculated for cells exposed to combination therapy and indicate how many folds the concentration of each single drug can be reduced to obtain a Fa value of 50%.

Drug formulation	Dm (μg/mL)		Dose-reduction index (DRI)			
	HeLa-P	HeLa-R	HeLa-P		HeLa-R	
			DTX	Ce6	DTX	Ce6
Ce6	0.708	0.799	-	-	-	-
Ce6-KNP	1.155	1.080	-	-	-	-
DTX	1.149	6.172	-	-	-	-
DTX-KNP	0.163	10.395	-	-	-	-
DTX + Ce6	0.549	2.139	3.25	3.61	4.48	1.04
DTX/Ce6-KNP	0.747	1.850	0.34	4.32	8.73	1.63
DTX-KNP + Ce6-KNP	0.758	2.363	0.33	4.26	6.84	1.27

On the contrary, the PDT phototoxic effects of Ce6 linked to KNPs were significantly worsened with respect to the free PS (Fig. 3a, Table 1; Dm of 0.708 and 1.155 for Ce6 and Ce6-KNPs, respectively). This result is unexpected considering that the cell uptake of the PS delivered by KNPs is increased with respect to free Ce6 (Fig. S3a), and Aluigi *et al.* reported increased photodynamic activity of Ce6 in KNPs [19]. Furthermore, the intracellular localization of the PS, that can affect photosensitizing activity, remained unaltered by using KNPs for the PS delivery. In HeLa cells, we found a clear accumulation in the endoplasmic reticulum, demonstrated by the co-localization of the red fluorescence of Ce6 and the green fluorescence of the ER-Tracker green probe (Fig. S3d, e) while we did not observe mitochondrial localization (Fig. S3b, c) as reported by others [27]. Thus, we exclude that the different PDT-response between Ce6 and Ce6-KNPs is related to a different compartmentalization of the PS within the cells.

In any case, when combination therapy was performed using bimodal KNPs (Fig. 3a), the Dm relative to the total drug concentration was only slightly increased compared to those obtained with the combination of the two drugs delivered without NPs (Dm of 0.747 and 0.549 for DTX/Ce6-KNPs and DTX + Ce6, respectively). A similar Dm value (0.758) was obtained when the cells were incubated with the drug loaded in separate NPs (DTX-KNPs + Ce6-KNPs). Notably, the inclusion of DTX in bimodal NPs enhanced Ce6 uptake (Fig. S3a), while the amount of Ce6 remain almost unvaried in the combination of DTX + Ce6 and DTX-KNPs + Ce6-KNPs.

Furthermore, to assess if the combination of DTX-chemotherapy and Ce6-PDT was synergic in the drug ratio considered, we

uploaded in the Compusyn software the values of Fraction affected (Fa) *vs* the total drug concentration used in the cell viability curves established for calculating the CI values. As shown in the Fa *vs* CI Plot (Fig. 3b), none of the three combinations produced synergic effects for Fa values lower than 0.5 (CI > 1, antagonism), very likely because at very low drug concentrations the contribution to the overall cytotoxic effect comes almost exclusively from DTX. The lowest CI values (CI < 1, synergism) were measured for the combination of the free drugs, especially in the Fa range 0.5-0.7, while for Fa > 0.7 the extent of synergism was comparable; for DTX/Ce6-KNPs and DTX-KNPs + Ce6-KNPs the curves are quite superimposable. Along with the CI values, also the DRI values were calculated to assess the extent of drug reduction for each type of combination; DRI values >1 and < 1 indicate favorable and not favorable dose-reduction, respectively. In Table 1 are reported the DRI values for Fa = 0.5 which have been calculated with Compusyn using the dose of each single drug giving a cell mortality of 50% when delivered alone or in combination with or without KNPs (Table S1). The calculated DRI values indicate the possibility of dose reduction of both drugs in DTX + Ce6 combination (DRI ~ 3), while using bimodal KNPs or DTX-KNPs + Ce6-KNPs only the PS dose can be reduced by 4.3 times. Combination therapy, CI and DRI analysis were assessed also in HeLa cells resistant to DTX (HeLa-R) in order to evaluate if this new bimodal nanoformulation can bring some therapeutic improvements and can contrast the effects of the P-glycoprotein 1 (P-gp) membrane efflux pump. In fact, we have already reported that HeLa-R cells are at least 8-fold more resistant to DTX than the parental cells due to the over-expression of P-gp [13]. As visible in Fig. 3b and Table 1 and as expected, HeLa-R were significantly more resistant to DTX-chemotherapy than HeLa-P cells (Dm of 6.172 and 10.396 μg/ml for DTX and DTX-KNPs, respectively) while the sensitivity to Ce6-PDT remain almost unaltered. Interestingly, in HeLa-R bimodal KNPs were more efficient in inducing cell mortality than the combination of the free drugs and importantly, while DTX and Ce6 loaded in KNPs demonstrated synergistic interaction almost at all Fa considered, free DTX + free Ce6 showed clear antagonism. Accordingly, the synergism using bimodal KNPs was accompanied by the higher DRI value for DTX that was doubled with respect to the standard solvent formulation (8.738 vs 4.489, respectively), confirming that this keratin-based nanoformulation is a good candidate to contrast acquired chemotherapeutic resistance at least in the cell line considered in our studies.

3.3. Cytotoxicity and CI analysis in 3D cell cultures

The *in vitro* use of multicellular spheroids as avascular tumor models, mimicking solid tumors more closely than monolayers, represent useful tools for investigating the efficacy of combo-nanotherapy and the extent of drug penetration before moving to *in vivo* studies on animal models. Thus, to assess whether bimodal KNPs were effective in producing synergism also in cells cultured *in vitro* in a tridimensional arrangement, HeLa-P and HeLa-R spheroids were generated using the liquid overlay technique and exposed to combination therapy after 3 days of growth. Combination therapy was performed with the 3 h incubation protocol (3 + 24 h) but the total light fluence was increased to 30 J/cm^2 to compensate the reduced PS uptake in cells of the 3D model with respect to cell in monolayers. Photo-toxicity curves of HeLa-P (Fig. 4b) and HeLa-R (Fig. 5b) spheroids showed enhanced cell mortality using bimodal KNPs with respect to the NPs loaded with the single drugs.

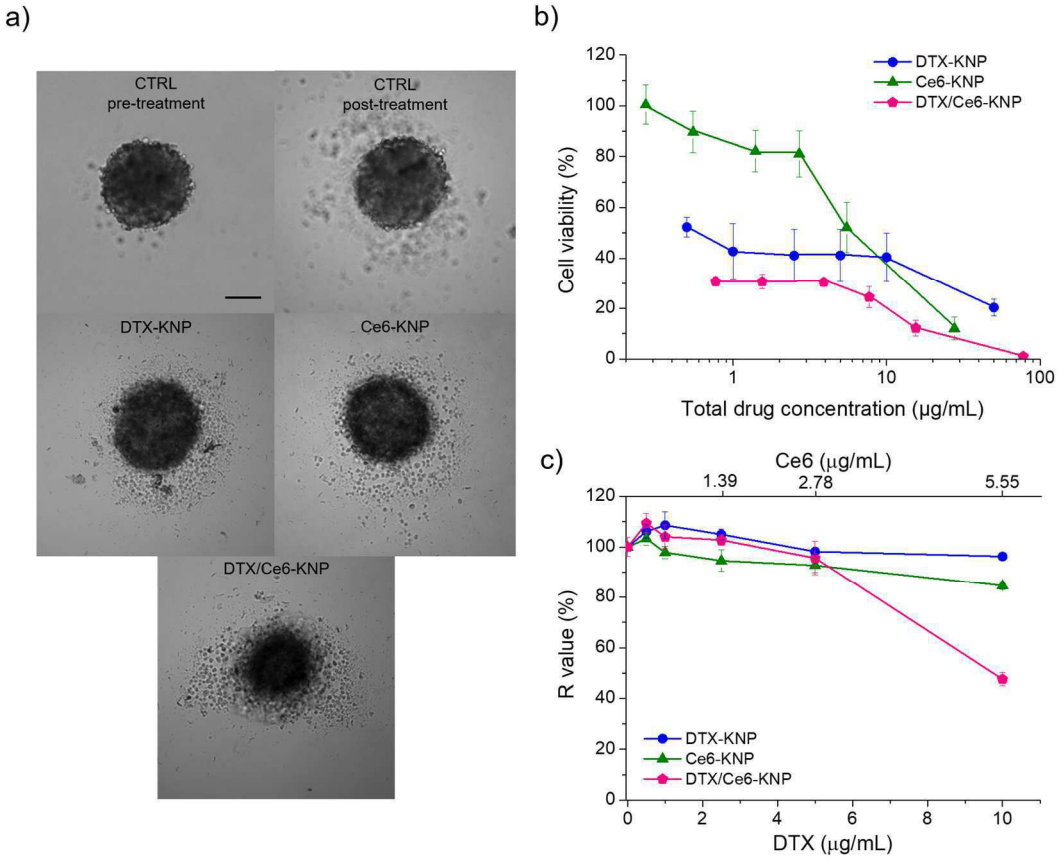

Figure 4. Mono and combined therapy in HeLa-P spheroids. a) Bright field images of a representative spheroid before drug treatment (CTRL pre-treatment; e.g. 3 day-old spheroid) and after the treatment (CTRL post-treatment; e.g. 4 day-old spheroid). The spheroids incubated with the 3 different nanoformulations were exposed for 3 h to KNPs on day 3, irradiated with red light at a fluence of 30 J/cm^2 and photographed 24 h post-PDT. The Ce6 dose was 5.55 μg/mL while the DTX dose was 10 μg/mL. Scale bar: 100 μm, 10X objective. b) Dose-response curves of spheroids incubated for 3 h with the different KNP formulations, irradiated and assessed for cell viability 24 h post-PDT using the 3D-Glo Assay. The control used was CTRL post-treatment. Data are expressed as mean percentage ± S.D. of at least two independent experiments in triplicate. c) Spheroid volume reduction through the calculation of the R value (%) as a function of the increasing drug dose.

As one can see in the bright field images of Fig. 4a and 5a, acquired 24 h post-irradiation and immediately before cell viability assessment, while untreated spheroids show spherical and compact morphologies (CTRL post-treatment), drug treatments generally induced the release of the external rim of cells from the core of the spheroids. This event was significantly more evident in spheroids of both of cell types treated with bimodal KNPs, accordingly to the higher cytotoxicity measured. Consequent to the loss of external cells due to death, the volume of the spheroid significantly decreased (Fig. 4c and 5c), as shown by the R value percentages, which are indicative of spheroid volume variations before and after treatment. In both types of spheroids only using the bimodal nanoformulation the R values decreased significantly administering a total drug dose of 15.5 μg/ml. As expected, based on the higher sensitivity to combo-nanotherapy, volume reduction was more consistent in HeLa-P with respect to HeLa-R spheroids, with R values of 48% and 65%, respectively, at the highest total drug tested in the experiment.

.

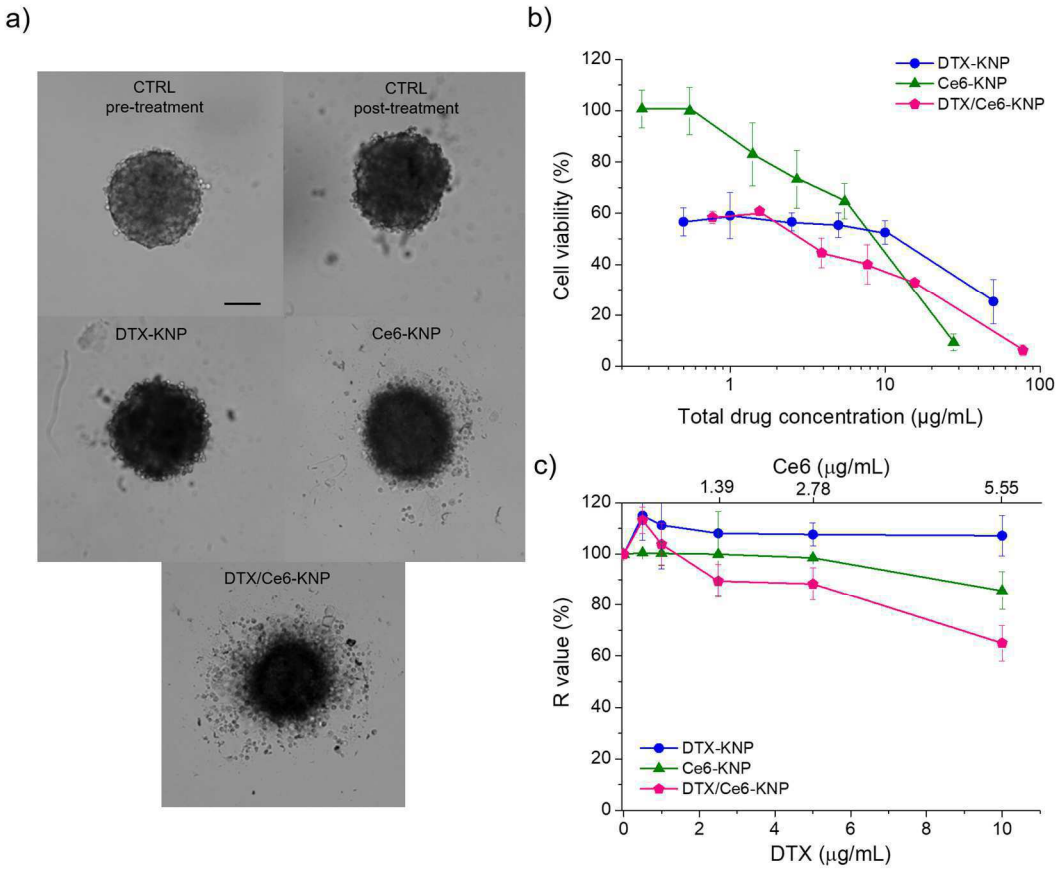

Figure 5. Mono and combined therapy in HeLa-R spheroids. a) Bright field images of a representative spheroid before drug treatment (CTRL pre-treatment; e.g. 3 day-old spheroid) and after the treatment (CTRL post-treatment; e.g. 4 day-old spheroid). The spheroids incubated with the 3 different nanoformulations were exposed for 3 h to KNP on day 3, irradiated with red light at a fluence of 30 J/cm^2 and photographed 24 h post-PDT. The Ce6 dose was 5.55 µg/ml while the DTX dose was 10 µg/ml. Scale bar: 100 µm, 10X objective. b) Dose-response curves of spheroids incubated for 3 h with the different KNP formulations, irradiated and assessed for cell viability 24 h post-PDT using the 3D-Glo Assay. The control used was CTRL post-treatment. Data are expressed as mean percentage ± S.D. of at least two independent experiments in triplicate. c) Spheroid volume reduction through the calculation of the R value (%) as a function of the increasing drug dose.

Table 2. Dm values and DRI calculated by Compusyn in HeLa-P and HeLa-R spheroids. Dm was calculated for cells exposed to DTX-chemotherapy and/or Ce6-PDT (time point 3 + 24 h) using NP formulations. The DRI values were calculated for cells exposed to combination therapy and indicate how many folds the concentration of each single drug can be reduced to obtain a Fa value of 50%.

Drug formulation	**Dm (µg/mL)**		**Dose-reduction index (DRI)**			
	HeLa-P	**HeLa-R**	**HeLa-P**		**HeLa-R**	
			DTX	**Ce6**	**DTX**	**Ce6**
Ce6-KNP	5.859	6.273	-	-	-	-
DTX-KNP	0.716	4.162	-	-	-	-
DTX/Ce6-KNP	0.700	2.567	1.58	23.41	2.52	6.84

Indeed, HeLa-R cells cultured as spheroids retain resistance to DTX compared to HeLa-P spheroids with a 6-times higher Dm value for DTX-KNPs (Table 2). Notwithstanding the doubling of the light fluence, both types of spheroids demonstrated less sensitivity to Ce6-PDT, with Dm at least 6 times higher with respect to those observed in monolayer cell cultures (Table 1 and 2). Accordingly, in combination therapy, the calculated DRI values for bimodal NPs were in favor of Ce6 dose reduction rather than for DTX (Table 2), with DRIs of 23.41 and 6.84 for Ce6 in HeLa-P and HeLa-R spheroids, respectively. In any case, the possibility of DTX dose reduction was higher in HeLa-R spheroids (DRI of 2.52 vs 1.58), confirming once again the better performances of the bimodal nanoformulation in drug-resistant cells. Regarding Ce6 and DTX interaction in multicellular tumor spheroids, synergism was measured exclusively for Fa values higher than 0.5 (Fig. S4a and b), in both cell lines considered.

3.4. Drug and NP penetration in 3D cell cultures

It is well established that drug and NP penetration inside solid tumors is hampered by several factors such as the presence of the extracellular matrix components and the high interstitial pressure at the tumor site. Multicellular tumor spheroids represent one of the simplest and reliable *in vitro* systems to study NP transport across several layers of cells [28]. HeLa-P spheroids incubated for 3 h with the different formulations were used as model to study the intracellular transport of the PS, by exploiting the red fluoresce of Ce6 and confocal microscopy.

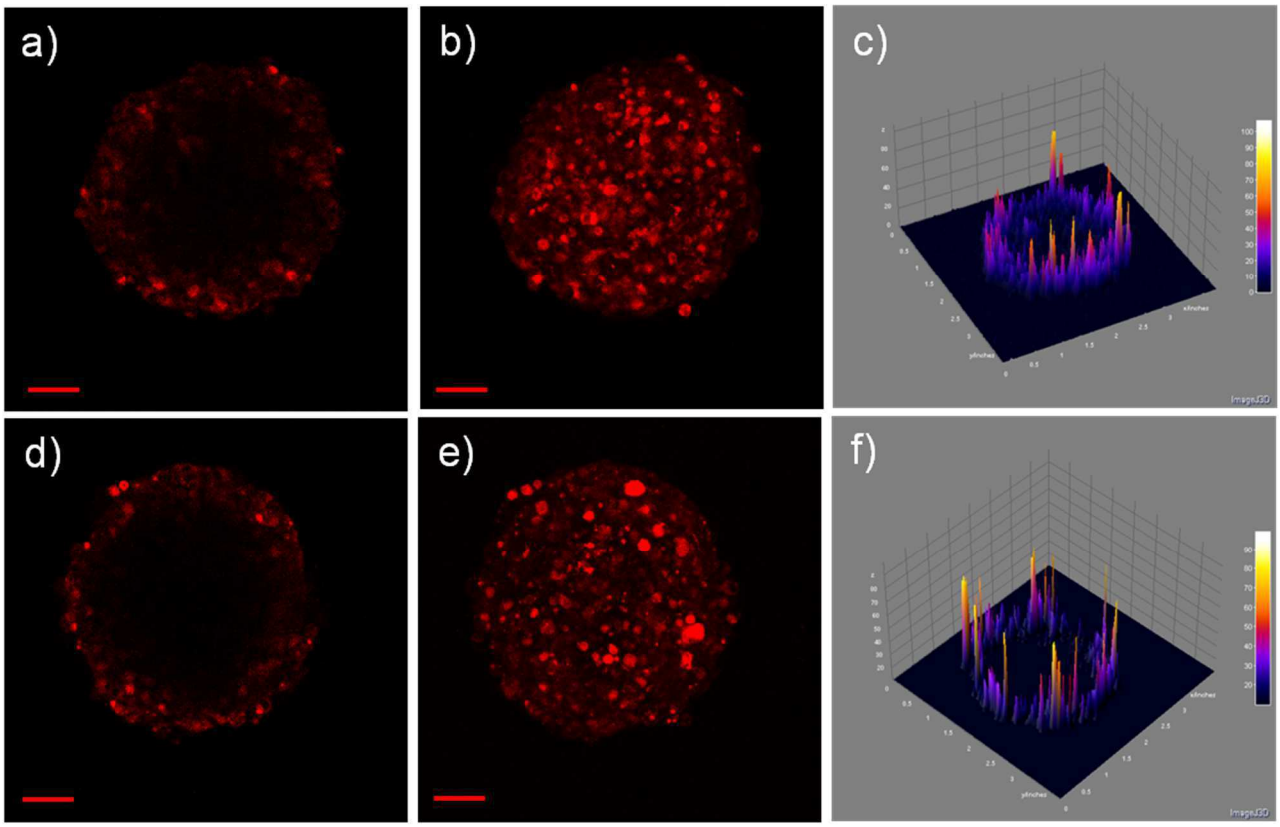

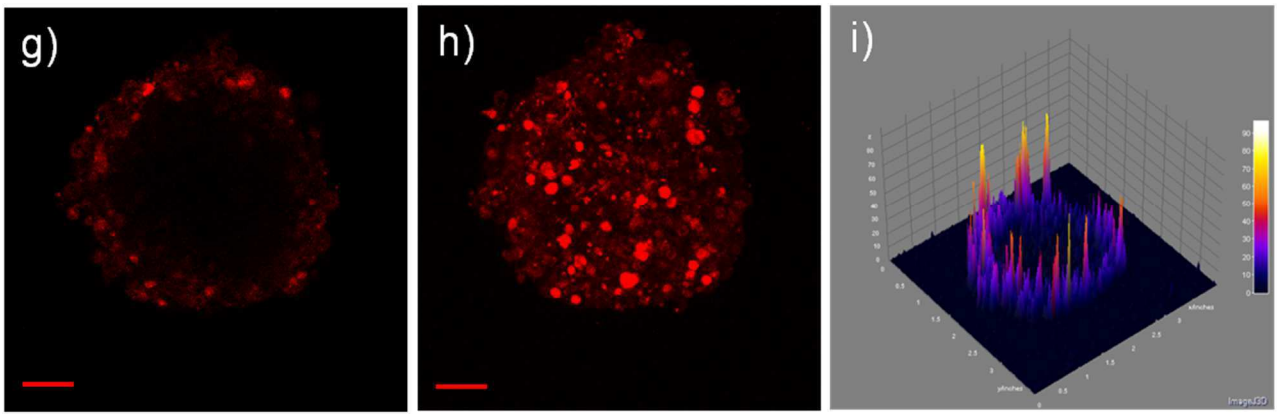

Figure 6. Ce6 penetration in HeLa-P spheroids incubated for 3 h with 5 μg/mL free Ce6 (a-c), Ce6-KNP (d-f) and DTX/Ce6-KNP (g-i). a,d,g) Ce6 fluorescence at the equatorial plane of spheroids; b,e,h) maximum projection obtained from the superimposition of 20 different acquired focal planes; c,f,i) 3D reconstruction of Ce6 fluorescence distribution in the equatorial plane of the spheroids. Scale bar 50 μm.

As visible in the images of Fig. 6 showing Ce6 fluorescence in the equatorial plane of a spheroid incubated with free Ce6 (a), Ce6-KNPs (d) and DTX/Ce6-KNPs (g), the different formulations shared a very similar pattern of distribution exclusively in the outer rims of cells of the spheroids. From the maximum projection images (Fig. 6b, e, h), reconstructed by the super-imposition of the different focal planes acquired along the entire spheroid structure, it can be observed that, independently from the formulation, the PS distribution was rather heterogeneous and varied from cell to cell. The majority of the cells that exhibited the highest fluorescence signals were located in the periphery of the spheroids as confirmed by the 3D reconstruction plots (Fig. 6c, f, i) generated with the ImageJ software. From the tridimensional reconstruction it is possible to observe in the z-axis an increased numbers of peaks of high fluorescence values (yellow) in the spheroids incubated with Ce6-KNPs (f) and DTX/Ce6-KNPs (i), indicating a higher extent of PS association/uptake when transported in NPs. Moreover, for the bimodal nanoformulation the extent of penetration appeared increased with respect to Ce6-KNPs, but quite similar to that of the undelivered PS. A further analysis of PS penetration (Fig. S5) confirmed the observation of the 3D plots, indicating that Ce6 delivered in the bimodal formulation was able to penetrate up to 60 μm inside the spheroid mass compared to the 40 μm when included in KNPs. In any case, even if the extent of penetration of the bimodal nanoformulation was quite comparable (about 50 μm) with those of the Ce6 delivered in the standard solvent, the extent of intracellular uptake was significantly improved as already mentioned. Thus, it is worth to note that the capability of KNPs to deliver Ce6 in higher amount with respect to the PS standard solution is maintained from monolayer to tridimensional cell culture models.

4. Conclusions

We have herein reported for the first time the encapsulation of DTX and the covalent loading of the PS Ce6 in bimodal KNPs, simply obtained in aqueous solution by avoiding the use of organic solvents and/or cross-linking agents. Notwithstanding the reduced capacity of aggregation method to obtained stable NPs by varying the ratio between DTX and Ce6 but allowing the co-loading of the two drugs in the ratio 1.8:1, we found some synergistic interactions between DTX-chemotherapy and Ce6-PDT by using bimodal KNPs to treat DTX-sensitive HeLa cells cultured as monolayers. Importantly, when DTX-resistant HeLa cells were exposed to combination therapy, while the administration of the drugs in the standard formulation resulted in an antagonistic interaction, bimodal KNPs photo-killed the

cells in a synergic way. Moreover, even when HeLa-P and HeLa-R cells were cultured as spheroids to approximate the complexity of tumors *in vivo*, the bimodal DTX/Ce6-KNPs demonstrated to be more effective in inducing mortality and in reducing spheroid volume than DTX-KNPs and Ce6-KNPs. Combination therapy in spheroids determine the damage and the release from the central core especially of the cells of external rim, accordingly to the limited delivery/penetration of PS/KNPs inside spheroid.

Acknowledgements
The financial support of the University of Padova (fondi ex 60%) is gratefully acknowledged.

Appendix A. Supplementary data

References

[1] R.L. Siegel, K.D. Miller, A. Jemal, Cancer statistics, 2018, CA. Cancer J. Clin. 68 (2018) 7–30. doi:10.3322/caac.21442.

[2] X. Qu, C. Eugen Hagemeyer, N. Paolocci, S. Hua Susan, S. Hua, M.B. C de Matos, J.M. Metselaar, G. Storm, Current Trends and Challenges in the Clinical Translation of Nanoparticulate Nanomedicines: Pathways for Translational Development and Commercialization, Front. Pharmacol. | Www.Frontiersin.Org. 1 (2018) 790. doi:10.3389/fphar.2018.00790.

[3] E. Bernabeu, M. Cagel, E. Lagomarsino, M. Moretton, D.A. Chiappetta, Paclitaxel: What has been done and the challenges remain ahead, Int. J. Pharm. 526 (2017) 474–495. doi:10.1016/j.ijpharm.2017.05.016.

[4] M. Kundranda, J. Niu, Albumin-bound paclitaxel in solid tumors: clinical development and future directions, Drug Des. Devel. Ther. 9 (2015) 3767. doi:10.2147/DDDT.S88023.

[5] M. Farhan Sohail, M. Rehman, H. Shoaib Sarwar, S. Naveed, O. Salman, N. Irfan Bukhari, I. Hussain, T.J. webster, G. Shahnaz, Advancements in the oral delivery of Docetaxel: challenges, current state-of-the-art and future trends, Int. J. Nanomedicine Dovepress. 13 (2018) 3145–3161. doi:10.2147/IJN.S164518.

[6] B. Li, Z. Feng, L. He, W. Li, Q. Wang, J. Liu, J. Huang, Y. Zheng, Y. Ma, X. Yang, K. Wang, Self-Assembled Supramolecular Nanoparticles for Targeted Delivery and Combination Chemotherapy, ChemMedChem. (2018). doi:10.1002/cmdc.201800291.

[7] R.K. Thapa, J.Y. Choi, B. Gupta, T. Ramasamy, B.K. Poudel, S.K. Ku, Y.S. Youn, H.G. Choi, C.S. Yong, J.O. Kim, Liquid crystalline nanoparticles encapsulating cisplatin and docetaxel combination for targeted therapy of breast cancer., Biomater. Sci. 4 (2016) 1340–50. doi:10.1039/c6bm00376a.

[8] V. Kushwah, S.S. Katiyar, C.P. Dora, A. Kumar Agrawal, D.A. Lamprou, R.C. Gupta, S. Jain, Co-delivery of docetaxel and gemcitabine by anacardic acid modified self-assembled albumin nanoparticles for effective breast cancer management, Acta Biomater. 73 (2018) 424–436. doi:10.1016/j.actbio.2018.03.057.

[9] L. Wang, D. Li, Y. Hao, M. Niu, Y. Hu, H. Zhao, J. Chang, Z. Zhang, Y. Zhang, Gold nanorod–based poly(lactic-co-glycolic acid) with manganese dioxide core–shell structured multifunctional nanoplatform for cancer theranostic applications, Int. J. Nanomedicine. Volume 12 (2017) 3059–3075. doi:10.2147/IJN.S128844.

[10] S. Maiolino, F. Moret, C. Conte, A. Fraix, P. Tirino, F. Ungaro, S. Sortino, E. Reddi, F. Quaglia, Hyaluronan-decorated polymer nanoparticles targeting the CD44 receptor for the combined photo/chemo-therapy of cancer, Nanoscale. 7 (2015). doi:10.1039/c4nr06910b.

[11] C. Conte, A. Scala, G. Siracusano, G. Sortino, R. Pennisi, A. Piperno, A. Miro, F. Ungaro, M.T. Sciortino, F. Quaglia, A. Mazzaglia, Nanoassemblies based on non-ionic amphiphilic cyclodextrin

hosting Zn(II)-phthalocyanine and docetaxel: Design, physicochemical properties and intracellular effects, Colloids Surfaces B Biointerfaces. 146 (2016) 590–597. doi:10.1016/j.colsurfb.2016.06.047.

[12] C. Conte, F. Ungaro, G. Maglio, P. Tirino, G. Siracusano, M.T. Sciortino, N. Leone, G. Palma, A. Barbieri, C. Arra, A. Mazzaglia, F. Quaglia, Biodegradable core-shell nanoassemblies for the delivery of docetaxel and Zn(II)-phthalocyanine inspired by combination therapy for cancer, J. Control. Release. 167 (2013) 40–52. doi:10.1016/j.jconrel.2012.12.026.

[13] E. Gaio, C. Conte, D. Esposito, G. Miotto, F. Quaglia, F. Moret, E. Reddi, Co-delivery of docetaxel and disulphonate tetraphenyl chlorin in one nanoparticle produces strong synergism between chemo- and photodynamic therapy in drug-sensitive and -resistant cancer cells, Mol. Pharm. (2018) acs.molpharmaceut.8b00597. doi:10.1021/acs.molpharmaceut.8b00597.

[14] P. Agostinis, K. Berg, K.A. Cengel, T.H. Foster, A.W. Girotti, S.O. Gollnick, S.M. Hahn, M.R. Hamblin, A. Juzeniene, D. Kessel, M. Korbelik, J. Moan, P. Mroz, D. Nowis, J. Piette, B.C. Wilson, J. Golab, Photodynamic therapy of cancer: An update, CA. Cancer J. Clin. 61 (2011) 250–281. doi:10.3322/caac.20114.

[15] F. Moret, E. Reddi, Strategies for optimizing the delivery to tumors of macrocyclic photosensitizers used in photodynamic therapy (PDT), J. Porphyr. Phthalocyanines. 21 (2017). doi:10.1142/S1088424617300014.

[16] K. DeFrates, T. Markiewicz, P. Gallo, A. Rack, A. Weyhmiller, B. Jarmusik, X. Hu, K. DeFrates, T. Markiewicz, P. Gallo, A. Rack, A. Weyhmiller, B. Jarmusik, X. Hu, Protein Polymer-Based Nanoparticles: Fabrication and Medical Applications, Int. J. Mol. Sci. 19 (2018) 1717. doi:10.3390/ijms19061717.

[17] V. Verma, P. Verma, P. Ray, A.R. Ray, Preparation of scaffolds from human hair proteins for tissue-engineering applications., Biomed. Mater. 3 (2008) 025007. doi:10.1088/1748-6041/3/2/025007.

[18] J.S. Desgrosellier, D.A. Cheresh, Integrins in cancer: biological implications and therapeutic opportunities, Nat. Rev. Cancer. 10 (2010) 9–22. doi:10.1038/nrc2748.

[19] A. Aluigi, G. Sotgiu, C. Ferroni, S. Duchi, E. Lucarelli, C. Martini, T. Posati, A. Guerrini, M. Ballestri, F. Corticelli, G. Varchi, Chlorin e6 keratin nanoparticles for photodynamic anticancer therapy, RSC Adv. 6 (2016) 33910–33918. doi:10.1039/C6RA04208B.

[20] A. Aluigi, M. Ballestri, A. Guerrini, G. Sotgiu, C. Ferroni, F. Corticelli, M.B. Gariboldi, E. Monti, G. Varchi, Organic solvent-free preparation of keratin nanoparticles as doxorubicin carriers for antitumour activity, Mater. Sci. Eng. C. 90 (2018) 476–484. doi:10.1016/j.msec.2018.04.088.

[21] F. Foglietta, G.C. Spagnoli, M.G. Muraro, M. Ballestri, A. Guerrini, C. Ferroni, A. Aluigi, G. Sotgiu, G. Varchi, Anticancer activity of paclitaxel-loaded keratin nanoparticles in two-dimensional and perfused three-dimensional breast cancer models, Int. J. Nanomedicine. Volume 13 (2018) 4847–4867. doi:10.2147/IJN.S159942.

[22] E. Gaio, D. Scheglmann, E. Reddi, F. Moret, Uptake and photo-toxicity of Foscan®, Foslip® and Fospeg® in multicellular tumor spheroids, J. Photochem. Photobiol. B Biol. 161 (2016). doi:10.1016/j.jphotobiol.2016.05.011.

[23] Y. Chen, W. Zhang, Y. Huang, F. Gao, X. Fang, Dual-functional c(RGDyK)-decorated Pluronic micelles designed for antiangiogenesis and the treatment of drug-resistant tumor., Int. J. Nanomedicine. 10 (2015) 4863–81. doi:10.2147/IJN.S86827.

[24] T.-C. Chou, Theoretical basis, experimental design, and computerized simulation of synergism and antagonism in drug combination studies., Pharmacol. Rev. 58 (2006) 621–81. doi:10.1124/pr.58.3.10.

[25] A. Rezaei, A. Nasirpour, H. Tavanai, M. Fathi, A study on the release kinetics and mechanisms of vanillin incorporated in almond gum/polyvinyl alcohol composite nanofibers in different aqueous food simulants and simulated saliva, Flavour Fragr. J. 31 (2016) 442–447. doi:10.1002/ffj.3335.

[26] J.A. Kemp, M.S. Shim, C.Y. Heo, Y.J. Kwon, "Combo" nanomedicine: Co-delivery of multi-modal therapeutics for efficient, targeted, and safe cancer therapy, Adv. Drug Deliv. Rev. 98 (2016) 3–18. doi:10.1016/j.addr.2015.10.019.

[27] W. Luo, R.-S. Liu, J.-G. Zhu, Y.-C. Li, H.-C. Liu, Subcellular location and photodynamic therapeutic effect of chlorin e6 in the human tongue squamous cell cancer Tca8113 cell line., Oncol. Lett. 9 (2015) 551–556. doi:10.3892/ol.2014.2720.

[28] H. Lu, M.H. Stenzel, Multicellular Tumor Spheroids (MCTS) as a 3D In Vitro Evaluation Tool of Nanoparticles, Small. 14 (2018) 1702858. doi:10.1002/smll.201702858.

Supplementary Data

Keratin nanoparticles co-delivering Docetaxel and Chlorin e6 for synergic chemo- and photodynamic anticancer effect

Elisa Gaio[a#], Andrea Guerrini[b#], Marco Ballestri[b], Greta Varchi[b], Claudia Ferroni[b], Annalisa Aluigi[b], Francesca Moret[a*], Elena Reddi[a].

[a]Cell Biology Unit, Department of Biology, University of Padova, Padova, Italy

[b]Institute of Organic Synthesis and Photoreactivity, Italian National Research Council, Bologna, Italy

[#]Contributed equally

*Corresponding author

Supplementary Figures

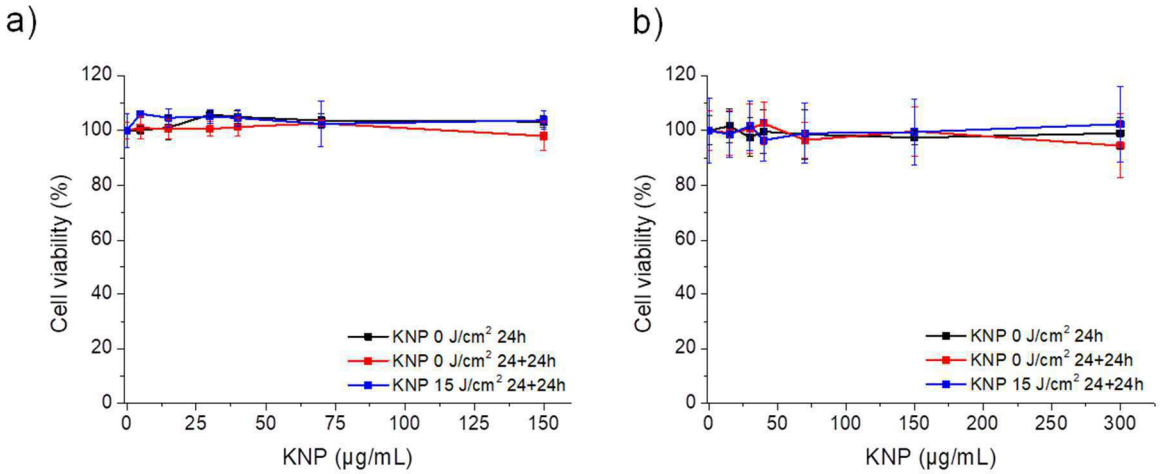

Figure S1. Viability measured in HeLa (a) and MDA-MB-231 (b) cells exposed to unloaded KNPs. Cytotoxicity profiles were measured in cells not exposed to light irradiation immediately after a 24 h treatment with KNPs (24 h) or after additional 24 h of cell release in NP-free medium (24 + 24 h). Some samples were incubated with KNPs for 24 h, exposed to 15.3 J/cm^2 of red light and assessed for cytotoxicity 24 h post-irradiation. Data are expressed as mean ± S.D. of at least two independent experiments in triplicate.

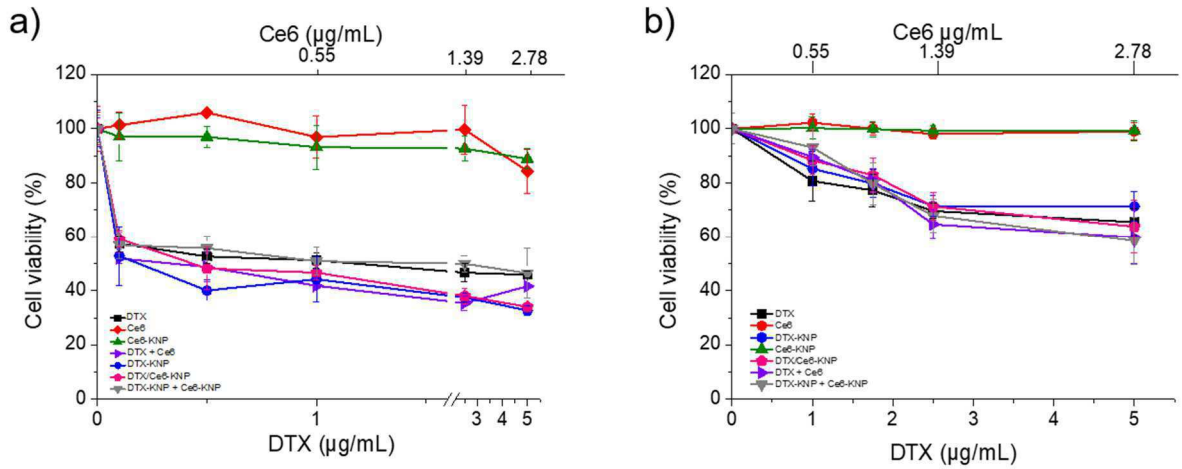

Figure S2. Dark cytotoxicity in monolayers of HeLa-P (a) and HeLa-R (b) cells exposed to the different DTX and/or Ce6 formulations for 3 h. Cytotoxicity profiles were measured with the MTS assay after additional 24 h of cell release in drug-free medium (3 + 24 h). Data are expressed as mean ± S.D. of at least two independent experiments in triplicate.

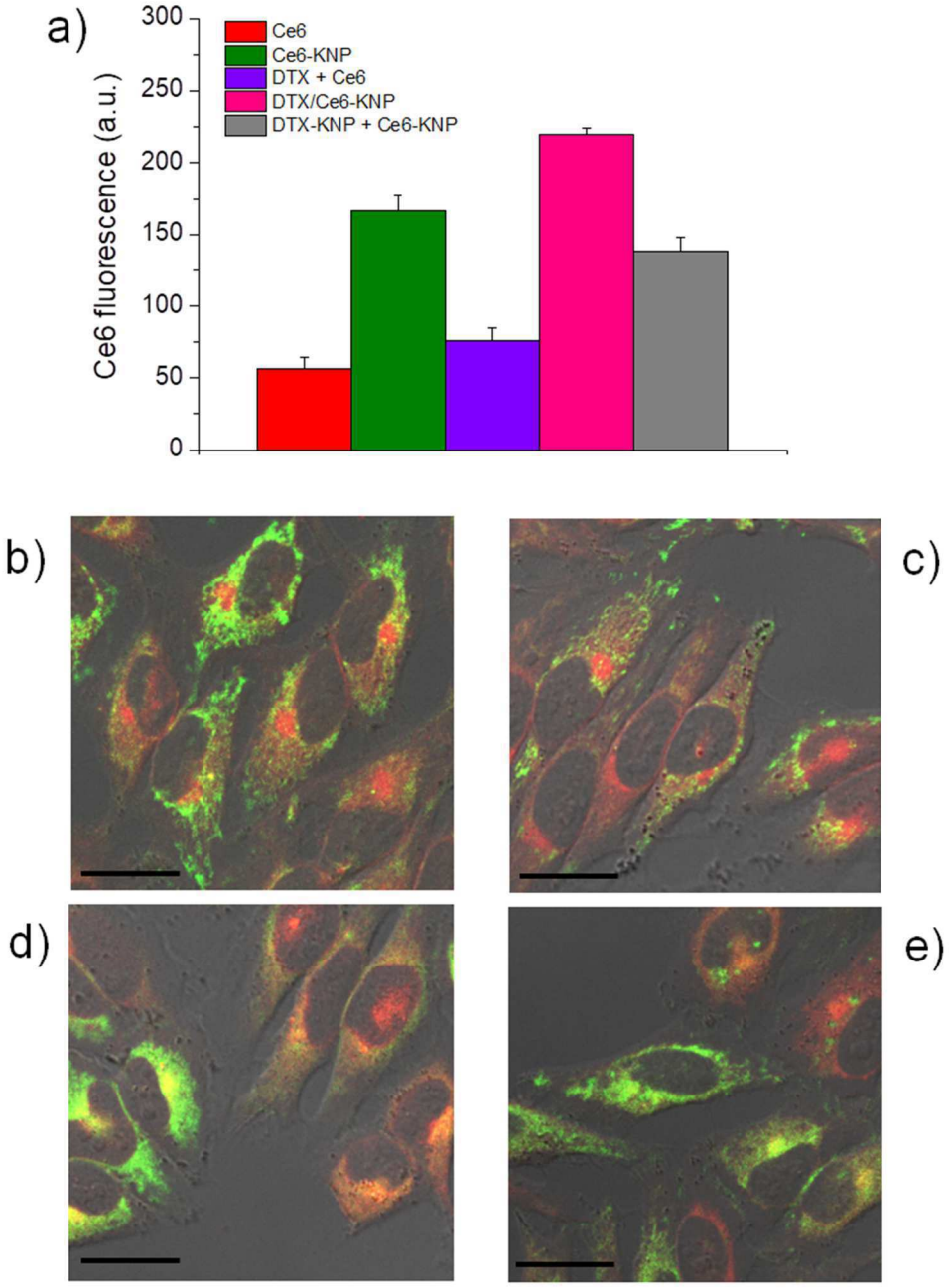

Figure S3. Intracellular uptake (a) and co-localization studies (b-e) of the different Ce6 formulations on HeLa cells. a) Flow cytometry measurements of Ce6 uptake in cells incubated for 3 h with 1 μg/mL of Ce6, absence and presence of 1.8 μg/mL DTX, delivered by the different formulations. Data are expressed as mean ± S.D. of at least two independent experiments.
Confocal microscopy images showing the co-localization of the red fluorescence of free Ce6 (b, d) and Ce6-KNP (c, e) with the green fluorescence of MitoTracker used as mitochondria probe (b, c) and ER-Tracker used as probe for endoplasmic reticulum (d, e). Scale bar: 25 μm.

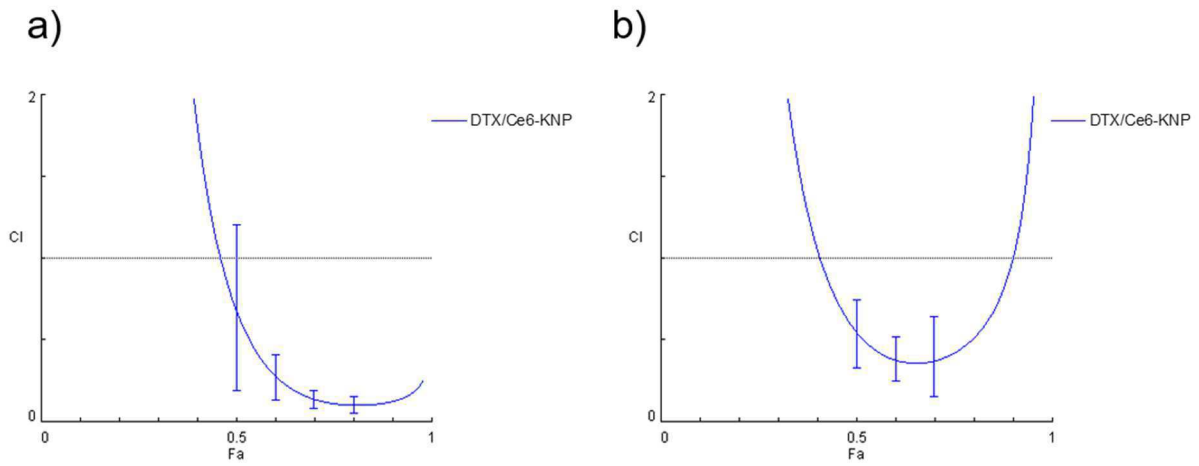

Figure S4. Combination Index Plots (Fa *vs* CI plots) of HeLa-P (a) and HeLa-R (b) spheroids exposed to combination therapy using the bimodal KNP formulation.

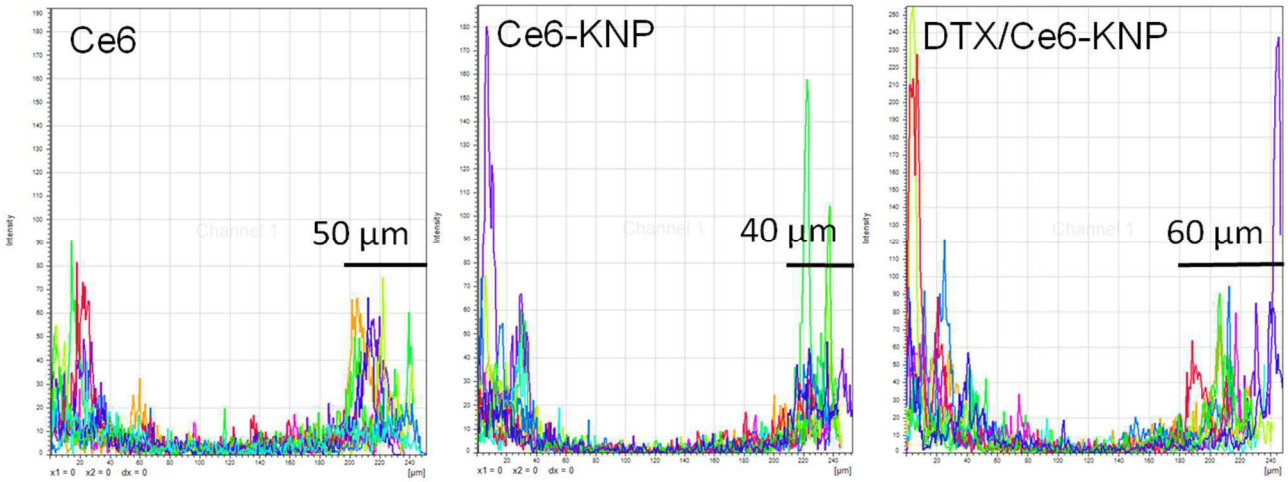

Figure S5. Comparison of Ce6 penetration in HeLa spheroids incubated for 3 h with the different Ce6 formulations. The analysis was carried out drawing 10 ROIs in the equatorial plane of selected spheroids and collecting the fluorescence signal using the program LAS AFLite.

Supplementary Tables

Table S1. Drug dose corresponding to Fa = 0.5 of HeLa-P and HeLa-R cells cultured in monolayer. The data were used to calculate the DRI values.

Data for Fa = 0.5	Drug dose (μg/ml)			
Drug Formulation	**Ce6**	**DTX**	**Ce6-KNP**	**DTX-KNP**
HeLa-P				
Ce6	0.70831			
DTX		1.14953		
Ce6-KNP			1.15541	
DTX-KNP				0.16345
DTX + Ce6	0.19618	0.35312		
DTX/Ce6-KNP			0.26685	0.48032
DTX-KNP + Ce6-KNP			0.27083	0.48749
HeLa-R				
Ce6	0.79933			
DTX		6.17230		
Ce6-KNP			1.08033	
DTX-KNP				10.3956
DTX + Ce6	0.76395	1.37510		
DTX/Ce6-KNP			0.66096	1.18973
DTX-KNP + Ce6-NP			0.84404	1.51928

Table S2. Drug dose corresponding to Fa = 0.5 of HeLa-P and HeLa-R spheroids. The data were used to calculate the DRI values.

Data for Fa = 0.5	Drug dose (μg/ml)	
Drug Formulation	**Ce6-KNP**	**DTX-KNP**
HeLa-P		
Ce6-KNP	5.85921	
DTX-KNP		0.71625
DTX/Ce6-KNP	0.25027	0.45048
HeLa-R		
Ce6-KNP	6.27371	
DTX-KNP		4.16246
DTX/Ce6-KNP	0.91690	1.65042

Conclusions

The combinatorial therapies, based on the use of drug cocktails or the association of different treatment modalities are increasingly considered as first line treatments for cancer therapy. The development of several nanomaterials used to synthetize nanoparticles with very different properties offers the possibility to improve treatment efficacy and increase the benefits expected with combination therapy reducing side effects to normal cells and tissues and, in some cases, to overcome drug resistance often developed following treatment with single drugs. Important advantages of the drug nanodelivery are the possibility of loading the nanoparticles (NPs) with well defined drug concentration ratios and to carry the drugs at the fixed ratio to target cells, differently from that occurs when drugs are delivered in their free formulation.

The work presented in this PhD thesis highlights the advantages arising from the use of two different nanocarriers for optimizing the killing effects of the combination of chemotherapy and PDT on 2D and 3D tumor cell models. PLGA-based hyaluronic acid (HA)-targeted NPs and keratin NPs were used in which, for the first time, the payload drugs (DTX and TCPS2a or Ce6) are co-loaded in a fixed concentration ratio. The cell killing efficiency, the ability to induce synergistic effects evaluated by calculation of the Combination Index (CI) with the dedicated software Compusyn, and the capability to overcome drug resistance of these nanoparticle-based formulations were evaluated. The studies on PLGA NPs, used for the co-delivery of the chemotherapeutic docetaxel (DTX) and the photosensitizer (PS) meso-tetraphenyl chlorin disulphonate (TPCS2a), namely DTX/TPCS2a-NPs, exhibited high killing efficiency and ability in inducing synergistic effect both in DTX –sensitive (HeLa and MDA-MB-231, MCF-7) and –resistant (HeLa-R) cancer cells in 2D cell monolayers and 3D cultures as spheroids and mammospheres. The advantage of using this nanoformulation is more evident in chemo-resistant cells where an impressive dose reduction index (DRI) for DTX is observed (~100). Nevertheless, the concentration ratio of 1:35 between DTX and TPCS2a, identified as optimal for producing synergism in cell monolayers, resulted inadequate in multicellular tumor spheroid and showed antagonistic effect. In this more complex in vitro tumor model, in which drug availability is limited by diffusion, synergistic interaction between DTX-chemotherapy and TPCS2a-PDT was observed using 1:5 and 1:3 concentration

ratios. This latter formulation produced the strongest synergism also in spheroids generated from HeLa-R cells. These observations highlight the importance to select the optimal drug ratio in order to elicit synergistic effects and underline that data obtained on cell monolayers could be used only as an indication of optimized conditions for combination treatment and studies performed in more complex models are required to obtain data that very likely can be translated *in vivo*. Considering that one major reason of cancer treatment failure is caused by cancer stem cells (CSCs), in this work we demonstrated the higher ability of DTX/TPCS2a-NPs to suppress sphere formation in MCF-7 and MDA-MB-231 mammospheres compared to the effect of nanoparticles loaded with DTX (DTX-NPs) and TPCS2a (TPCS2a-NPs) delivered separately. An overall evaluation of the data produced indicates that the PLGA HA-targeted NPs, used in this work, represent useful nanocarriers in which the chemotherapeutic and the PS can be loaded at their optimal drug ratio to perform successful combo photo-chemo therapy. DTX was also employed in combination with Ce6 using keratin NPs as delivery vehicle (DTX/Ce6-KNP). Despite the ratio of drugs loaded in NPs was not optimal, due to limits imposed by the aggregation method used for preparation, the nanoformulation DTX/Ce6-KNP 1.8:1 showed the capacity to induce some extent of synergism in chemo –sensitive and, more importantly, –resistant cells grown in adherent and tridimensional arrangement. In conclusion, in this PhD thesis, the potentials of the use of NPs as useful tools to perform the simultaneous delivery of different therapeutic agents to cancer cells *in vitro* have been discussed. The data underline that combination therapy represents a promising strategy for cancer treatment and offer particular advantages in overcoming drug resistance. Moreover, it is demonstrated that, despite nanotechnology allows to obtain the fine control of the drug ratio loaded in NPs, essential to obtain synergistic effects in the combination, the optimal concentration ratio between two therapeutic agents could be very different in 2D and 3D tumor models. This observation suggests the need to extend drug screening studies to 3D tumor models beside the widely employed analysis performed in cell monolayer, before to translate the *in vitro* results to *in vivo* studies or to clinical applications.

References

1. Estanqueiro M, Amaral MH, Conceição J, Sousa Lobo JM, "Nanotechnological carriers for cancer chemotherapy: The state of the art", 2015, *Colloids Surf B Biointerfaces*, **126**, 631-648.

2. Li Z, Tan S, Li S, Shen Q, Wang K, "Cancer drug delivery in the nano era: An overview and perspective (Review)", 2017, *Oncol Rep*, **38**, 611-624.

3. Pakunlu RI, Wang Y, Tsao W, Pozharov V, Cook TJ, Minko T, "Enhancement of the efficacy of chemotherapy for lung cancer by simultaneous suppression of multidrug resistance and antiapoptotic cellular defense: novel multicomponent delivery system", 2004, *Cancer Res*, **64**, 6214-6224.

4. Zhang J, Tang H, Liu Z, Chen B, "Effects of major parameters of nanoparticles on their physical and chemical properties and recent application of nanodrug delivery system in targeted chemotherapy", 2017, *Int J Nanomedicine*, **12**, 8483-8493.

5. Thrall JH, "Nanotechnology and medicine", 2004, *Radiology*, **230**, 315-318.

6. Gmeiner WH, Ghosh S, "Nanotechnology for cancer treatment", 2015, *Nanotechnol Rev*, **3**, 111-122.

7. Sanvicens N, Marco MP, "Multifunctional nanoparticles-properties and prospects for their use in human medicine", 2008, *Trends Biotechnol*, **26**, 425-433.

8. Peer D, Karp JM, Hong S, Farokhzad OC, Margalit R, Langer R, "Nanocarriers as an emerging platform for cancer therapy", 2007, *Nat Nanotechnol*, **2**, 751-760.

9. Lee PI, Li JX, "Evolution of oral controlled release dosage forms", in: Wen H, Park K (Eds.), Oral Controlled Release Formulation Design and Drug Delivery, John Wiley &Sons, Inc., Hoboken, NJ 2010, pp.21-31.

10. James ND, Coker RJ, Tomlinson D, Harris JR, Gompels M, Pinching AJ, Stewart JS, "Liposomal doxorubicin (Doxil): an effective new treatment for Kaposi's sarcoma in AIDS", 1994, *Clin Oncol (R Coll Radiol)*, **6**, 294-296.

11. Kamaly N, Xiao Z, Valencia PM, Radovic-Moreno AF, Farokhzad OC, "Targeted polymeric therapeutic nanoparticles: design, development and clinical translation", 2012, *Chem Soc Rev*, **41**, 2971-3010.

12. Miele E, Spinelli GP, Miele E, Tomao F, Tomao S, "Albumin-bound formulation of paclitaxel (Abraxane ABI-007) in the treatment of breast cancer", 2009, *Int J Nanomedicine*, **4**, 99-105.

13. Ahn HK, Jung M, Sym SJ, Shin DB, Kang SM, Kyung SY, Park JW, Jeong SH, Cho EK, "Aphase II trial of Cremorphor EL-free paclitaxel (Genexol-PM) and gemcitabine in patients with advanced non-small cell lung cancer", 2014, *Cancer Chemother Pharmacol*, **74**, 277-282.

14. Bertrand N, Wu J, Xu X, Kamaly N, Farokhzad OC, "Cancer nanotechnology: the impact of passive and active targeting in the era of modern cancer biology", 2014, *Adv Drug Deliv Rev*, **66**, 2-25.

15. Wilhelm S, Tavares AJ, Dai Q, Ohta S, Audet J, Dvorak HF, Chan WCW, "Analysus of nanoparticle delivery to tumours", 2016, *Nat Rev Mater*, **1**, 16014.

16. McNeil S, "Nanotechnology for the biologist", 2005, *J Leukoc Biol*, **78**, 585-594.

17. Sriraman SK, Aryasomayajula B, Torchilin VP, "Barriers to drug delivery in solid tumors", 2014, *Tissue Barriers*, 2:e29528.

18. Torchilin VP, Papisov M, 2Why do polyethylene glycol-coated liposomes circulate so long?. Molecular mechanism of liposome steric protection with polyethylene glycol. Role of polymer chain flexibility", 1994, *J Liposome Res*, **4**, 725-739.

19. Kobayashi H, Watanabe R, Choyke PL, “Improving conventional enhanced permeability and retention (EPR) effects; what is the appropriate target?”, 2013, *Theranostics,* **4**, 81-89.

20. Duncan R, “The dawning era of polymer therapeutics”, 2003, *Nat Rev Drug Discov*, **2**, 347-360.

21. Danhier F, Feron O, Préat V, “To exploit the tumor microenvironment: passive and active tumor targeting of nanocarriers for anti-cancer drug delivery”, 2010, *J Control Release*, **148**, 135-146.

22. Maruyama K, “Intracellular targeting delivery of liposomal drugs to solid tumors based on EPR effects”, 2011, *Adv Drug Deliv Rev*, **63**, 161-169.

23. Cabral H, Matsumoto Y, Mizuno K, Chen Q, Murakami M, Kimura M, Terada Y, Kano MR, Miyazono K, Uesaka M, Nishiyama N, Kataoka K, “Accumulation of sub-100 nm polymeric micelles in poorly permeable tumours depends on size”, 2011, *Nat Nanotechnol*, **6**, 815-823.

24. Bartczak D, Muskens OL, Nitti S, Sanchez-Elsner T, Millar TM, Kanaras AG, “Interactions of human endothelial cells with gold nanoparticles of different morphologies”, 2012, *Small*, **8**, 122-130.

25. Klibanov AL, Maruyama K, Torchilin VP, Huang L, “Amphipathic polyethyleneglycols effectively prolong the circulation time of liposomes”, 1990, *FEBS Lett*, **268**, 235-237.

26. Wang X, Li J, Wang Y, Koenig L, Gjyrezi A, Giannakakou P, Shin EH, Tighiouart M, Chen ZG, Nie S, Shin DM, “A folate receptor-targeting nanoparticle minimizes drug resistance in a human cancer model”, 2011, *ACS Nano*, **5**, 6184-6194.

27. Gu FX, Karnik R, Wang AZ, Alexis F, Levy-Nissenbaum E, Hong S, Langer RS, Farokhzad OC, “Targeted nanoparticles for cancer therapy”, 2007, *Nano Today* **2**, 14–21.

28. Yang SJ, Lin FH, Tsai KC, Wei MF, Tsai HM, Wong JM, Shieh MJ, “Folic acid-conjugated chitosan nanoparticles enhanced protoporphyrin IX accumulation in colorectal cancer cells”, 2010, *Bioconjug Chem,* **21**, 679-689.

29. Platt VM, Szoka FC, “Anticancer therapeutics: targeting macromolecules and nanocarriers to hyaluronan or CD44, a hyaluronan receptor”, 2008, *Mol Pharm*, **5**, 474–486.

30. Sahoo SK, Ma W, Labhasetwar V, “Efficacy of transferrin-conjugated paclitaxel-loaded nanoparticles in a murine model of prostate cancer”, 2004, *Int. J. Cancer*, **112**, 335–340.

31. Dhar S, Gu FX, Langer R, Farokhzad OC, Lippard SJ, “Targeted delivery of cisplatin to prostate cancer cells by aptamer functionalized Pt(IV) prodrug- PLGA-PEG nanoparticles”, 2008, *Proc Natl Acad Sci USA*, **105**, 17356–17361.

32. Adams GP, Weiner LM, “Monoclonal antibody therapy of cancer”, 2005, *Nat. Biotechnol*, **23**, 1147–1157.

33. Byrne JD, Betancourt T, Brannon-Peppas L, “Active targeting schemes for nanoparticle systems in cancer therapeutics”, 2008, *Adv Drug Deliv Rev*, **60**, 1615-1626.

34. Toole BP, “Hyaluronan-CD44 Interactions in Cancer: Paradoxes and Possibilities”, 2009, *Clin Cancer Res*, **15**, 7462-7468.

35. Yu M, Jambhrunkar S, Thorn P, Chen J, Gu W, Yu C, “Hyaluronic acid modified mesoporous silica nanoparticles for targeted drug delivery to CD44-overexpressing cancer cells”, 2013, *Nanoscale*, **5**, 178-183.

36. Qhattal HS, Liu X, “Characterization of CD44-mediated cancer cell uptake and intracellular distribution of hyaluronan-grafted liposomes”, 2011, *Mol Pharm*, **8**, 1233-1246.

37. Yu MK, Park J, Jon S, “Targeting strategies for multifunctional nanoparticles in cancer imaging and

therapy", 2012, *Theranostics*, **2**, 3-44.

38. Aslan B, Ozpolat B, Sood AK, Lopez-Berestein G, "Nanotechnology in cancer therapy", 2013, *J Drug Target*, **21**, 904-913.

39. Bobo D, Robinson KJ, Islam J, Thurecht KJ, Corrie SR, "Nanoparticle-Based Medicines: A Review of FDA-Approved Materials and Clinical Trials to Date", 2016, *Pharm Res,* **33**, 2373-2387.

40. Ventola CL, "The nanomedicine revolution: part 1: emerging concepts", 2012, *P T*, **37**, 512-525.

41. Maier-Hauff K, Ulrich F, Nestler D, Niehoff H, Wust P, Thiesen B, Orawa H, Budach V, Jordan A, "Efficacy and safety of intratumoral thermotherapy using magnetic iron-oxide nanoparticles combined with external beam radiotherapy on patients with recurrent glioblastoma multiforme", 2011, *J Neurooncol*, **103**, 317-324.

42. Elahi N, Kamali M, Baghersad MH, "Recent biomedical applications of gold nanoparticles: A review", 2018, *Talanta,* **184**, 537-556.

43. Cui T, Liang JJ, Chen H, Geng DD, Jiao L, Yang JY, Qian H, Zhang C, Ding Y, "Performance of Doxorubicin-Conjugated Gold Nanoparticles: Regulation of Drug Location", 2017, *ACS Appl Mater Interfaces*, **9**, 8569-8580.

44. Sun TM, Wang YC, Wang F, Du JZ, Mao CQ, Sun CY, Tang RZ, Liu Y, Zhu J, Zhu YH, Yang XZ, Wang J, "Cancer stem cell therapy using doxorubicin conjugated to gold nanoparticles via hydrazone bonds", 2014, *Biomaterials*, **35**, 836-845.

45. Wang L, Zhang M, Zhang N, Shi J, Zhang H, Li M, Zhang Z, "Synergidtic enhancement of cancer therapy using a combination of docetaxel and photothermal ablation indiced by single-walled carbon nanotubes", 2011, *Int J Nanomedicine,* **6**, 2641-2652.

46. Datir SR, Das M, Singh RP, Jain S, "Hyaluronate tethered, "smart" multiwalled carbon nanotubes for tumor-targeted delivery of doxorubicin", 2012, *Bioconjug Chem*, **23**, 2201-2213.

47. Noble GT, Stefanick JF, Ashley JD, Kiziltepe T, Bilgicer B, "Ligand-targeted liposome design: challenges and fundamental considerations", 2014, *Trends Biotechnol*, **32**, 32-45.

48. Chonn A, Cullis PR, "Recent advances in liposomal drug-delivery systems", 1995, *Curr Opin Biotechnol*, **6**, 698-708.

49. Allen TM, Cullis PR, "Liposomal drug delivery systems: from concept to clinical applications", 2013, *Adv Drug Deliv Rev*, **65**, 36-48.

50. Kolate A, Baradia D, Patil S, Vhora I, Kore G, Misra A, "PEG – a versatile conjugating ligand for drugs and drug delivery systems", 2014, *J Control Release*, **192**, 67-81.

51. Bondurant B, Mueller A, O'Brien DF, "Photoinitiated destabilization of sterically stabilized liposomes", 2001, *Biochim Biophys Acta,* **1511**, 113-122.

52. Huang SL, MacDonald RC, "Acoustically active liposomes for drug encapsulation and ultrasound triggered release", 2004, *Biochim Biophys Acta*, **1665**, 134-141.

53. Simões S, Moreira JN, Fonseca C, Düzgüneş N, de Lima MC, "On the formulation of pH-sensitive liposomes with long circulation times", 2004, *Adv Drug Deliv Rev*, **56**, 947–965.

54. Kono K, Ozawa T, Yoshida T, Ozaki F, Ishizaka Y, Maruyama K, Kojima C, Harada A, Aoshima S, "Highly temperature-sensitive liposomes based on a thermosensitive block copolymer for tumor-specific chemotherapy", 2010, *Biomaterials*, **31**, 7096–7105.

55. Safari J, Zanegar Z, “Advanced drug delivery systems: nanotechnology of health design. A review”, 2013, *Journal of Saudi Chemical Society,* **18**, 85-99.

56. Svenson S, “Dendrimers as versatile platform in drug delivery applications”, 2009, *Eur. J. Pharm. Biopharm*, **71**, 445–462.

57. Malik N, Evagorou EG, Duncan R, “Dendrimer-platinate: a novel approach to cancer chemotherapy”, 1999, *Anticancer Drugs*, **10**, 767-776.

58. Liu P, Zhang H, Wu X, Guo L, Wang F, Xia G, Chen B, Yin H, Wang Y, Li X, “Tf-PEG-PLL-PLGA nanoparticles enhanced chemosensitivity for hypoxia-responsive tumor cells”, 2016, *Onco Targets Ther*, **9**, 5049-5059.

59. Wang X, Wang Y, Chen ZG, Shin DM, “Advances of cancer therapy by nanotechnology”, 2009, *Cancer Res Treat,* **41**, 1-11.

60.Kumari A, Yadav SK, Yadav SC, “Biodegradable polymeric nanoparticles based drug delivery systems”, 2010, *Colloids Surf B Biointerfaces*, **75**, 1-18.

61. Hammond PT, “Polyelectrolyte multilayered nanoparticles: using nanolayers for controlled and targeted systemic release”, 2012, *Nanomedicine (Lond)*, **7**, 619-622.

62. Deng ZJ, Morton SW, Ben-Akiva E, Dreaden EC, Shopsowitz KE, Hammond PT, “Layer-by-Layer nanoparticles for systemic codelivery of an anticancer drug and siRNA for potential triple-negative breast cancer treatment”, 2013, *ACS Nano* **7**, 9571-9584

63. Morton SW, Poon Z, Hammond PT, “The architecture and biological performance of drug- loaded LbL nanoparticles”, 2013, *Biomaterials* **34**, 5328-5335.

64. Hawkins MJ, Soon-Shiong P, Desai N, “Protein nanoparticles as drug carriers in clinical medicine”, 2008, *Adv Drug Deliv Res*, **60**, 876-885.

65. Xu H, Shi Z, Reddy N, Yang Y, “Intrinsically water-stable keratin nanoparticles and their in vivobiodistribution for targeted delivery”, 2014, *J Agric Food Chem*, **62**, 9145-9150.

66. Zhi X, Wang Y, Li P, Yuan J, Shen J, “Preparation of keratin/chlorhexidine complex nanoparticles for long-term and dual stimuli responsive release”, 2015, *RSC Adv*, **5**, 82334-82341.

67. Aluigi A, Sotgiu G, Ferroni C, Duchi S, Lucarelli E, Martini C, Posati T, Guerrini A, Ballestri M, Corticelli F, Varchi G, “Chlorin e6 keratin nanoparticles for photodynamic anticancer therapy”, 2016, *RSC Adv*, **6**, 33910-33918.

68. Lage H, “An overview of cancer multidrug resistance: a still unsolved problem”, 2008, *Cell Mol Life Sci*, **65**, 3145-3167.

69. Frei E, Karon M, Levin RH, Freireich EJ, Taylor RJ, Hananian J, Selawry O, Holland jf, Hoogstraten B, Wolman IJ, Abir E, Sawitsky A, Lee S, Mills SD, Burgert EO, Spurr CL, Patterson RB, Ebaugh FG, James GW, Moon JH, “The effectiveness of combinations of antileukemic agents in inducing and maintaining remission in children with acute leukemia”, 1965, *Blood*, **26**, 642-656.

70. Corn PG, Agarwal N, Araujo JC, Sonpavde G, “Taxane-based Combination Therapies for Metastatic Prostate Cancer”, 2017, *Eur Urol Focus,* DOI: 10.1016/j.euf.2017.11.009.

71. Lee A, Djamgoz MBA, “Triple negative breast cancer: Emerging therapeutic modalities and novel combination therapies”, 2018, *Cancer Treat Rev*, **62**, 110-122.

72. Mao H, Xie Y, Ju H, Mao H, Zhao L, Wang Z, Hua L, Zhao C, Li Y, Yu RT, Liu HM, "Design of tumor microenvironment responsive drug-drug micelle for cancer radiochemotherapy", 2018, *ACS Appl Mater Interfaces*, DOI: 10.1021/acsami.8b11159.

73. Chang JE, Yoon IS, Sun PL, Yi E, Jheon S, Shim CK, "Anticancer efficacy of photodynamic therapy with hematoporphyrin-modified, doxorubicin-loaded nanoparticles in liver cancer", 2014, *J Photochem Photobiol B*, **140**, 49-56.

74. Liu H, Chen D, Li L, Liu T, Tan L, Wu X, Tang F, "Multifunctional Gold Nanoshells on Silica Nanorattles: A Platform for the Combination of Photothermal Therapy and Chemotherapy with Low Systemic Toxicity", 2011, *Angew Chem Int Ed Engl*, **50**, 891-895.

75. Susa M, Iyer AK, Ryu K, Choy E, Hornicek FJ, Mankin H, Milane L, Amiji MM, Duan Z, "Inhibition of ABCB1 (MDR1) expression by ab siRNA nanoparticulate delivery system to overcome drug resistance in osteosarcoma", 2010, *PLoS One*, **5**: e10764.

76. Tian F, Dahmani FZ, Qiao J, Ni J, Xiong H, Liu T, Zhou J, Yao J, "A targeted nanoplatform co-delivering chemotherapeutic and antiangiogenic drugs as a tool to reverse multidrug resistance in breast cancer", 2018, *Acta Biomater*, **75**, 398-412.

77. Xu X, Ho W, Zhang X, Bertrand N, Farokhzad O, "Cancer nanomedicine: from targeted delivery to combination therapy", 2015, *Trends Mol Med*, **21**, 223-232.

78. Waterhouse DN, Gelmon KA, Klasa R, Chi K, Huntsman D, Ramsay E, Bally MB, "Development and assessment of conventional and targeted drug combina- tions for use in the treatment of aggressive breast cancers", 2006, *Curr. Cancer Drug Targets*, **6**, 455–489.

79. Zhang RX, Wong HL, Xue HY, Eoh JY, Wu XY, "Nanomedicine of synergistic drug combinations for cancer therapy–Strategies and perspectives", 2016, *J Control Release*, **240**, 489-503.

80. Ramsay EC, Dos Santos N, Dragowska WH, Laskin JJ, Bally MB, "The formulation of lipid-based nanotechnologies for the delivery of fixed dose anticancer drug combinations", 2005, *Curr Drug Deliv*, **2**, 341-351.

81. Mayer LD, Harasym TO, Tardi PG, Harasym NL, Shew CR, Johnstone SA, Ramsay EC, Bally MB, Janoff AS, "Ratiometric dosing of anticancer drug combinations: controlling drug ratios after systemic administration regulates therapeutic activity in tumor-bearing mice", 2006, *Mol Cancer Ther*, **5**, 1854-1863.

82. Wu J, Lu Y, Lee A, Pan X, Yang X, Zhao X, Lee RJ, "Reversal of multidrug resistance by transferrin-conjugated liposomes co-encapsulating doxorubicin and verapamil", 2007, *J Pharm Pharm Sci*, **10**, 350-357.

83. Tekade RK, Dutta T, Gajbhiye V, Jain NK, "Exploring dendrimer towards dual drug delivery: pH responsive simultaneous drug.release kinetics", 2009, *J Microencapsul*, **26**, 287-296.

84. Li R, Wu R, Zhao L, Wu M, Yang L, Zou H, "P-glycoprotein antibody functionalized carbon nanotube overcomes the multidrug resistance of human leukemia cells", 2010, *ACS Nano*, **4**, 1399-1408.

85. Misra R, Sahoo SK, "Coformulation of doxorubicin and curcumin in poly(D,L-lactide-co-glycolide) nanoparticles suppresses the development of multidrug resistance in K562 cells", 2011, *Mol Pharm*, **8**, 852-866.

86. Wong HL, Bendayan R, Rauth AM, Wu XY, "Simultaneous delivery of doxorubicin and GG918 (Elacridar(by new polymer-lipid hybrid nanoparticles (PLN) for enhanced treatment of multidrug-resistant breast cancer", 2006, *J Control Release*, **116**, 275-284.

87. Shuhendler AJ, O'Brien PJ, Rauth AM, Wu XY, "On the synergistic effect of doxorubicin and mitomycin C against breast cancer cells", 2007, *Drug Metabol Drug Interact*, **22**, 201-233.

88. Dai W, Wang X, Song G, Liu T, He B, Zhang H, Wang X, Zhang Q, "Combination antitumor therapy with targeted dual-nanomedicines", 2017, *Adv Drug Deliv Rev*, **115**, 23-45.

89. Gao JQ, Lv Q, Li LM, Tang XJ, Li FZ, Hu YL, Han M, "Glioma targeting and blood-brain barrier penetration by dual-targeting doxorubicin liposomes", 2013, *Biomaterials*, **22**, 5628-5639.

90. Allison RR, "Photodynamic therapy: oncologic horizons", 2014, *Future Oncol*, **10**, 123-142

91. Master A, Livingston M, Sen Gupta A, "Photodynamic nanomedicine in the treatment of solid tumors: perspectives and challenges", 2013, *J Control Release*, **168**, 88-102.

92. Dolmans DE, Fukumura D, Jain RK, "Photodynamic therapy for cancer", 2003, *Nat Rev Cancer*, **3**, 380-387.

93. Konan YN, Gurny R, Allémann E, "State of the art in the delivery of photosensitizers for photodynamic therapy", 2002, *J Photochem Photobiol B*, **66**, 89-106.

94. Agostinis P, Berg K, Cengel KA, Foster TH, Girotti AW, Gollnick SO, Hahn SM, Hamblin MR, Juzeniene A, Kessel D, Korbelik M, Moan J, Mroz P, Nowis D, Piette J, Wilson BC, Golab J, "Photodynamic therapy of cancer: an update", 2011, *CA Cancer J Clin*, **6**, 250-281.

95. Allison RR, Sibata CH, "Oncologic photodynamic therapy photosensitizers: a clinical review", 2010, *Photodiagnosis Photodyn Ther*, **7**, 61-75.

96. Senge MO, "mTHPC-A drug on its way from second to third generation photosensitizer?", 2012, *Photodiagnosis Photodyn Ther*, **9**, 170-179.

97. Wang JT, Berg K, Høgset A, Bown SG, MacRobert AJ, "Photophysical and photobiological properties of a sulfonated chlorin photosensitizer TPCS(2a) for photochemical internalization (PCI)", 2013, *Photochem Photobiol Sci*, **12**, 519-526.

98. Olsen CE, Weyergang A, Edwards VT, Berg K, Brech A, Weisheit S, Høgset A, Selbo PK, "Development of resistance to photodynamic therapy (PDT) in human breast cancer cells is photosensitizer-dependent: Possible mechanisms and approaches for overcoming PDT-resistance", 2017, *Biochem Pharmacol*, **144**, 63-77.

99. Lee LS, Thong PS, Olivo M, Chin WW, Ramaswamy B, Kho KW, Lim OL, Lau WK, "Chlorin e6-polyvinylpyrrolidone mediated photodynamic therapy-A potential bladder sparing option for high risk non-muscle invasive bladder cancer", 2010, Photodiagnosis Photodyn Ther, **7**, 213-220.

100. Orenstein A, Kostenich G, Roitman L, Shechtman Y, Kopolovic Y, Ehrenberg B, Malik Z, "A comparative study of tissue distribution and photodynamic therapy selectivity of chlorin e6, Photofrin II and ALA-induced protoporphyrin IX in a colon carcinoma model", 1996, Br J Cancer, **73**, 937-944.

101. Sheleg SV, Zhavrid EA, Khodina TV, Kochubeev GA, Istomin YP, Chalov VN, Zhuravkin IN, "Photodynamic therapy with chlorin e(6) for skin metastases of melanoma", 2004, Photodermatol Photoimmunol Photomed, **20**, 21-26.

102. Collaud S, Juzeniene A, Moan J, Lange N, "On the selectivity of 5-aminolevulinic acid-induced protoporphyrin IX formation", 2004, *Curr Med Chem Anticancer Agents*, **4**, 301-316.

103. Huang HC, Mallidi S, Liu J, Chiang CT, Mai Z, Goldschmidt R, Ebrahim-Zadeh N, Rizvi I, Hasan T, "Photodynamic Therapy Synergizes with Irinotecan to Overcome Compensatory Mechanisms and Improve Treatment Outcomes in Pancreatic Cancer", 2016, *Cancer Res*, **76**,1066-1077.

104. Ali S, Muhammad S, Khurshid A, Ikram M, Maqsood M, Fisher C, Cathcart J, Lilge L, "Effective Phthalocyanines mediated Phoyodynamic Therapy with Doxorubicin or Methotrexate combination therapy at sub-micromolar concentrations in vitro", 2018, *Photodiagnosis Photodyn Ther*, **22**, 51-64.

105. Khdair A, Chen D, Patil Y, Ma L, Dou QP, Shekhar MP, Panyam J, "Nanoparticle-mediated combination chemotherapy and photodynamic therapy overcomed tumor drug resistance", 2010, *J Control Release*, **141**, 137-144.

106. Postiglione I, Chiaviello A, Palumbo G, "Enhancing photodynamyc therapy efficacy by combination therapy: dated, current and oncoming strategies", 2011, *Cancers (Basel)*, **3**, 2597-2629.

107. Nonaka M, Ikeda H, Inokuchi T, "Effect of combined photodynamic and chemotherapeutic treatment on lymphoma cells in vitro", 2002, *Cancer Lett*, **184**, 171-178.

108. Kasimova K, Lilge L, Wilson BC, "In-vitro efficacy of indocyanine green-mediated photodynamic therapy in combination with cisplatin or etoposide", 2015, *Photon Lasers Med*, **4**, 281-290.

109. Zhang Y, Huang F, Ren C, Yang L, Liu J, Cheng Z, Chu L, Liu J, "Targeted Chemo-Photodynamic Combination Platform Based on the DOX Prodrug Nanoparticles for Enhanced Cancer Therapy", 2017, *ACS Appl Mater Interfaces*, **9**, 13016-13028.

110. Xu S, Zhu X, Zhang C, Huang W, Zhou Y, Yan D, "Oxygen and Pt(II) self-generating conjugate for synergistic photo-chemo therapy of hypoxic tumor", 2018, *Nat Commun*, **9**, 2053.

111. Nieuweboer AJ, de Morrée ES, de Graan AJ, Sparreboom A, de Wit R, Mathijssen RH, "Inter-patient variability in docetaxel pharmacokinetics: A review", 2015, *Cancer Treat Rev*, **41**, 605-613.

112. Chou TC, "Derivation and properties of Michaelis-Menten type and Hill type equations for reference ligands", 1976, *J Theor Biol*, **59**, 253-276.

113. Chou TC, Talalay P, "Generalized equations for the analysis of inhibitions of Michaelis-Menten and higher-order kinetic systems with two or more mutually exclusive and non exclusive inhibitors", 1981, *Eur J Biochem*, **115**, 207-216.

114. Chou TC, "Theoretical basis, experimental design, and computerized simulation of synergism and antagonism in drug combination studies", 2006, *Pharmacol Rev*, **58**, 621-681.

115. Hongrapipat J, Kopeckova P, Prakongpan S, Kopecek J, "Enhanced antitumor activity of combinations of free and HPMA copolymer-bound drugs", 2008, *Int J Pharm*, **351**, 259-270.

116. Zhang N, Fu JN, Chou TC, "Synergistic combination of microtubule targeting anticancer fludelone with cytoprotective panaxytriol derived from panax ginseng against MX-1 cells in vitro: experimental design and data analysis using the combination index method", 2015, *Am J Cancer Res*, **6**, 97-104.

117. Dewangan J, Tandon D, Srivastava S, Verma AK, Yapuri A, Rath SK, "Novel combination of salinomycin and resveratrol synergistically enhances the anti-proliferative and pro-apoptotic effects on human breast cancer cells", 2017, *Apoptosis*, **22**, 1246-1259.

118. Peterson OW, Rønnov-Jessen L, Howlett AR, Bissel MJ, "Interaction with basement membrane served to rapidly distinguish growth and differentiation pattern of normal and malignant human breast epithelial cells", 1992, *Proc Natl Acad Sci USA*, **89**, 9064-9068.

119. Mseka T, Bamburg JR, Cramer LP, "ADF/cofilin family proteins control formation of oriented actin-filament bundles in the cell body to trigger fibroblast polarization", 2007*, J Cell Sci*, **120**, 4332-4344.

120. Birgersdotter A, Sandberg R, Ernberg I, "Gene expression perturbation in vitro-a growing case for three-dimensional (3D) culture systems", 2005, *Semin Cancer Biol*, **15**, 405-412.

121. Leong D, Ng KW, "Probing the relevance of 3D cancer models in nanomedicine research", 2014, *Adv Drug Deliv Rev*, DOI: 10.1016/j.addr.2014.06.007.

122. Katt ME, Placone AL, Wong AD, Xu ZS, Searson PC, "In vitro Tumor Models: Advantages, Disadvantages, Variables, and Selecting the Right Platform", 2016, *Front Bioeng Biotechnol*, **4**, 12.

123. Kramer N, Walzl A, Unger C, Rosner M, Krupitza G, Hengstschläger M, Dolznig H, “In vitro cell migration and invasion assays”, 2013, *Mutat Res*, **752**, 10-24.

124. Gottfried E, Kunz-Schughart LA, Andreesen R, Kreutz M, “Brave little world: spheroids as an in vitro model to study tumor-immune-cell interactions”, 2006, *Cell Cycle*, **5**, 691-695.

125. Lin RZ, Chang HY, “Recent advances in three-dimensional multicellular spheroid culture for biomedical research”, 2008, *Biotechnol J*, **3**, 1172-1184.

126. Yabushita H, Ohnishi M, Komiyama M, Mori T, Noguchi M, Kishida T, Noguchi Y, Sawaguchi K, Noguchi M, “Usefulness of collagen gel droplet embedded culture drug sensitivity testing in ovarian cancer”, 2004, *Oncol Rep*, **12**, 307-311.

127. Bogorad MI, DeStefano J, Karlsson J, Wong AD, Gerecht S, Searson PC, “Review: in vitro microvessel models”, 2015, *Lab Chip*, **15**, 4242-4255.

128. Hirschhaeuser F, Menne H, Dittfeld C, West J, Mueller-Klieser W, Kunz-Schughart LA, “Multicellular tumor spheroids: an underestimated tool is catching up again”, 2010, *J Biotechnol*, **148**, 3-15.

129. Poland J, Sinha P, Siegert A, Schnölzer M, Korf U, Hauptmann S, “Comparison of protein expression profiles between monolayer and spheroid cell culture of HT-29 cells revealed fragmentation of CK18 in three-dimensional cell culture”, 2002, *Electrophoresis*, **23**, 1174-1184.

130. Dufau I, Frongia C, Sicard F, Dedieu L, Cordelier P, Ausseil F, Ducommun B, Valette A, “Multicellular tumor spheroid model to evaluate spatio-temporal dynamics effect of chemotherapeutics: application to the gemcitabine/CHK1 inhibitor combination in pancreatic cancer”, 2012, *BMC Cancer*, **12**, 15.

131. Vinci M, Gowan S, Boxall F, Patterson L, Zimmermann M, Court W, Lomas C, Mendiola M, Hardisson D, Eccles SA, “Advances in establishment and analysis of three-dimensional tumor spheroid-based functional assays for target validation and drug evaluation”, 2012, *BMC Biol*, **10**, 29.

132. Page H, Flood P, Reynaud EG, “Three-dimensional tissue cultures: current trends and beyond”, 2013, *Cell Tissue Res*, **352**, 123-131.

133. Ponti D, Costa A, Zaffaroni N, Pratesi G, Petrangolini G, Coradini D, Pilotti S, Pierotti MA, Daidone MG, “Isolation and in vitro propagation of tumorigenic breast cancer cells with stem/progenitor cell properties”, 2005, *Cancer Res*, **65**, 5506-5511.

134. Choi YH, Yu AM, “ABC transporters in multidrug resistance and pharmacokinetics, and strategies for drug development”, 2014, *Curr Pharm Des*, **20**, 793-807.

135. Baccelli I, Trumpp A, “The evolving concept of cancer and metastasis stem cells”, 2012, *J Cell Biol*, **198**, 281-293.

136. Al-Hajj M, Wicha MS, Benito-Hernandez A, Morrison SJ, Clarke MF, “Prospective identification of tumorigenic breast cancer cells”, 2003, *Proc Natl Acad Sci U S A*, **100**, 3983-3988.

137. Bao B, Ahmad A, Azmi AS, Ali S, Sarkar FH, “Overview of Cancer Stem Cells (CSCs) and Mechanisms of Their Regulation: Implications for Cancer Therapy”, 2013, *Curr Protoc Pharmaco*l, 14: Unit–14.25. DOI:10.1002/0471141755.ph1425s61.

138. Dontu G, Abdallah WM, Foley JM, Jackson KW, Clarke MF, Kawamura MJ, Wicha MS, “In vitro propagation and transcriptional profiling of human mammary stem/progenitor cells”, 2003, *Genes Dev*, **17**, 1253-1270.

139. Usacheva M, Swaminathan SK, Kirtane AR, Panyam J, “Enhanced photodynamic therapy and effective elimination of cancer stem cells using surfactant-polymer nanoparticles”, 2014, *Mol Pharm*, **11**, 3186-3195.

140. Wang H, Agarwal P, Zhao S, Yu J, Lu X, He X, “Combined cancer therapy with hyaluronan-decorated fullerene-silica multifunctional nanoparticles to target cancer stem-like cells”, 2016, *Biomaterials*, **97**, 62-73.